Scuola Normale Superiore

Ph. D. Thesis in chemistry

A dynamical approach to the calculation of thermal reaction rate constants

Candidate: Riccardo Conte

Supervisor: Prof. Giovanni Paolo Arrighini

Contents

Introduction **1**

1 A brief introduction to reaction rate theory **6**
1.1 Classical rate theory 9
1.2 Transition State Theory (TST) 11
1.3 Quantum Transition State Theory 14
1.3.1 Long-Time Fictitious-Dynamics Quantum Transition State Theory (LTFDQTST) 16
1.3.2 Short-time Quantum Transition State Theory (STQTST) . . . 18
1.4 Main features of SCIVR 23

2 Quantum mechanical propagators in the case of simple Hamiltonian operators **26**
2.1 Propagators for the free particle 28
2.2 The harmonic oscillator case 29
2.3 Real-time propagator for the complete oscillator potential 31
2.4 Thermal density matrices for parabolic barriers 32

3 A dynamical approach to the calculation of thermal reaction rates **34**
3.1 First quantum mechanical steps 36
3.2 The ininfluent dynamics limit ($t = 0$) 38
3.3 Reaction rate constants for parabolic barrier models 41
3.3.1 The simple parabolic barrier 41
3.3.2 The complete parabolic barrier 45
3.4 Treatment of forms of barrier not analytically solvable 50

4 Computational strategies **52**
4.1 Step 1: the thermal density matrix 53
4.1.1 Some properties of density matrices 53
4.2 Calculation of the thermal density matrix elements 56
4.2.1 Diagonal elements 56
4.2.2 Off-diagonal elements 61

4.3 The density matrix for the Eckart barrier 66
4.4 Confined systems 69
4.5 A different algorithm for Boltzmann path integrals 71
4.6 Step 2: dynamics and integration 73

5 Reaction rates and conclusions **77**
5.1 The truncated parabolic barrier 78
5.2 The Eckart barrier 80
5.2.1 Symmetrical Eckart barrier 82
5.2.2 Asymmetrical Eckart barrier 83
5.3 Conclusions and perspectives 86

A A remarkable relation between a principal value integral and a complex error function **88**

B Calculation of an integral of the error function **91**

C Basic path integral method for the calculation of thermal density matrix elements **93**

Bibliography **95**

Introduction

The microscopic comprehension of the kinetic aspects of a chemical reaction is recognized a challenge in theoretical and computational chemistry because of the many facets of the problem. Role of temperature, influence of the phase in which the reaction takes place, significance of quantum effects, along with their reciprocal influences, are only a few points which need elucidation.

One of the first attempts to construct an accurate theory of reaction rates dates back to 1930s, with the introduction of *TST* (Transition State Theory) by M. Polanyi, H. Eyring and E. Wigner[1]. In occasion of the famous General Discussion of the Faraday Society held in Manchester in 1937, two different perspectives in Transition State Theory (TST) were illustrated, leading to a dualism still present in modern strategies: Eyring (together with Evans) introduced the thermodynamic picture, based on the assumption of a quasi-equilibrium between the Transition State (TS) and reactants, which dominated the field in the first decades due to its large number of applications to realistic systems and reactions; Wigner, instead, focused his attention on the dynamical point of view, through the hypothesis of no-recrossing dynamics (also called the dynamical bottleneck assumption) for trajectories pointing towards the products when leaving the transition state.
Furthermore, Wigner gave an even today valid snapshot of the kinetic problem in his 'three threes': three groups (1), (2), (3), each composed of three items, describing (1) the three steps which are necessarily involved in kinetic theory, (2) the three groups of elementary reactions to deal with and, most of all, (3) the three basic assumptions of TST, i.e. electronic adiabaticity next to the dynamical bottleneck, the validity of classical mechanics for nuclear motion and the presence of a dividing surface separating reactants from products.

Transition state theory, indeed, was born as a classical theory, which aims to compute one-way rate constants at equilibrium and gives the best results for multidimensional systems, at low energy, a situation where quantum effects like tunneling grow in importance with the lowering of temperature. For these reasons, many attempts have been made and keep on being made to extend transition state theory to

the realm of quantum mechanics, by inclusion of tunneling and interference contributions.
A relatively recent review of *TST* and its state-of-art appeared in 1996 [3], essentially in the form of bibliographical collection, (a list that would be actually much longer nowadays), confirming the vivacity and plenty of interest in the matter. Advancements in the calculation of rate constants, related to improvements of the electronic structure description, the inclusion of solvent effects and the accuracy of approximations in treating quantum dynamics, were widely illustrated.

Eyring's work was based on a time independent interpretation of the assumed quasi-equilibrium, while Wigner opened up a route, centered on real-time dynamics, that led, actually some decades later, to various and stimulating approaches to the problem.
Present-day thermodynamic approaches intend to introduce quantum effects by extrapolating thermal rate constants without explicitly considering the real-time dynamics of the reactive process. Two major classes can be identified:
i) the Centroid Rate theory developed mainly by Gillan, Voth et al.[4, 5], in which a classical transition state theory treatment is adopted in the presence of a quantum potential of mean force defined by the centroid density: since the centroid density is computed from the diagonal elements of the imaginary-time propagator, this represents a legitimate thermodynamic strategy;
ii) methods which can be reconducted to the Hansen-Andersen approach to the time dependent flux-side or flux-flux correlation function formulation [6, 7]. Here one finds, for the true potential, the first two initial-time derivatives of the correlation function, which depend only on matrix elements of the imaginary time propagator, and then, by means of analytic continuation, extrapolates the result to large (formally infinite) time.

Coming to Wigner, a preliminary step to grasp his dynamical view brings us to Yamamoto [8], who suggested a flux-flux correlation function formalism. Yamamoto's idea lays on classical-mechanics grounds, while quantum calculations should rigorously set up the problem in terms of state-to-state reactive scattering (evaluation of the $S-$matrix). Actually, if one is interested principally in evaluating thermal rate constants, a lot of work can be avoided by estimating the long-time limit of the quantum mechanical trace of the thermalized flux times a time-dependent projecton operator [9, 10]. This result, initially derived for the thermal penetration of a barrier with asymptotically vanishing boundary interaction, can also be successfully applied to the decay of metastable states.
The formally exact Miller's expression can be elaborated in different ways, and, consequently, many paths have been explored: amongst them, we cite the direct evalu-

ation of the trace in different complete basis sets (trace invariance with respect to the choice of the representation); the development of a non-separable transition state theory; the formulation of a rigorous semiclassical theory of rate constants, along with a stationary-phase procedure to evaluate the trace.
The assumption of separability of the Hamiltonian operator about the potential saddle point is a poor one, due to the corner-cutting effect [11], and can be avoided by means of semiclassical approximations to the Boltzmann operator [12]. Tunneling, in this semiclassical picture, takes place along a periodic classical trajectory on the upside-down potential energy surface [13, 14].

Miller et al arrived to a quantum analog of Yamamoto's correlation function [15] that provides exact reaction rates if calculations are pushed to long times.
Long-time quantum dynamics is synonymic of impossible task. The best we can do for its approximate implementation involves a first step where thermal and dynamical contributions are separated out, followed by a second step in which dynamics is approximated more or less drastically, either avoiding direct real-time propagation (long-time fictitious-dynamics approaches) or limiting its duration to a brief period (short-time approaches).

Ankerhold, Grossmann and Tannor [16] studied the partition between dynamical and thermal factors in quantum rate calculations by means of a coherent-state approach, suitable to analyze the different contributions to the rate constant from various phase space regions. The parabolic barrier approximation in the asymptotic limit ($\omega_b t \gg 1$) leads to introduce a complex-valued error function, a feature which deserves to be remarked because a similar quantity plays a role in our approach.

Voth, Chandler and Miller, in a different formulation of quantum transition state theory [17], arrived to Miller's quantum reactive formula for the thermal rate constant starting from Zwanzig's work on correlation functions [18]. Here, the factorization is between the thermal density matrix and the so-called (dynamical) z factor, which is calculated at large times for a few models: free particle, parabolic barrier and one-dimensional barriers (semiclassical limit).

More recently, quantum transition state theory has been revisited by Pollak and Liao [19]. Their new rate expression, based on a parabolic barrier approximation to the dynamics is similar to that put forward by Voth, Chandler and Miller, the main difference deriving from the adoption of a symmetrized form of the thermal flux operator.

A different formulation of quantum transition state theory encompasses short-time approaches, sometimes referred to as Short Time Quantum Transition State Theory (STQTST). In short time quantum transition state theory, (real-time) dynamics is not completely avoided, but rather considered for just the brief period necessary to

get the main contribution to the reaction rate, or to reach the regime behavior.
In this view, Tromp and Miller [20, 21] proposed an approach based on the correlation functions introduced by Miller, Schwartz and Tromp: the calculation of the flux-flux autocorrelation function is stopped as soon as its value tumbles to zero. As a consequence, the integration needed to get the rate constant is limited to a short time. Any negative lobe of the function at longer times is interpreted as a recrossing flux through the chosen dividing surface, unveiling, in this way, the route towards a possible variational theory.
In the context of short time quantum transition state theory, through a series of recent papers, Craig and Manolopoulos have proposed a formulation for calculating reaction rates [22, 23, 24] based on the Ring Polymer Molecular Dynamics method (RPMD). According to this approach, the "harmonic ring polymer" involved, initially centered around the dividing surface, is made to evolve classically. The long-time limit of an appropriately approximated version of the Kubo-transformed flux-side correlation function depends on the behavior of the centroid, and the final result is that the correlation function converges to its long-time limit rapidly.

In general, the main problem plaguing any quantum transition state theory (of course we understand that there is not a unique one) is the difficulty to perform quantum calculations. While it is well documented that simulations relative to a great variety of dynamical processes (including chemical reactions) can be carried out in classical terms, even for complex molecular systems, a full quantum dynamical treatment for many degrees of freedom is out of question, due to the unendurable computational costs. The adoption of approaches able to give account of tunnel and interference effects, but based on the evolution, over effective potential energy surfaces, of classical trajectories determined entirely by the initial conditions, represents an attempt to get sensible results with tolerable computational efforts.

The standard Van Vleck's Semi-Classical approximation to the real time quantum-mechanical propagator [25] leads to a general procedure of this kind. Developed mainly by W.H.Miller and coworkers, the approach, known as Semi-Classical Initial Value Representation (SCIVR) [26], has been widely improved since its first formulation [27] and extended to the study of complex systems. In SC-IVR, all the degrees of freedom are treated semiclassically and the non-linear boundary value problem, associated with Van Vleck's approximation is replaced by an average over the initial conditions of classical trajectories. The integrations involved in the evaluation of the real-time propagator, instead of being performed via Stationary Phase Approximation (SPA), are carried out numerically, by resorting to Monte Carlo techniques, providing a way to deal with classically forbidden phenomena in terms of real-valued trajectories.

The goal of the present work is the evaluation of the rate constant for reactive processes, described by simple onedimensional barriers. The approach is an elaboration of a previous result suggested by W.H.Miller for bimolecular rate constants under a fully quantum mechanical treatment. After separating out thermal and dynamical contributions to the rate constant, the introduction of a specific parabolic-barrier approximation to dynamics allows us through short-time classical simulations, to get, finally, the observable (rate constant). It should be observed that, while the dynamical problem is overcome by resorting to the parabolic barrier approximation, the thermal factor is calculated exactly, by means of the Feynman-Kac relation. Results have been obtained for the truncated parabola, symmetrical and asymmetrical Eckart barriers, in addition to the parabolic barrier.

In chapter one, a brief summary of a number of techniques adopted in transition state theory is presented. Exact classical rate theory, classical and quantum transition state theory and some of the main features of Miller's semiclassical initial value representation are described in a concise way, with the goal of introducing the basic themes of reaction rate theory, while focusing on the strategy adopted by those approaches.

In chapter two, quantum mechanical propagators for a few Hamiltonian operators involving simple potential energy functions are recalled and derived by means of analytical procedures. Both real-time and imaginary-time propagators are taken into consideration. Analytic continuation, a technique frequently adopted in thermodynamic methods to face the reaction rate problem, constitutes the interrelation between the two propagators.

In chapter three, the approach adopted in the present work is introduced and described. Starting from preceding results suggested by Miller, pushing through quantum mechanical operations, the final shore is represented by the extension to the case of not analytically solvable barriers.

Chapter four is devoted to the description and analysis of the computational strategies employed. The general procedure involves two steps: initially, the determination of the (off-diagonal) elements of the thermal density matrix; then, the integration of the evolved trajectories to obtain the rate constant.
The Feynman-Kac formula is described, together with applications to some kinds of activation barrier. Filon's formula for the integration of oscillatory integrands and Gautschi's algorithm for complex error functions are briefly discussed in view of their importance in this work.

Finally, in chapter five, results are reported for the truncated parabolic barrier and Eckart barrier (both symmetrical and asymmetrical): these represent the onedimensional barriers to which the approach, here developed, is applied.

Chapter 1

A brief introduction to reaction rate theory

Reaction rate theory is a vast field of theoretical research, with so many possible approaches of a different kind and so many problems to face, depending on features like type of reaction, nature of reactants, operating temperature (to name only a few), that an exhaustive description cannot be achieved in this context.

Two main methodological branches can be recognized: thermodynamic approaches and dynamical approaches. The former are based on the assumption of quasi-equilibrium between reactants and transition state (with all information extracted from the thermal density matrix), while the latter are based on the study of trajectories over a potential energy surface.
It is in the dynamical-approach area that the approach presented in this work finds his placement. Some of the most common methods employed, like classical TST, the attempts for a quantum version of it, called Quantum Transition State Theory (QTST), or semiclassical formulations like the SemiClassical Initial Value Representation (SCIVR) [26], are firstly presented and successively our specific approach is introduced and developed.

Going back to the large number of contributions to the field, consider that, just as an example, a relative recent review [3] of TST and its state-of-art appeared in 1996: it was filled with bibliographic items, a list that would be actually longer nowadays, confirming the vivacity and plenty of interest in the subject. Advancements in topics related to the calculation of rate constants like electronic-structure theory, the inclusion of solvent effects or the accuracy of various approximations to quantum dynamics were illustrated. By the way, all that stuff was referred to TST, which is just one (even though, perhaps, the best known) of the possible approaches to the kinetic problem. Nowadays, many scientists and research groups are involved in the

improvement of theoretical techniques to efficiently describe chemical reactions.

In a classical world, accurate reaction rate constants could be evaluated by means of molecular-dynamics simulations, even for fairly complex reactions. The dynamical problem posed by the necessity of monitoring the microscopic evolution of the system to long times, although very exacting, would be superable.

TST is an approximation to the exact classical treatment which assumes the instantaneous flux of reactant trajectories through a dividing surface (between reactants and products) to be the net reactive flux. From a dynamical point of view, this assumption is equivalent to that of zero-time dynamics: the initial momenta of reactants on the dividing surface is, in fact, all that is needed to quarry the rate constant. TST is verified to lead to predictions in good accordance with exact classical results in the low-energy range and for multidimensional systems. Due to these features, it is normal to try exporting TST in the realm of quantum mechanics, since it is at low energies that quantal phenomena are more influent. From now, anyway, we emphasize that there is no unique quantum analogue of TST and that many QTST approaches have been proposed.

Exact quantum rate constants should actually be determined by solving the associated reactive scattering problem, a difficult and expensive (in computational terms) procedure, particularly if the interest is addressed to calculate primarily reaction rate constants. The fact that the knowledge of the scattering S-matrix for all the possible reactive channels results in a costly excess of information has directed the efforts to search for alternative routes. Fundamental contributions in this direction are the result of much work by W.H.Miller and his group at Berkeley [14, 15]. Here we limit ourselves to recall that, through his formulations, Miller has shown how the evaluation of a rate constant is reducible to that of a time-dependent quantum mechanical trace at long times or, equivalently, of appropriate correlation functions (a difficult task, in any case).

Many different kinds of approximations have been introduced into Miller's original formulation, leading to different versions of QTST. Since, in quantum mechanics, Heisenberg's uncertainty principle prevents us from the possibility of following particle trajectories, the TST fundamental assumption must be replaced by some other kind of assumption or by resorting to semiclassical methods. In particular, developments of Miller's formula in the coherent-state space, which adopt an overcomplete basis set, have been pursued [16].

A central role in quantum treatments is played by the calculation of propagators at real and imaginary times. Path integration techniques [28] or semiclassical dynamical methods, originated from the standard Van Vleck's approximation [29], have been employed in these computations. In quantum mechanics, statistics and dynamics are

strictly intertwined, since both of them are entirely described in terms of wave functions; the possibility of achieving a clear separation between thermal and dynamical effects, surely coexisting in rate constant calculations, represents an interesting goal which our approach aims at.

1.1 Classical rate theory

Prerequisite of all the considerations we are about to make is the assumption of knowing the Potential Energy Surface (PES) on which the nuclear motions are bound to take place in the frame of the adiabatic Born-Oppenheimer approximation. The PES is expected to be known with good accuracy, especially for the reactant and product regions and for first-order saddle points.

If a reactive process is treated from a purely classical point of view, the following exact expression for the reaction rate constant is readily determined [12, 30]

$$k_{cl}(T) = Q_r(T)^{-1}(2\pi\hbar)^{-L} \int d\mathbf{p} \int d\mathbf{q}\, e^{-\beta H(\mathbf{p},\mathbf{q})} F(\mathbf{p},\mathbf{q})\chi_r(\mathbf{p},\mathbf{q}) \tag{1.1}$$

The factor $\hbar^{-L}$, where L is the number of degrees of freedom of the system, is customarily included in the classical partition function so as to ensure an approximately correct quantum state counting [30]; $Q_r(T)$ is the reactant partition function per unit volume, $\beta = (kT)^{-1}$, $H(\mathbf{p},\mathbf{q})$ is the Hamiltonian for the complete molecular system. Finally, $F(\mathbf{p},\mathbf{q})$ is the flux factor and $\chi_r(\mathbf{p},\mathbf{q})$ the characteristic function for the reaction.

The presence of a flux factor implies the presence of a surface to which the flux is referred. This particular surface (a subspace of the potential energy surface) is called the dividing surface, because it separates the reactant region from the product one. Topologically, it is defined by the equation

$$f(\mathbf{q}) = 0 \tag{1.2}$$

reactants being referred to the $f(\mathbf{q}) < 0$ region and products to the $f(\mathbf{q}) > 0$ one.

The flux can therefore be expressed as

$$F(\mathbf{p},\mathbf{q}) = \frac{d}{dt}\Theta[f(\mathbf{q})] \tag{1.3}$$

where $\Theta(\xi)$ is the Heaviside function

$$\Theta(\xi) = \begin{cases} 1 & \xi > 0 \\ 0 & \xi < 0 \end{cases} \tag{1.4}$$

Assuming the vectors $(\mathbf{p},\mathbf{q})$ to be expressed in terms of Cartesian components, the flux tranforms as follows

$$F(\mathbf{p},\mathbf{q}) = \delta[f(\mathbf{q})]\frac{\partial f}{\partial \mathbf{q}} \cdot \frac{\mathbf{p}}{m} \tag{1.5}$$

$\chi_r(\mathbf{p},\mathbf{q})$, the characteristic function, can be defined in a way allowing a direct quantum mechanical generalization

$$\chi_r(\mathbf{p},\mathbf{q}) = \lim_{t\to\infty} \Theta[f(\mathbf{q}(t))] \tag{1.6}$$

Here $\mathbf{q}(t)$ is the t-time evolved trajectory originated from the initial conditions $(\mathbf{p},\mathbf{q})$ at time $t = 0$. In this way, $\chi_r(\mathbf{p},\mathbf{q}) = 1$ if the trajectory with initial conditions $(\mathbf{p},\mathbf{q})$ is on the product side in the limit $t \to \infty$; otherwise, χ_r equals 0. Therefore, in the classical rate constant formula, eq.(1.1), the canonical ensemble statistics is represented by the $e^{-\beta H(\mathbf{p},\mathbf{q})}$ term, while the dynamics is exclusively contained in the characteristic function $\chi_r(\mathbf{p},\mathbf{q})$.

According to another purely classical approach, one can define a microcanonical rate constant, i.e. the rate constant for reactions at fixed energy E

$$k(E) = (2\pi\hbar\rho_r(E))^{-1} N(E) \tag{1.7}$$

where ρ_r is the density of reactant states (per unit energy) and $N(E)$ the cumulative reaction probability

$$N(E) = 2\pi\hbar(2\pi\hbar)^{-F} \int d\mathbf{p} \int d\mathbf{q}\, \delta[E - H(\mathbf{p},\mathbf{q})] F(\mathbf{p},\mathbf{q}) \chi_r(\mathbf{p},\mathbf{q}) \tag{1.8}$$

Its relation to the canonical rate constant is

$$k(T) = (2\pi\hbar Q_r)^{-1} \int dE e^{-\beta E} N(E) \tag{1.9}$$

Since the integrations in eq. (1.1) and eq. (1.8) are extended to the whole phase space, the knowledge of $\chi_r(\mathbf{p},\mathbf{q})$ for each starting point would imply the study of the complete dynamics of the system. Actually, the presence of the Dirac delta in the flux definition requires to evolve trajectories starting from the dividing surface only and the multi-dimensional integrations involved can then be performed by resorting to convenient Monte Carlo methods [31, 32]. It is a fact that, according to Liouville's theorem, the rate is independent of the choice of the dividing surface; a good choice, based on both energetic and entropic considerations (i.e. considering a free energy rather than potential energy surface), however, can be of noticeable aid making calculations easier.

1.2 Transition State Theory (TST)

Transition State Theory (*TST*) provides a powerful approximation to the classical determination of rate constants. The fundamental assumption of *TST* is that trajectories leaving the dividing surface and pointing towards the products will be unable to recross it in the opposite direction (direct dynamics). In mathematical terms, therefore, the approximate characteristic function $\chi_r(\mathbf{p}, \mathbf{q})$ enjoys the peculiar property

$$\chi_{TST}(\mathbf{p}, \mathbf{q}) = \begin{cases} 1 & \mathbf{p} \cdot \mathbf{n} > 0 \\ 0 & \mathbf{p} \cdot \mathbf{n} \leq 0 \end{cases} \tag{1.10}$$

where $\mathbf{n}$ is the direction normal to the dividing surface and pointing towards the products. In a compact form,

$$\chi_{TST}(\mathbf{p}, \mathbf{q}) = \Theta \left[\frac{\partial f(\mathbf{q})}{\partial \mathbf{q}} \cdot \frac{\mathbf{p}}{m} \right] \tag{1.11}$$

The characteristic function defined by eq.(1.10) can be interpreted as a short-time approximation to dynamics, because, more than the whole evolution of the trajectory, from its generation at the dividing surface until its long-time behavior, what counts is in this view the orientation of the component of the momentum normal to the surface as the trajectory originates.

Use of eq. (1.11) provides an upper bound to the correct classical reaction rate constant ($k_{TST}(T) \geq k_{cl}(T)$), with the equality valid only if $\chi_{TST} = \chi_r$ (see eq. (1.1)). For a one-dimensional barrier, the transition state is univocally determined on the basis of energetic considerations, i.e. the best dividing surface (actually a point) is located at the top of the barrier, and, in this case, $k_{TST}(T) = k_{cl}(T)$. If the dividing surface were chosen away from the maximum of the barrier, transition state theory would lead to a result higher than expected. This is because both $\chi_r(p, q)$ and $\chi_{TST}(p, q)$ would equal 0 for $p < 0$, but, on the contrary, for $p > 0$ χ_{TST} would always be 1, while χ_r would be 0 in case the particle had not sufficient kinetic energy to climb over the barrier.

The accuracy of the *TST* approximation clearly depends on the particular location of the dividing surface. The search for a dividing surface which optimizes the calculated value of the rate constant has originated a variational procedure, called variational transition state theory (*VTST*). It is out of our scope to treat *VTST* (a detailed review can be found for instance in [33, 34, 35]) but it is a fact and a peculiar characteristic that the results from *TST* computations depend on the choice of the dividing surface. In a one-dimensional space, naturally, it is trivial to find the best location for the dividing surface according to energetic considerations, but in two or

even higher-dimensional systems the task becomes more difficult, due to the role of entropic factors, clearly in competition with the purely energetic ones. For this reason, many approaches proposed rely on the consideration of free energy rather than potential energy surfaces.

Anyway, calculations are made easier if the dividing surface is planar; if q_F denotes the normal coordinate, in fact, the surface is defined by the equation $f(\mathbf{q}) = q_F^*$ and the choice $q_F^* = 0$ allows to reduce eq. (1.8) to the form

$$N_{TST}(E) = 2\pi\hbar(2\pi\hbar)^{-F} \int d\mathbf{p} \int d\mathbf{q}\, \delta\left[E - V(\mathbf{q}) - \frac{\mathbf{p^2}}{2m}\right] \delta q_F \frac{p_F}{m}\, \Theta(p_F) \tag{1.12}$$

and after performing the integrations with respect to p_F, q_F

$$N_{TST}(E) = (2\pi\hbar)^{-(F-1)} \int d\mathbf{p}' \int d\mathbf{q}'\, \Theta(E - H^{\neq}(\mathbf{p}', \mathbf{q}')) \tag{1.13}$$

Here $\mathbf{p}', \mathbf{q}'$ label coordinates and momenta relative to the motion on the $(F-1)$-dimensional dividing surface and

$$H^{\neq}(\mathbf{p}', \mathbf{q}') = \sum_{k=1}^{F-1} \frac{p_k^2}{2m} + V(\mathbf{q}', q_F = 0) \tag{1.14}$$

Eq.(1.13) states that the cumulative reaction probability (CRP) is the volume of the phase space of the activated complex with energy less or equal to E.
Finally,

$$k_{TST}(T)Q_r(T) = \frac{kT}{h}\, Q^{\neq}(T) \tag{1.15}$$

$$Q^{\neq}(T) = (2\pi\hbar)^{-(F-1)} \int d\mathbf{p}' \int d\mathbf{q}'\, e^{-\beta H^{\neq}(\mathbf{p}', \mathbf{q}')} \tag{1.16}$$

In the particular case of a one-dimensional barrier of height $V^{\neq}$,

$$k_{TST}Q_r = \frac{kT}{h} e^{-\beta V^{\neq}} \tag{1.17}$$

which for a free particle reduces to

$$k_{TST}^{f.p.} = \frac{kT}{h} \tag{1.18}$$

an exact result expected to be valid for both the classical and the quantum treatments.

TST is found to be an accurate approximation at sufficiently low energy [10, 36], i.e. a little above the potential energy barrier, while at higher energy it breaks down because of the great number of trajectories which recross back the dividing surface.

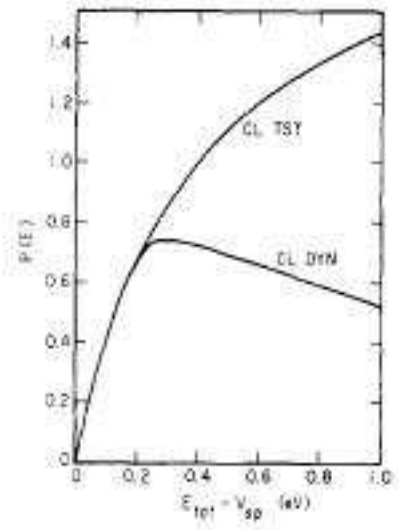

Figure 1.1: Comparison between *TST* and classical molecular dynamics

This point can be appreciated in fig.1.1, where the ratio between reactive and incident flux is plotted against energy for a collinear $H + H_2$ reaction, according to *TST* and classical molecular dynamics calculations carried out by Porter and Karplus many years ago [37].
So far, our considerations have been limited only to classical rate theory. An accurate estimation of the rate constant, however, must also take into account quantum effects like tunneling. A quantum mechanical formulation of the problem is possible; however, the fact that *TST* works better for multidimensional systems and at low energy (where quantum effects are more prominent), suggests that it would be extremely interesting to find out a quantum analogue of *TST*.

1.3 Quantum Transition State Theory

Chemical reactions can be treated rigorously from a quantum mechanical point of view in terms of a formulation based on the scattering S-matrix associated to the reaction.
The cumulative reaction probability can be shown to be expressible in the form

$$N(E) = \sum_{n_p} \sum_{n_r} \left| S_{n_p,n_r}(E) \right|^2 \tag{1.19}$$

The sums in eq.(1.19) run over the quantum numbers labeling the states of reactants and products, the square moduli of the S-matrix elements representing reaction probabilities for the $n_r \rightarrow n_p$ transitions (channels).
The knowledge of the S-matrix elements provides the most detailed information about the reaction, surely much more than necessary to evaluate an averaged quantity like the reaction rate constant. Besides, the solution of the reactive scattering problem is generally a difficult and computationally expensive task, so that the implementation of a more direct procedure would be desirable.

A first attack to the problem could be based on the direct quantization of the classical TST expression for $N(E)$ [38]. In this view, the phase-space integration in eq.(1.13) becomes a quantum mechanical trace, with the Hamiltonian operator $\hat{H}^{\neq}$ bounded on the dividing surface

$$N_{QTST}(E) = Tr\ \left[\Theta(E - \hat{H}^{\neq})\right] = \sum_n \Theta(E - E_n^{\neq}) \tag{1.20}$$

The expression for $k(T)$ which stems from eq.(1.20) is

$$k_{QTST}(T) Q_r(T) = \frac{kT}{h} Q^{\neq}(T) \tag{1.21}$$

Eqs.(1.20),(1.21) neglect the motion along the reaction coordinate and the associated tunneling effect. Eq.(1.20) can be improved by replacing the step function with a tunneling probability, which depends on the energy difference $E_F = E - E_n^{\neq}$

$$N_{QTST}(E) = \sum_n P_F(E - E_n^{\neq}) \tag{1.22}$$

Eq.(1.22) leads to

$$k_{QTST}(T) Q_r(T) = \kappa(T) \frac{kT}{h} Q^{\neq}(T) \tag{1.23}$$

where $\kappa(T)$ is the one-dimensional tunneling factor, defined by

$$\kappa(T) = \beta \int_{-\infty}^{+\infty} dE_F\, e^{-\beta E_F}\, P_F(E_F) \tag{1.24}$$

The fact that in eq.(1.23) the quantum tunneling appears as a multiplicative factor means that the reaction coordinate has been considered uncoupled to the other degrees of freedom. This is, of course, an oversimplification [12] and different multidimensional tunneling corrections have been suggested [39, 40, 41], in many cases with better results, even though these procedures still rest on approximations to the coupling between the reaction coordinate and the remaining degrees of freedom.

In 1974, Miller proposed a direct formula, later rearranged in terms of correlation functions [9], to tackle the problem [15]

$$k(T)Q_r(T) = \lim_{t\to\infty} Tr\left[e^{-\beta\hat{H}}\hat{F}\Theta(\hat{p}(t))\right] \tag{1.25}$$

In eq.(1.25) the rate constant is calculated as the long-time limit of a quantum mechanical trace. The operators involved are the statistical Boltzmann operator, a flux operator and a projection operator onto the product states. The role of these operators will be widely discussed in chapter 3. At the moment, it is interesting to notice that eq.(1.25) involves the quantum propagation of the momentum operator at long times. Needless to say that resorting to approximate treatments of dynamics is the rule in actual calculations.

The necessity of including quantum effects in the estimation of rate constants, along with the possibility of avoiding long-time simulations, makes the search for a quantum version of transition state theory a fundamental topic in reaction rate theory.

A central role in this search is held by the partitioning of dynamical from thermal effects. Ankerhold, Grossmann and Tannor [16] have investigated this aspect by means of a coherent-state approach. Coherent states constitute an overcomplete expansion basis set. The evaluation of the quantum mechanical trace present in Miller's formula in terms of such basis set leads to the following expression for the rate constant

$$k(T)Q_r(T) = Re\int \frac{dx_0\,dp_0}{2\pi\hbar}\int \frac{dp_0''}{2\pi\hbar}\langle x_0|e^{-\beta\hat{H}}|x_0''=0\rangle\frac{p_0''}{m}\langle\tilde{z}_{p_0'',x_0''=0};\alpha|\hat{P}|\tilde{z}_{p_0,x_0};\alpha\rangle \tag{1.26}$$

where $|\tilde{z};\alpha\rangle$ denote coherent states in the notation adopted by Caratzoulas and Pechukas [42]. Eq.(1.26) involves a position representation for the Boltzmann operator and the coherent-state representation for the projector operator which takes into account the dynamics.

The application of the formalism to two typical one-dimensional models, parabolic barrier and symmetrical Eckart barrier, along with a detailed analysis of the phase-space dynamics has led to ascertain the role of the two partitioned effects, quantifying their prominence in various temperature regimes. In particular, the long-time limit

for the parabolic barrier model leads to a very interesting result for the projection operator matrix element involved in eq.(1.26), that can be expressed as product of a coherent state overlap matrix element times a complex complementary error function

$$\langle \tilde{z}_{p_0'',x_0''=0};\alpha|\hat{P}|\tilde{z}_{p_0,x_0};\alpha\rangle = \langle \tilde{z}_{p_0'',x_0''=0};\alpha|\tilde{z}_{p_0,x_0};\alpha\rangle \xi(p_0'';p_0,x_0) \tag{1.27}$$

where

$$\xi(p_0'';p_0,x_0) = \frac{1}{\sqrt{\pi}} \int_{-\infty}^{u(p_0'';p_0,x_0)} dx\, e^{-x^2} \tag{1.28}$$

with u a complex function depending also on the barrier curvature (for more details see [16]). Our emphasis on this point, the occurrence of an error function as a consequence of an approximation based on the parabolic barrier, is related to the fact that the result is similar to our findings in the approach discussed in this thesis (see Chap. 3).

It has been argued that a rigorous quantum formulation of the transition state theory should share with its classical analogue some basic features [19]:

a) To be a first-principle theory;

b) Rate constant deducible directly from the thermal density matrix;

c) The theory overestimates the exactly measured rate constant;

d) The theory is variational and the result can be optimized by proper location of the dividing surface;

e) The QTST expression is the leading term in a possible expansion of the rate constant with respect to some suitable, small parameter.

In conclusion, there is not an unambiguous generalization of the transition state theory to the realm of quantum mechanics, but, instead, there exist a bunch of different approaches aimed at adding tunneling and interference effects onto a classical-born theory.

1.3.1 Long-Time Fictitious-Dynamics Quantum Transition State Theory (LTFDQTST)

The acronym adopted tries to capture the main characteristics of some QTST approaches where the true (real-time) dynamics is replaced by a fictitious one, exactly tractable, so as to suggest an easy guess for the required Long-Time quantum evolution. In this way, the estimation of the kinetic rate constant is essentially reduced to

a calculation involving the "exact" thermal density matrix and a (time-independent) matrix element associated with the asymptotic fictitious dynamics.

Voth, Chandler and Miller (VCM) [17] arrived at two different expressions for the rate constant which yield the same results, provided that exact calculations are performed for both thermal density matrix $\rho(x, x'; \beta)$ and dynamical factor $z(x, x'; \Delta t)$. In the first formula

$$k(T)Q_r(T) = \frac{2}{\hbar\beta} \int dx \int dx' \, \Theta_r(x)\Theta_p(x')\rho(x, x'; \beta)z(x, x'; \Delta t) \tag{1.29}$$

$\Theta_r(x)$ ($\Theta_p(x')$) represents the Heaviside function associated with the population operator of reactants (products), while

$$z(x, x'; \Delta t) = Im\langle x|\hat{\Theta}_r(\Delta t)|x'\rangle = -Im\langle x|\hat{\Theta}_p(\Delta t)|x'\rangle \tag{1.30}$$

is the dynamical factor.
The second formula is (x^* corresponds to the location of the dividing surface)

$$k(T)Q_r(T) = \frac{\hbar}{m} \int dx \frac{\partial\rho(x, x^*; \beta)}{\partial x^*} z(x^*, x; \Delta t) \tag{1.31}$$

VCM calculated the general matrix element of the real-time propagator (hence the z-factor) for a few models: free particle (exact), parabolic barrier (exact), general one-dimensional barrier (semiclassical limit).
For the free particle (f.p.) and parabolic barrier (p.b.) cases, the long-time limit of the respective z-factors

$$z_{f.p.}(x, x'; \infty) = \frac{1}{2\pi(x' - x)} \tag{1.32}$$

$$z_{p.b.}(x, x'; \infty) = \frac{1}{2\pi} \frac{1}{(x' - x)} \cos\left[\frac{m\omega_b}{2}(x^2 - x'^2)\right] \tag{1.33}$$

provides working approximations for the dynamical factor of Eqs. (1.29),(1.31). For a symmetrical Eckart barrier, for instance, results in appreciable agreement with the exact ones have been obtained. The same cannot be said in the case of asymmetric Eckart barriers, at low temperatures, where some unphysical findings emerged in their study.

Pollak and Liao (PL) [19] proposed a slightly different approach still derived from first principles, which adopts the long-time behavior of the parabolic-barrier system as approximate dynamics. For long times ($\omega^{\neq}$ is the curvature of the parabolic barrier which fits the actual barrier at the dividing surface)

$$\hat{x}_{p.b.}(t) \approx \frac{1}{2} e^{\omega^{\neq} t} \left[\hat{x} + \frac{\hat{p}}{m\omega^{\neq}}\right] \tag{1.34}$$

so that

$$\lim_{t\to\infty} e^{i\hat{H}_{pb}t/\hbar}\,\Theta(\hat{x})\,e^{-i\hat{H}_{pb}t/\hbar} = \Theta\left(\hat{x} + \frac{\hat{p}}{m\omega^{\neq}}\right) \tag{1.35}$$

For any one-dimensional Hamiltonian $\hat{H}$, it is possible to separate out a parabolic barrier component $\hat{H}_{p.b.}$, so that $\hat{H} = \hat{H}_{pb} + \hat{H}'$. In this way, the result in eq.(1.35) can be considered the leading-order term in the expansion of the time evolution of the Heaviside operator.
The formula for the rate constant becomes

$$k_{QTST}(T)Q_r(T) = Tr\left[\hat{F}(\beta, x^*)\Theta(\omega\hat{x} + \hat{p}/m)\right] \tag{1.36}$$

The next steps of the PL procedure involve the adoption, differently from VCM, of a symmetrized form of the thermal flux operator and the choice to represent the trace appearing in eq. (1.36) in the form (Wigner transform method)

$$Tr[\hat{A}\hat{B}] = 2\pi\hbar \int_{-\infty}^{+\infty} dp \int_{-\infty}^{+\infty} dx A_w(p,x)B_w(p,x) \tag{1.37}$$

Since the Wigner representation of the Heaviside operator is easily found, one arrives at the central result

$$k_{QTST}(T)Q_r(T) = \int_{-\infty}^{+\infty} dp \int_{-\infty}^{+\infty} dx\,\Theta(p + m\omega^{\neq}x)\rho_w\left[\hat{F}(\beta, x^*); p, x\right] \tag{1.38}$$

Through this formulation, PL have obtained good results for symmetrical and asymmetric Eckart barriers, even in those cases where VCM where only partially successful.

1.3.2 Short-time Quantum Transition State Theory (STQTST)

Short-time approaches, differently from the previous ones, do not discard the real-time propagation in the true potential. In this kind of approaches, some approximation on the dynamics is introduced and in this way the long-time limit, which would rigorously be required to attain the correct result for the rate constant, is actually reached after a short time.

Tromp and Miller proposed [20, 21] a new quantum transition state theory version, based on the reactive flux correlation function formalism suggested by Miller, Schwartz and Tromp [15]. The thermal rate constant for a bimolecular reaction can be expressed in the form

$$k(T)Q_r(T) = \int_0^{\infty} C_f(t)dt \tag{1.39}$$

where $C_f(t)$ is a flux-flux autocorrelation function. Fig.1.2 shows the behavior of

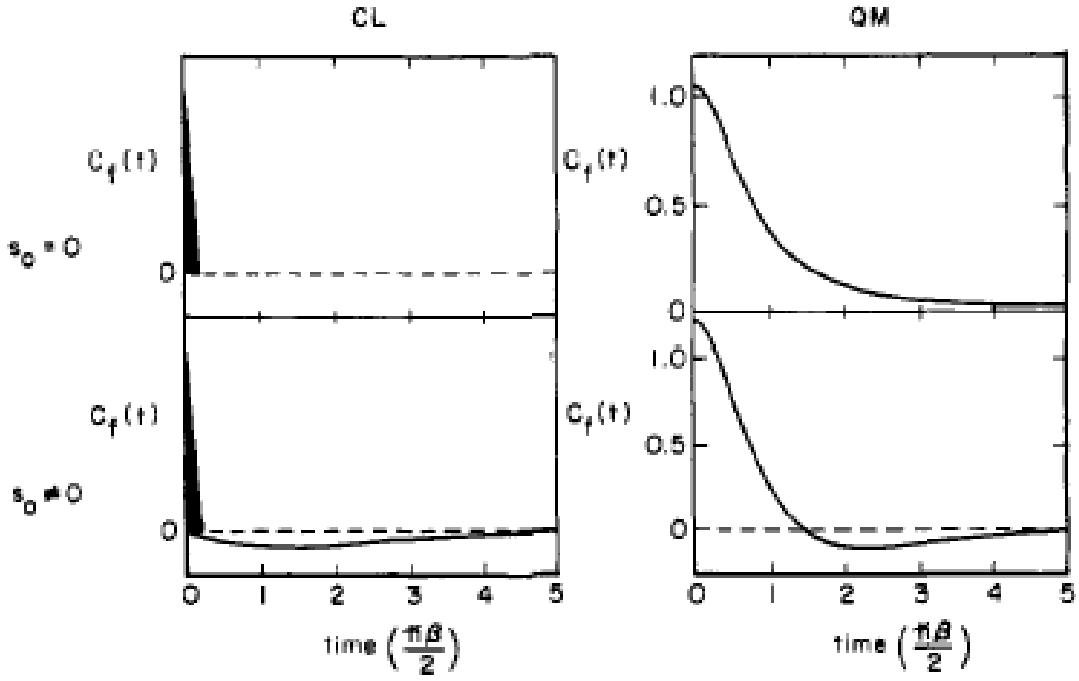

Figure 1.2: Classical (CL) and quantum mechanical (QM) flux-flux correlation functions are shown for the symmetrical Eckart barrier for the case that the dividing surface is chosen at the top of the barrier ($s_0 = 0$) or displaced from it ($s_0 \neq 0$). The shaded regions in the classical (CL) case simulates the Dirac delta function at $t = 0$.

the classical (on the left) and quantum (on the right) correlation function for a symmetrical one-dimensional Eckart barrier. The upper parts of the figures refer to a choice of the dividing surface located at the top of the barrier, while, in the lower parts, the dividing surface has been displaced. Incidentally, the quantum calculations were performed by adopting a finite-basis set approximation to the trace, in terms of standard harmonic oscillator eigenfunctions.

The main feature of the classical simulation is the presence of a Dirac delta-like behavior at time $t = 0$, with no recrossing flux if the dividing surface is chosen at the top of the barrier.
The classical rate constant can be evaluated from the flux-flux autocorrelation function according to

$$k_{TST}^{cl}(T)Q_r(T) = \lim_{\varepsilon \to 0} \int_0^{\varepsilon} dt C_f^{cl}(t) \tag{1.40}$$

It must be observed, however, that the expression provides the correct (classical) result only if the dividing surface is chosen properly, in a way that no recrossing flux takes place; otherwise, it overestimates the true rate constant. As a consequence, a

variational theory should be performed, to the aim of minimizing the rate constant by shifting the dividing surface.

The quantum results for the flux-flux autocorrelation function are characterized by a different behavior: the δ function at $t = 0$ is replaced by smoother curves, which drop to zero in a time of the order $\hbar\beta$. Even in this case, the results are affected by the choice of the position of the dividing surface; even though the time integral of the correlation function is invariant, in fact, the correlation function does not display negative contributions only if the dividing surface is chosen at the top of the barrier. The quantum transition state approach suggested by Tromp and Miller is based on the evaluation of the contribution arising from the first positive lobe of the quantum correlation function

$$k_{TST}^{qm} = \int_0^{t_0} dt C_f^{qm}(t) \tag{1.41}$$

where t_0 corresponds to the first zero of $C_f^{qm}(t)$. A number of methods have been explored to calculate the quantum correlation function at short times [43, 44] and eq.(1.41) provides an example of short-time quantum transition state theory.

Craig and Manolopoulos (CM), in a series of recent papers [22, 23, 24], have developed a procedure, known as Ring Polymer Molecular Dynamics (RPMD) approach, which arrives to a short-time quantum transition state theory, starting from the Kubo-transformed version of the reaction rate theory. The procedure is based on the recognized isomorphism between path integral representation of the quantum partition function and the classical partition function of a harmonic ring polymer [45, 46, 47]. Concisely, if $\hat{A}$ and $\hat{B}$ are two coordinate-dependent operators, their correlation function can be expressed as

$$\langle \hat{A}(0)\hat{B}(t)\rangle_n = \frac{1}{(2\pi\hbar)^n Z_n} \int d\mathbf{p}_0 \int d\mathbf{x}_0 \, e^{-\beta_n H_n(\mathbf{p}_0,\mathbf{x}_0)} A_n(\mathbf{x}_0) B_n(\mathbf{x}_t) \tag{1.42}$$

where n is the number of beads that constitute the harmonic ring, $\beta_n = \beta/n$ the scaled Boltzmann factor, while $H_n(\mathbf{p}, \mathbf{x})$ denotes the classical Hamiltonian of a harmonic ring polymer subjected to an external potential $V(x)$

$$H_n(\mathbf{p}, \mathbf{x}) = \sum_{i=1}^{n} \frac{p_i^2}{2m} + \frac{m}{2\beta_n^2\hbar^2} \sum_{i=1}^{n} (x_i - x_{i-1})^2 + \sum_{i=1}^{n} V(x_i) \tag{1.43}$$

$A_n(\mathbf{x}_0)$ and $B_n(\mathbf{x}_t)$ represent averages over the beads, respectively at two different times

$$A_n(\mathbf{x}_0) = \frac{1}{n} \sum_{i=1}^{n} A[\mathbf{x}_i(0)] \tag{1.44}$$

$$B_n(\mathbf{x}_t) = \frac{1}{n}\sum_{i=1}^{n} B[\mathbf{x}_i(t)] \tag{1.45}$$

The expression in Eq.(1.42) gives the correct result for the correlation function in the limit $n \to \infty$ if the external potential is harmonic. If both $\hat{A}$ and $\hat{B}$ are operators linearly coordinate dependent (i.e. the case of the position autocorrelation function), and the external potential is harmonic, the classical result ($n = 1$) is valid too. For the general case of an external potential $V(x)$ which is not harmonic, eq.(1.42) yields an approximation to the exact result.

As already mentioned, the starting point of the RPMD approach is the approximate Kubo-transformed side-side correlation function

$$\tilde{c}_{ss}(t) \approx \frac{1}{(2\pi\hbar)^n}\int d\mathbf{p}_0 \int d\mathbf{x}_0\, e^{-\beta_n H_n(\mathbf{p}_0,\mathbf{x}_0)}\Theta_n(\mathbf{x}_0)\Theta_n(\mathbf{x}_t) \tag{1.46}$$

which can be rearranged to the following flux-side correlation function

$$\tilde{c}_{fs}(t) \approx \frac{1}{(2\pi\hbar)^n}\int d\mathbf{p}_0 \int d\mathbf{x}_0\, e^{-\beta_n H_n(\mathbf{p}_0,\mathbf{x}_0)}\delta_1(\mathbf{x}_0)v_1(\mathbf{p}_0)\Theta_n(\mathbf{x}_t) \tag{1.47}$$

with $\delta_1(\mathbf{x}) = \delta(x_1 - x^*)$, $v_1(\mathbf{p}) = p_1/m$ and $\Theta_n(\mathbf{x}) = 1/n\sum_{i=1}^{n}\Theta(x_i - x^*)$.
Eq.(1.47) means that the first bead is initially ($t = 0$) in correspondence of the dividing surface and its initial velocity is correlated with the fraction of the ring polymer that lies on the product side at time t.

The strategy just described can be improved (i.e. it can be formulated in a manner which permits to reach more rapidly convergence to the long-time limit) by considering the dynamics of the ring-polymer centroids, the centroid of the ring-polymer coordinates being defined as

$$\bar{x} = \frac{1}{n}\sum_{i=1}^{n} x_i \tag{1.48}$$

Eq.(1.47) can be shown to be equivalently calculable as

$$\tilde{c}_{fs}(t) = \frac{1}{(2\pi\hbar)^n}\int d\mathbf{p}_0 \int d\mathbf{x}_0\, e^{-\beta_n H_n(\mathbf{p}_0,\mathbf{x}_0)}\delta(\bar{x}_0 - x^*)\frac{\bar{p}_0}{m}\Theta(\bar{x}_t - x^*) \tag{1.49}$$

a result very similar to the preceding one, provided the first bead is replaced by the centroid.
Eq.(1.49) appears preferable to eq.(1.47) due to the improved phase-space average and the faster convergence to the long-time limit. The phase-space average is better calculated by means of Monte Carlo methods in the centroid approach: most contributions, in fact, are positive, since it is not very probable (and of course less

probable than for the first bead in the first-bead approach) that a starting centroid, characterized by $\bar{p}_0 < 0$, is found on the product side at time t.
The fact that the long-time limit is soon achieved, makes the CM approach an example of short-time quantum transition state theory.

1.4 Main features of SCIVR

In the previous sections, we have tried to underline the limitations of a classical description of chemical kinetics, evidencing that intrinsically quantum mechanical effects, such as coherences, tunneling, selection rules have a role and cannot be ignored. At the same time, the quantum problem associated with chemically reactive events is recognized as one generally difficult to treat, mainly when a highly dimensional description is involved. In this view, all the quantum transition state approaches examined in precedence have been tested over low-dimensionality systems (usually one-dimensional barrier models).

The adoption of mixed quantum/classical approaches, where only a limited number of degrees of freedom are treated rigorously, i.e. assuming acceptable for all the remaining ones a classical description, is a possible way to face the problem.
A viable alternative is offered in principle by semiclassical approaches, employing Van Vleck's approximation for the matrix element (transition amplitude) of the real-time propagator in the coordinate representation [25]. The required evolution of classical trajectories leads unfortunately to deal with a non-linear boundary value problem, usually difficult to solve.

The SemiClassical Initial Value Representation (SCIVR) formalism [26, 27] is an approach where all the degrees of freedom (even electronically non-adiabatic) are treated on the same footing and nowadays constitutes possibly the leading strategy for studying complex reactions, even in condensed phase. It takes its origins from Van Vleck's approximation, so that in all respects we are confronting with a semiclassical theory. In its main lines, the approach starts from the standard Van Vleck's approximation for the general matrix element of the quantum propagator,

$$\langle 2|e^{-i\hat{H}t/\hbar}|1\rangle = \sum_{roots} \int\int dx_1 dx_2 \Psi_2^*(x_2)\Psi_1(x_1) \left[(2\pi i\hbar)^f \left|\frac{\partial x_2}{\partial p_1}\right|\right]^{-1/2} e^{\frac{i}{\hbar}S_t(x_2,x_1)-i\pi\nu(t)/2} \tag{1.50}$$

with

$$S_t(x_2,x_1) = \int_0^t dt' \left[p(t')\frac{dx(t')}{dt'} - H(p(t'),x(t'))\right] \tag{1.51}$$

the classical action (time integral of the Lagrangian) for trajectories starting from x_1 at $t'=0$ and ending at x_2 at time $t'=t$.

$$\left|\frac{\partial x_2}{\partial p_1}\right| = \left|\frac{\partial x_t(x_1,p_1)}{\partial p_1}\right| \tag{1.52}$$

is the Jacobian factor, while the phase factor (or Maslov index) $\nu(t)$ counts how many times the determinant $|\partial x_t/\partial p_1|$ vanishes in the time interval $[0,t]$, f being finally the

number of degrees of freedom of the system.
A straightforward application of the Van Vleck's approximation leads, as already mentioned above, to deal with a rather difficult non-linear numerical problem with given boundary value conditions. As a matter of fact, x_t is not necessarily a monotone function of p_1, with consequent occurrence of solutions to find out, because the problem solution requires that all the roots (trajectories) are calculated.

The novelty introduced by SCIVR is based on the recognition that classical trajectories are univocally determined by initial conditions rather than by multiple roots defined by boundary conditions. This feature allows the following replacement

$$\sum_{roots} \int dx_2 \rightarrow \int dp_1 \left| \frac{\partial x_t}{\partial p_1} \right| \tag{1.53}$$

so that eq.(1.50) transforms into

$$\langle 2|e^{-i\hat{H}t/\hbar}|1\rangle = \int dx_1 \int dp_1 \Psi_2^*(x_t)\Psi_1(x_1) \left[\frac{|\partial x_t/\partial p_1|}{(2\pi i\hbar)^f} \right]^{1/2} e^{\frac{i}{\hbar}[S_t(p_1,x_1) - i\pi\nu(t)/2]} \tag{1.54}$$

From a formal point of view, eqs.(1.50) and (1.54) are equivalent but the implementation of the latter introduces computational facilities, in addition to the advantageous replacement of the sum over different roots with a single integral mentioned before. Furthermore, the new Jacobian factor removes the singularities and keeps the integrand going to zero, preserving its continuity each time the Maslov index is null.

Among various virtues, SCIVR is able to provide an approximate description of dynamical tunneling, while maintaining the interference structure proper of semiclassical theories. Finally, SCIVR can be seen as a way to add quantum effects over purely classical simulations. The only problem affecting the approach seems to lie in the oscillatory nature of the integrand, even though some Monte Carlo techniques have been formulated to tackle this aspect [48, 49, 50, 51].

The SCIVR application to time correlation functions of the form

$$C_{AB}(t) = Tr[\hat{A}e^{it\hat{H}}\hat{B}e^{-it\hat{H}}]$$

leads to

$$C_{AB}(t) = (2\pi\hbar)^{-f} \int d\mathbf{p}_0 d\mathbf{x}_0 d\mathbf{p}_0' d\mathbf{x}_0' \, \langle \mathbf{x}_0|\hat{A}|\mathbf{x}_0'\rangle\langle \mathbf{x}_t'|\hat{B}|\mathbf{x}_t\rangle e^{i(S_t - S_t')/\hbar} \left| \frac{\partial \mathbf{x}_t}{\partial \mathbf{p}_0} \right|^{1/2} \left| \frac{\partial \mathbf{x}_t'}{\partial \mathbf{p}_0'} \right|^{1/2} \tag{1.55}$$

We are particularly interested to the reactive flux correlation function (its long-time limit is involved in the rate constant calculation), where

$$\hat{A} = e^{-\beta\hat{H}/2}\hat{F}e^{-\beta\hat{H}/2} \tag{1.56}$$

$$\hat{B} = \Theta(s(\hat{x})) \tag{1.57}$$

A way to deal with eq.(1.55) is by adopting the linearization approximation: the oscillatory integrand in the double phase-space integration is treated by assuming that the only important contribution comes from trajectories close to one another. This kind of approximation reduces SCIVR to the classical Wigner approximation [52]

$$C_{AB}(t) \approx (2\pi\hbar)^{-f} \int d\bar{\mathbf{p}}_0 \int d\bar{\mathbf{x}}_0 A_w(\bar{\mathbf{p}}_0, \bar{\mathbf{x}}_0) B_w(\bar{\mathbf{p}}_t, \bar{\mathbf{x}}_t) \tag{1.58}$$

where $\bar{\mathbf{p}}_0 = \frac{1}{2}(\bar{\mathbf{p}}_0 + \bar{\mathbf{p}}'_0)$ and $\bar{\mathbf{x}}_0 = \frac{1}{2}(\bar{\mathbf{x}}_0 + \bar{\mathbf{x}}'_0)$, while A_w and B_w are the Wigner functions associated to the operators $\hat{A}$ and $\hat{B}$ respectively. Various tests on several benchmark model problems confirm that the linear approximation describes the short-time quantum behavior well, so that it must rightfully be added to the number of quantum transition state theory.

Overcoming the linearized SCIVR approach without becoming involved in the double phase-space integrations (see (1.55)) has motivated the growth of other approaches (which will not be reviewed). Among them, we cite the forward-backward IVR, suggested by Thompson and Makri [53, 54] and developed by Miller.

Chapter 2

Quantum mechanical propagators in the case of simple Hamiltonian operators

A key role in modern quantum-mechanical theories devised to provide a rationale as well as viable computational routes for chemical kinetics investigations is played by the (quantum) propagator both at real time and at imaginary time.
The expansion of the imaginary-time propagator into a coordinate basis set ($\langle x|e^{-\beta\hat{H}}|x'\rangle$) yields a matrix representation of the Boltzmann operator $e^{-\beta\hat{H}}$ in the form of an integral characterized by a non-oscillatory integrand, that can be evaluated numerically by resorting to Monte Carlo techniques based on the Feynman path integration formalism [57].
On the contrary, the computation of the real-time propagator ($\langle x|e^{-i\hat{H}t}|x'\rangle$), a quantity seemingly similar to the preceding one, involves a much more difficult task, related to the oscillatory behavior of the integrand. Modified Monte Carlo procedures have been suggested and developed to attack this kind of integrals [48, 49, 58], even though it must be remarked the frequent recourse to appropriate approximations to the real-time dynamics so as to avoid the heavy difficulties of the direct calculation.

Real-time propagators can be analytically calculated in some particular cases and the result extended to the correspondent imaginary-time propagators by resorting to analytic continuation procedures, a standard technique often adopted in thermodynamic approaches to reaction rate theory (see, for instance, the Hansen-Andersen work [6, 7]).
Needless to say that real-time propagators can be obtained quite easily for a free particle (sec.(2.1)) and, at the cost of some efforts, for the harmonic oscillator potential (sec.(2.2), sec.(2.3)). An ordinary presentation is based on the calculation of the

Feynman propagator for a quadratic-Lagrangian system [60, 61]. At our craftsman level, we shall look at the problem of the harmonic oscillator according to Beauregard's theorem [59].
For simplicity, in the forthcoming formulae, the choice $\hbar = 1$ has been maintained.

2.1 Propagators for the free particle

The trivial case of a free particle is the first type of propagator to take into consideration. Of course, the free-particle system is not of great importance in the context of the reaction rate theory. Neverthless, the results relative to this system serve as a starting point for treating more complex cases and represent a basic tool in view of the algebraic techniques employed.

The Hamiltonian contains only the kinetic energy operator: $\hat{H} = \hat{p}^2/2m$, so that

$$K(x, x'; t) = \langle x|e^{-i\hat{H}t}|x'\rangle = \langle x|e^{-i\frac{\hat{p}^2}{2m}t}|x'\rangle \tag{2.1}$$

which is easily elaborated by switching from the position to the momentum representation

$$\begin{aligned} K(x, x'; t) &= \langle x|e^{-i\frac{\hat{p}^2}{2m}t}|x'\rangle = \\ &= \frac{1}{2\pi}\int_{-\infty}^{+\infty} dp\, e^{-ip(x'-x)}e^{-i\frac{p^2}{2m}t} \end{aligned} \tag{2.2}$$

By the following standard result

$$\int_{-\infty}^{+\infty} ds\, e^{-As^2+Bs} = \sqrt{\frac{\pi}{A}}\, e^{B^2/4A} \tag{2.3}$$

we get without effort

$$K_{f.p.}(x, x'; t) = \left(\frac{m}{2\pi i t}\right)^{1/2} e^{-\frac{m(x-x')^2}{2it}} \tag{2.4}$$

Analytic continuation allows one to find the expression of the free-particle thermal density matrix. In fact, analytic continuation in the complex field is obtained by means of the substitution $t \to -i\beta$, so that

$$\langle x|e^{-\beta\frac{p^2}{2m}}|x'\rangle = \rho_{f.p.}(x, x'; \beta) = \left(\frac{m}{2\pi\beta}\right)^{1/2} e^{-\frac{m(x-x')^2}{2\beta}} \tag{2.5}$$

In conclusion, the imaginary-time propagator for the free particle in the coordinate representation is a Gaussian function whose width depends on the temperature and the mass of the particle: the lower mass and temperature, the higher the spread of the density matrix element around the x' position at which it is centered. This result is also central in the evaluation of thermal density matrices by means of Feynman path integration.

2.2 The harmonic oscillator case

This calculation is a bit more complex and difficult than the previous one and requires some additional efforts.
The Hamiltonian for a particle under the influence of the harmonic potential can be expressed as follows

$$\hat{H}_{h.p.} = \frac{\hat{p}^2}{2m} + \frac{1}{2}m\omega^2\hat{x}^2 \tag{2.6}$$

where ω is the frequency of the harmonic oscillator.

The searched solution for the propagator is attained by reduction of the problem to that of a free particle, invoking the following theorem due to Beauregard:

Theorem. *Let $\hat{P}$ and $\hat{Q}$ be two linear operators obeying the following commutation relations*

$$\begin{cases} [[\hat{Q},\hat{P}],\hat{P}] = 2\hat{P} \\ [[\hat{P},\hat{Q}],\hat{Q}] = 2\hat{Q} \end{cases} \tag{2.7}$$

Let λ be a dimensionless parameter. Then[59, 62]

$$e^{2\lambda(\hat{P}+\hat{Q})} = \exp\{\hat{Q}\tan(\lambda)\}\exp\{\hat{P}\sin(2\lambda)\}\exp\{\hat{Q}\tan(\lambda)\} \tag{2.8}$$

Beauregard's theorem was first stated (without demonstration) by Fujiwara. It provides a way to factorize the exponential of a sum of non-commuting operators defined by the commutation relations in Eqs. (2.7).

Defining the operators $\hat{P}$, $\hat{Q}$ and the parameter λ as follows (it is easy to demonstrate that they satisfy the conditions in Eqs.(2.7))

$$\begin{cases} \hat{P} = -\dfrac{i}{2m\omega}\hat{p}^2 \\ \hat{Q} = \dfrac{m\omega}{2i}\hat{x}^2 \\ 2\lambda = \omega t \end{cases} \tag{2.9}$$

the real-time propagator can be expressed as follows

$$K_{h.p.}(x,x';t) = \langle x|e^{-i\hat{H}t}|x'\rangle = \langle x|e^{\hat{Q}\tan(\lambda)}e^{\hat{P}\sin(2\lambda)}e^{\hat{Q}\tan(\lambda)}|x'\rangle \tag{2.10}$$

and therefore

$$K_{h.p.}(x,x';t) = A\langle x|e^{\hat{P}\sin(2\lambda)}|x'\rangle, \qquad A = e^{\frac{m\omega}{2i}(x^2+x'^2)\tan(\omega t/2)} \tag{2.11}$$

The matrix element is easily evaluated in the momentum representation,

$$K_{h.p.}(x,x';t) = A\left(\frac{m\omega}{2\pi i\sin(\omega t)}\right)^{1/2} e^{-\frac{m\omega(x-x')^2}{2i\sin(\omega t)}} \tag{2.12}$$

Easy manipulations of eq.(2.12), based on simple trigonometry, lead to the well known formula of the propagator for the harmonic oscillator in its usual form

$$\langle x|e^{-i\hat{H}t}|x'\rangle = \left(\frac{m\omega}{2\pi i\sin(\omega t)}\right)^{1/2}\exp\left\{\frac{im\omega}{2\sin(\omega t)}\left[(x^2+x'^2)\cos(\omega t)-2xx'\right]\right\} \tag{2.13}$$

Actually, eq.(2.13) is not completely correct, since a double-valued analytic continuation has been adopted while extending the validity of the result of the basic Gaussian integral of eq.(2.3) to the corresponding one with imaginary parameters ($\int_{-\infty}^{\infty} e^{-i\alpha x^2}dx = \sqrt{i\pi/\alpha}$ [61]). The consequence is that a phase ambiguity arises at caustic points (values of $t = n\pi/\omega$, n integer). Once removed this ambiguity by exploiting the group property of the propagators and translational invariance in time [60], the final result is the following Feynman-Soriau formula

$$K_{h.p.}(x,x';t) =$$
$$e^{-i\frac{\pi}{2}(\frac{1}{2}+Ent[\frac{\omega t}{\pi}])}\left(\frac{m\omega}{2\pi|\sin(\omega t)|}\right)^{1/2}\exp\left\{\frac{im\omega}{2\sin(\omega t)}\left[(x^2+x'^2)\cos(\omega t)-2xx'\right]\right\} \tag{2.14}$$

where $Ent[\xi]$ denotes the entire part of ξ.
From the relations

$$\begin{cases}\sin(i\alpha) = i\sinh(\alpha)\\ \cos(i\alpha) = \cosh(\alpha)\end{cases} \tag{2.15}$$

and by analytic continuation of eq.(2.13) ($t \to -i\beta$), a straightforward procedure similar to that adopted for the free particle, leads to the thermal density matrix (imaginary time propagator),

$$\rho_{h.p.}(x,x';\beta) \equiv \langle x|e^{-\beta\hat{H}}|x'\rangle$$
$$= \left(\frac{m\omega}{2\pi\sinh(\beta\omega)}\right)^{1/2}\exp\left\{-\frac{m\omega}{2}\left[(x^2+x'^2)\coth(\beta\omega)-\frac{2xx'}{\sinh(\beta\omega)}\right]\right\} \tag{2.16}$$

This result will serve as a test for checking the reliability of the Path Integral Monte Carlo (PIMC) algorithm described in one of the following chapters (sec.(4.2)). It must be noticed that Eq.(2.16) is not normalized, $\int \rho_{h.p.}(x,x;\beta)dx \neq 1$, so that it does not represent a proper density matrix. The space integral of $\rho_{h.p.}$ in Eq.(2.16) (with $x' = x$), i.e. the trace of the operator $e^{-\beta\hat{H}}$ is the quantum partition function for the harmonic oscillator.

2.3 Real-time propagator for the complete oscillator potential

Another potential, for which a direct analytic treatment is possible, is represented by the complete oscillator potential, i.e. of the form $V(x) = a + bx + cx^2$, a complete second order polynomial.
The complete oscillator Hamiltonian is therefore

$$\hat{H}_x = \frac{\hat{p}^2}{2m} + \frac{1}{2}m\omega^2\hat{x}^2 + v_1\hat{x} + V_0 \tag{2.17}$$

To proceed, it is convenient to define the following translated position operator

$$\hat{y} = \hat{x} + \frac{v_1}{m\omega^2} \tag{2.18}$$

which allows to transform $\hat{H}_x$ into

$$\hat{H}_y = \frac{\hat{p}^2}{2m} + \frac{1}{2}m\omega^2\hat{y}^2 - \frac{v_1^2}{2m\omega^2} + V_0 \tag{2.19}$$

apart an additive constant, the Hamiltonian operator of a simple harmonic oscillator. The generic matrix element of the propagator is therefore

$$K(y, y'; t) = \langle y|e^{-i\hat{H}_y t}|y'\rangle \tag{2.20}$$

Taking into account the result of eq.(2.13), after the introduction of the auxiliary parameters $F = \left(\frac{m\omega}{2\pi i \sin(\omega t)}\right)^{1/2}$ and $F' = F\, e^{-iV_0 t}\, e^{iv_1^2 t/(2m\omega^2)}$, it is possible to go back to the $x-$representation

$$\begin{aligned}\langle x|e^{-it\hat{H}_x}|x'\rangle &= F' \exp\left\{\frac{im\omega}{2\sin(\omega t)}\left[\left((x+\frac{v_1}{m\omega^2})^2 + (x'+\frac{v_1}{m\omega^2})^2\right)\cos(\omega t) - 2(x+\frac{v_1}{m\omega^2})(x'+\frac{v_1}{m\omega^2})\right]\right\} \\ &= F' \exp\left\{\frac{im\omega}{2\sin(\omega t)}\left[\left(x^2 + x'^2 + \frac{2v_1^2}{(m\omega^2)^2} + \frac{2v_1}{m\omega^2}(x+x')\right)\cos(\omega t)\ + \right.\right. \\ &\qquad \left.\left. -2\left(xx' + \frac{v_1^2}{(m\omega^2)^2} + \frac{v_1}{m\omega^2}(x+x')\right)\right]\right\}\end{aligned} \tag{2.21}$$

Eq.(2.21) can be conveniently elaborated on the basis of the following simplifications involving different powers of the parameter v_1:

$$\begin{aligned}(v_1^2): \qquad & \exp\left\{\frac{im\omega}{2\sin(\omega t)}\left[\frac{2v_1^2}{(m\omega^2)^2}\cos(\omega t) - \frac{2v_1^2}{(m\omega^2)^2}\right]\right\} = \\ = \ & \exp\left\{\frac{iv_1^2 t}{m\omega^2}\frac{1}{\omega t}\left(\frac{1}{\tan(\omega t)} - \frac{1}{\sin(\omega t)}\right)\right\} = \\ = \ & \exp\left\{-\frac{iv_1^2 t}{m\omega^2}\frac{\tan(\omega t/2)}{\omega t}\right\}\end{aligned} \tag{2.22}$$

$$
\begin{aligned}
(v_1): \qquad & \exp\left\{\frac{im\omega}{2\sin(\omega t)}\left[\frac{2v_1}{m\omega^2}(x+x')\cos(\omega t)-\frac{2v_1}{m\omega^2}(x+x')\right]\right\}= \\
&= \exp\left\{\frac{iv_1(x+x')}{\omega}\left(\frac{1}{\tan(\omega t)}-\frac{1}{\sin(\omega t)}\right)\right\}= \\
&= \exp\left\{-iv_1(x+x')\frac{\tan(\omega t/2)}{\omega}\right\}
\end{aligned}
\tag{2.23}
$$

The terms independent of v_1, are expected to give rise to the same result found for the harmonic oscillator (Eq.(2.13)). A few manipulations along the lines of the above procedure lead to:

$$
\begin{aligned}
(v_1^0): \quad & F\exp\left\{\frac{im\omega}{2\sin(\omega t)}\left[(x^2+x'^2)\cos(\omega t)-2xx'\right]\right\}= \\
&= F\exp\left\{\frac{im\omega}{2\sin(\omega t)}\left[\left(\frac{(x+x')^2+(x-x')^2}{2}\right)\cos(\omega t)-\frac{(x+x')^2-(x-x')^2}{2}\right]\right\} \\
&= F\exp\left\{\frac{im\omega}{4\sin(\omega t)}\left[-(x+x')^2\tan(\omega t/2)+\frac{(x-x')^2}{\tan(\omega t/2)}\right]\right\}
\end{aligned}
\tag{2.24}
$$

Consequently, the real-time propagator for the complete oscillator potential, is

$$
\begin{aligned}
&\langle x|e^{-it\hat{H}_x}|x'\rangle = F\,e^{-iV_0t}\exp\left\{\frac{iv_1^2t}{2m\omega^2}\left(1-\frac{2\tan(\omega t/2)}{\omega t}\right)\right\}\times \\
&\exp\left\{i\left[\frac{m\omega}{4}\left(\frac{(x-x')^2}{\tan(\omega t/2)}-(x+x')^2\tan(\omega t/2)\right)-\frac{v_1}{\omega}(x+x')\tan(\omega t/2)\right]\right\}
\end{aligned}
\tag{2.25}
$$

Another kind of potential for which it is not complicated to get an expression for the propagator is the linear potential. The solution can be found, for instance, in [61]. Since the main interest for the purposes of this thesis is addressed to parabolic barriers, the case of a particle moving in an uniform force field will be omitted from our considerations.

2.4 Thermal density matrices for parabolic barriers

The harmonic potentials treated in precedence are not ideally suitable to describe a barrier involved in a reactive process, mainly because of their unbound shape over the whole space (in particular, their pathological behavior as $x \pm \infty$). In spite of their inadequacy, they are useful as a starting point to test the efficience of any strategy adopted to tackle the dynamical problem. The physical reason making this potential eligible as the main approximation in the study of a realistic kinetics is to be searched

in the fact that some features of the "true" barrier potentials are captured by simpler model potentials like the inverted harmonic one. Our present interest is addressed to the computation of the (unnormalized) thermal density matrix, in particular the matrix element $\langle x|e^{-\beta\hat{H}}|x'=0\rangle_{p.b.}$, for the case of a parabolic barrier, which plays a fundamental role in the following.
The procedure employed to get the searched results is, once again, the analytic continuation of eqs. (2.13) and (2.25) by the replacement

$$\omega \rightarrow i\omega \tag{2.26}$$

In fact, under such transformation, the Hamiltonian (2.6) (and in a similar way that for the complete oscillator potential) becomes the correct Hamiltonian for the parabolic barrier

$$\hat{H}_{p.b.} = \frac{\hat{p}^2}{2m} - \frac{1}{2}m\omega^2 x^2 \qquad \omega \in \Re \tag{2.27}$$

Some algebra and use of the trigonometric relations of eqs.(2.15) lead to

$$\langle x|e^{-\beta\hat{H}}|x'\rangle_{p.b.} = \left(\frac{m\omega}{2\pi\sin(\beta\omega)}\right)^{1/2} \exp\left\{-\frac{m\omega}{2}\left[(x^2+x'^2)\cot(\beta\omega) - \frac{2xx'}{\sin(\beta\omega)}\right]\right\} \tag{2.28}$$

$$\langle x|e^{-\beta\hat{H}}|0\rangle_{p.b.} = \left(\frac{m\omega}{2\pi\sin(\beta\omega)}\right)^{1/2} \exp\left\{-\frac{m\omega}{2}x^2\cot(\beta\omega)\right\} \tag{2.29}$$

A double analytic continuation procedure (in time and frequency) $\omega t \rightarrow \beta\omega$ of eq.(2.25) leads to the thermal density matrix elements for the complete parabolic barrier (*c.p.b.*)

$$\begin{aligned}\langle x|e^{-\beta\hat{H}}|x'\rangle_{c.p.b.} = &\left(\frac{m\omega}{2\pi\sin(\beta\omega)}\right)^{1/2} e^{-\beta V_0} \exp\left\{-\frac{\beta v_1^2}{2m\omega^2}\left[\frac{2\tan(\beta\omega/2)}{\beta\omega} - 1\right]\right\} \times \\ &\exp\left\{-\left[\frac{m\omega}{4}\left(\frac{(x-x')^2}{\tan(\beta\omega/2)} - (x+x')^2\tan(\beta\omega/2)\right) + \frac{v_1}{\omega}(x+x')\tan(\beta\omega/2)\right]\right\}\end{aligned} \tag{2.30}$$

$$\begin{aligned}\langle x|e^{-\beta\hat{H}}|0\rangle_{c.p.b.} = &\left(\frac{m\omega}{2\pi\sin(\beta\omega)}\right)^{1/2} e^{-\beta V_0} \exp\left\{-\frac{\beta v_1^2}{2m\omega^2}\left[\frac{2\tan(\beta\omega/2)}{\beta\omega} - 1\right]\right\} \times \\ &\exp\left\{-\left[\frac{m\omega x^2}{2}\cot(\beta\omega) + \frac{v_1 x}{\omega}\tan(\beta\omega/2)\right]\right\}\end{aligned} \tag{2.31}$$

Inspection of eqs.(2.28)-(2.31) highlights an unexpected behavior for $\beta\omega > \pi$, because the thermal density matrix elements give up being real. The problem is that the analytic continuation $\omega \rightarrow i\omega$ in certain situations can produce paradoxical consequences, and so it can be accepted only under strict conditions [65]. The mechanically unstable system involving a parabolic barrier, in fact, gives rise to an unacceptable (statistical) thermodynamics and the Boltzmann operator matrix elements exist only for $\beta\omega < \pi$ [17]. The temperature at which $\beta\omega = \pi$ is called the critical temperature.

Chapter 3

A dynamical approach to the calculation of thermal reaction rates

In the preliminary chapter addressed to introduce the reaction rate theory, the problem of the resolution of a (complex) scattering problem was reformulated by means of a time-dependent correlation function formalism introduced by Miller et al., whose long-time limit approaches the thermal (i.e. with reactants in Boltzmann equilibrium) rate constant (T is the absolute temperature)

$$k(t;T)Q_r(T) = Re\left\{Tr\left[e^{-\beta\hat{H}}\hat{F}\hat{P}(t)\right]\right\}, \quad k(T) = \lim_{t\to\infty} k(t;T) \tag{3.1}$$

The above expression implies the resolution of the quantum dynamical problem at long times, a goal usually difficult to reach, due to its complexity and, in any case, of high computational cost.

The purpose of this chapter is to suggest a dynamical approach, developed for one-dimensional systems, based on the expansion of eq.(3.1) in the ordinary position representation, which leads to a separation between thermal and dynamical effects. The procedure does not take origin from semiclassical approximations to the quantum mechanical propagators (like, for instance, SC-IVR, which moves from the known Van Vleck's approximation [25]); instead, it adopts a completely rigorous quantum mechanical treatment, joined with a parabolic-barrier approximation. Classical trajectories evolved for a rather short time then enable to approximate reasonably the dynamical factor and to arrive, finally, to the rate constant.

In eq. (3.1) $Q_r(T)$ represents the partition function for reactants (per unit of volume), while from now on, for simplicity, the explicit temperature dependence will

be omitted; $\hat{F}$ is the flux operator through a potential energy surface (in our one-dimensional system actually reduced to the point $x = 0$), which separates reactive species from products. The flux operator is chosen to be

$$\hat{F} = \frac{1}{m}\delta(\hat{x})\hat{p} \tag{3.2}$$

with $\hat{p}$ momentum operator. Besides,

$$\hat{P}(t) = e^{it\hat{H}}\Theta(\hat{p})\, e^{-it\hat{H}} \tag{3.3}$$

is the projection operator onto the product states, explicitly expressed in terms of the time evolution of the Heaviside operator $\Theta(\hat{p})$ (notice that the usual choice $\hbar = 1$ has been done).

Eq.(3.3) corresponds to identify the reaction products by means of the sign of the momentum, in agreement with the basic work by Miller, Schwartz and Tromp [15]. The procedure, fully correct for gas-phase reactions, breaks down in the case of condensed phases, due to cage effects which modify the dynamics, in the sense that products are not necessarily characterized by a definite-sign momentum [55]. The extension to kinetics under such conditions can be attained by replacing $\Theta(\hat{p})$ with $\Theta(\hat{x}-\bar{x})$ ($\bar{x}$ being the location of the dividing surface), the transformation being valid for bimolecular collisions in the long-time limit.
In our approach, the basic starting point is eq. (3.3), which will now be elaborated in a proper way.

3.1 First quantum mechanical steps

The trace operation in eq. (3.1) can be carried out in terms of the complete set of position eigenstates $|x\rangle$, so that

$$\begin{aligned} k(t)Q_r &= Re \int_{-\infty}^{+\infty} dx \ < x|e^{-\beta\hat{H}}\hat{F}\hat{P}(t)|x > \\ &= Re \int_{-\infty}^{+\infty} dx \int_{-\infty}^{+\infty} dx' < x|e^{-\beta\hat{H}}|x' >< x'|\hat{F}\hat{P}(t)|x > \end{aligned} \tag{3.4}$$

The matrix element involving the quantal flux $\hat{F}$ defined in precedence is readily evaluated,

$$\begin{aligned} < x'|\hat{F}\hat{P}(t)|x > &= \frac{1}{m} < x'|\delta(\hat{x})\hat{p}\hat{P}(t)|x > \\ &= \frac{\delta(x')}{m} < x'|\hat{p}\hat{P}(t)|x > \end{aligned} \tag{3.5}$$

The form of the operator $\hat{P}(t)$ suggests the introduction of a complet set of momentum eigenstates $\{|p\rangle\}$

$$< x'|\hat{F}\hat{P}(t)|x >= \frac{1}{\sqrt{2\pi}m} \int_{-\infty}^{+\infty} dp \, p < p|\hat{P}(t)|x > \ \delta(x') \, e^{ipx'} \tag{3.6}$$

After integrating with respect to x', we get a first fundamental result, characterized by the separation of the thermal factor from the dynamical one, a feature that appears both gratifying and computationally useful

$$k(t)Q_r = \frac{1}{\sqrt{2\pi}m} Re \int_{-\infty}^{+\infty} dx < x|e^{-\beta\hat{H}}|x = 0 > \int_{-\infty}^{+\infty} dp \, p < p|\hat{P}(t)|x > \tag{3.7}$$

The Boltzmann average involves off-diagonal elements of the thermal density matrix centered around $x = 0$, $\rho(x; 0; \beta) \equiv < x|e^{-\beta\hat{H}}|x = 0 >$, or, more generally, centered around the location of the dividing point (surface).
The dynamical matrix element can be developed efficiently by resorting to the integral representation of the Heaviside operator

$$\Theta(\hat{p}) = \frac{i}{2\pi} \lim_{\varepsilon \to 0} \int_{-\infty}^{+\infty} d\xi \frac{e^{-i\xi\hat{p}}}{\xi + i\varepsilon} \tag{3.8}$$

From

$$\lim_{\varepsilon \to 0} (\xi + i\varepsilon)^{-1} = p.p. \, [1/\xi] - i\pi\delta(\xi) \tag{3.9}$$

it follows

$$\Theta(\hat{p}) = \frac{1}{2} + \frac{i}{2\pi} \fint_{-\infty}^{+\infty} \frac{d\xi}{\xi}\, e^{-i\xi\hat{p}} \tag{3.10}$$

where $\fint$ stands for the principal value of the integral.
Therefore $\hat{P}(t)$ can be expressed in the form

$$\hat{P}(t) = \frac{1}{2} + \frac{i}{2\pi} \fint_{-\infty}^{+\infty} \frac{d\xi}{\xi} e^{-i\xi\hat{p}(t)}, \quad \text{where} \quad \hat{p}(t) = e^{i\hat{H}t}\hat{p}e^{-i\hat{H}t} \tag{3.11}$$

The calculation of the rate constant involves therefore two contributions,

$$\begin{aligned} k(t)Q_r = {} & \frac{1}{\sqrt{2\pi}m} Re \int_{-\infty}^{+\infty} dx < x|e^{-\beta\hat{H}}|x = 0 > \frac{1}{2}\int_{-\infty}^{+\infty} dp\, p < p|x > + \\ & + \frac{1}{\sqrt{2\pi}m} Re \int_{-\infty}^{+\infty} dx < x|e^{-\beta\hat{H}}|x = 0 > \frac{i}{2\pi} \fint_{-\infty}^{+\infty} \frac{d\xi}{\xi} \int_{-\infty}^{+\infty} dp\, p < p|e^{-i\xi\hat{p}(t)}|x > \end{aligned} \tag{3.12}$$

It is easy to verify that

$$\frac{1}{2}\int_{-\infty}^{+\infty} dp\, p < p|x >= \frac{\sqrt{2\pi}}{2} i \frac{\partial}{\partial x}\, \delta(x) \tag{3.13}$$

so that the first of the two terms of eq.(3.12) is purely immaginary and cannot contribute to the final real value.
Thus,

$$k(t)Q_r = \frac{1}{2\pi m\sqrt{2\pi}}\, Re \int_{-\infty}^{+\infty} dx < x|e^{-\beta\hat{H}}|x = 0 > \fint_{-\infty}^{+\infty} \frac{d\xi}{\xi}\, i \int_{-\infty}^{+\infty} dp\, p < p|e^{-i\xi\hat{p}(t)}|x > \tag{3.14}$$

Equation (3.14) is an important intermediate result of our approach. It will be further elaborated and characterized by investigating a few simple models of potential barriers.

3.2 The ininfluent dynamics limit ($t = 0$)

The evaluation of eq. (3.14) in the particular and extreme case $t = 0$ corresponds to ignore the fundamental role of dynamics of the system under investigation. Nevertheless, it can be considered an interesting calculation, since it can be related to the classical transition state theory assumption (instantaneous, i.e. time independent, reactive flux through the dividing surface). Under this condition,

$$\langle p|e^{-i\xi\hat{p}(0)}|x\rangle = \langle p|e^{-i\xi\hat{p}}|x\rangle = \frac{1}{\sqrt{2\pi}}e^{-ip(x+\xi)} \tag{3.15}$$

so that eq. (3.14) transforms into

$$k(0)Q_r = \frac{1}{(2\pi)^2 m} Re\left\{ i\int_{-\infty}^{+\infty} dx \langle x|e^{-\beta\hat{H}}|x=0\rangle \fint_{-\infty}^{+\infty} \frac{d\xi}{\xi} \int_{-\infty}^{+\infty} dp\, p\, e^{-ip(x+\xi)} \right\} \tag{3.16}$$

Introducing a partial differentiation with respect to x to treat the p-integral

$$k(0)Q_r = \frac{1}{(2\pi)^2 m} Re\left\{ i\int_{-\infty}^{+\infty} dx \langle x|e^{-\beta\hat{H}}|x=0\rangle \fint_{-\infty}^{+\infty} \frac{d\xi}{\xi} \left(i\frac{\partial}{\partial x} \int_{-\infty}^{+\infty} dp\, e^{-ip(x+\xi)} \right) \right\} \tag{3.17}$$

After exchanging properly the order of the integrations,

$$k(0)Q_r = -\frac{1}{2\pi m} Re\left\{ \fint_{-\infty}^{+\infty} \frac{d\xi}{\xi} \int_{-\infty}^{+\infty} dx \langle x|e^{-\beta\hat{H}}|x=0\rangle \frac{\partial}{\partial x}\delta(x+\xi) \right\} \tag{3.18}$$

an integration by parts on the x variable leads to the result

$$k(0)Q_r = \frac{1}{2\pi m} Re\left\{ \fint_{-\infty}^{+\infty} \frac{d\xi}{\xi} \frac{\partial}{\partial x} \langle x|e^{-\beta\hat{H}}|x=0\rangle \Big|_{x=-\xi} \right\} \tag{3.19}$$

As one could expect, ignoring the dynamics of the system transforms the problem in a purely thermodynamic one: the knowledge of the thermal density matrix elements is sufficient to get the value of the rate constant.

A trivial case, obviously unfit to depict realistic barriers, is that of the free particle, for which it is easy to find the requested matrix elements. From standard results for Gaussian integrals[1],

$$\begin{aligned} < x|e^{-\beta\hat{H}}|x=0 > &= \int_{-\infty}^{+\infty} dp < x|p >< p|e^{-\beta\hat{p}^2/2m}|x=0 > \\ &= \frac{1}{2\pi}\int_{-\infty}^{+\infty} dp\, e^{ipx}\, e^{-\beta p^2/2m} \\ &= \left(\frac{m}{2\pi\beta}\right)^{1/2} e^{-mx^2/2\beta} \end{aligned} \tag{3.20}$$

[1] $\int_{-\infty}^{+\infty} dx e^{-Ax^2+Bx} = \sqrt{\pi/A}\, e^{B^2/4A}$

Use of this result in eq.(3.19) leads to the ξ cancellation at the denominator and to the final result for the free particle,

$$k(0)Q_r = k_{f.p.}\, Q_r = \frac{1}{2\pi\beta} \tag{3.21}$$

In a more general frame (i.e. independently of the choice of the adopted units) eq.(3.21) can be written as $kQ_r = k_B T/h$, with k_B the Boltzmann constant, and h the Planck constant.
It is interesting to remark that for the free particle (but for it only) eq.(3.21) is valid at any time, since $\hat{p}(t) = \hat{p}(0) = \hat{p}$. As already remarked, eq.(3.21) is also the expression that would have been obtained in the realm of classical transition state theory.

An important delucidation, that is worth investigating at this point, is about the influence of the choice of the position of the dividing surface. We shall examine the problem in the present context, i.e. in the ininfluent-dynamics limit, but the results could be readily generalized to the general case of influent dynamics.
Shifting the location of the dividing surface from $x = 0$ to $x = x^*$ is seen immediately to imply the following changes in the flux operator and in the thermal matrix element

1.
$$\hat{F} = \frac{\delta(\hat{x} - x^*)}{m}\hat{p} \tag{3.22}$$

2.
$$\langle x|e^{-\beta\hat{H}}|x = 0\rangle \rightarrow e^{ipx^*}\langle x|e^{-\beta\hat{H}}|x^*\rangle \tag{3.23}$$

By inserting these changes in due places, it is readily verified that

$$\begin{aligned} k(0)Q_r &= -\frac{1}{2\pi m} Re \left\{ \oint_{-\infty}^{+\infty} \frac{d\xi}{\xi} \int_{-\infty}^{+\infty} dx \frac{d}{dx} \left(\langle x|e^{-\beta\hat{H}}|x^*\rangle \right) \delta\left[x - (x^* + \xi)\right] \right\} \\ &= -\frac{1}{2\pi m} Re \left\{ \oint_{-\infty}^{+\infty} \frac{d\xi}{\xi} \frac{d}{dx} \left(\langle x|e^{-\beta\hat{H}}|x^*\rangle \right)_{x=x^*+\xi} \right\} \end{aligned} \tag{3.24}$$

The exact result cannot be influenced by the location of the dividing surface, even though a crafty choice can simplify the problem by making calculations easier. A simple test can be performed by applying eq.(3.24) to the free-particle case:

$$\begin{aligned} k(0)Q_r &= -\frac{1}{2\pi m} Re \left\{ \oint_{-\infty}^{+\infty} \frac{d\xi}{\xi} \left[\frac{d}{dx} \left(\left(\frac{m}{2\pi\beta} \right)^{1/2} e^{-\frac{m(x-x^*)}{2\beta}} \right) \right]_{x=x^*+\xi} \right\} \\ &= \frac{1}{2\pi\beta} \left(\frac{m}{2\pi\beta} \right)^{1/2} \int_{-\infty}^{\infty} d\xi\, e^{-\frac{m\xi^2}{2\beta}} \end{aligned} \tag{3.25}$$

and, finally,

$$k(0)Q_r = \frac{1}{2\pi\beta} \tag{3.26}$$

3.3 Reaction rate constants for parabolic barrier models

The discussion of the simple parabolic barrier is important because it permits to go deeper into the nature of the general reactive problem, suggesting, together with the complete parabolic barrier case, some of the techniques and numerical strategies adopted in the present work. It provides also the main approximations used to mimic the crossing of more complicated and realistic barriers, especially in the high-temperature regime, as the majority of the contributions to the rate constant comes from states with energy close to the top of the barrier [55].

3.3.1 The simple parabolic barrier

The Hamiltonian operator for the simple parabolic barrier is

$$\hat{H} = \frac{\hat{p}^2}{2m} - \frac{1}{2}m\omega^2\hat{x}^2 \qquad \omega \in \Re \tag{3.27}$$

The thermal density matrix elements, obtained by analytic continuation in sec.(2.4) are

$$\langle x|e^{-\beta\hat{H}}|x'\rangle_{p.b.} = \left(\frac{m\omega}{2\pi\sin(\beta\omega)}\right)^{1/2} \exp\left\{-\frac{m\omega}{2}\left[(x^2+x'^2)\cot(\beta\omega) - \frac{2xx'}{\sin(\beta\omega)}\right]\right\} \tag{2.28}$$

The next step involves the resolution of the quantum dynamical problem, before we can use eq.(3.14).
The strategy employed is standard. The starting point is the quantum mechanical time evolution of the momentum operator

$$\frac{d}{dt}\hat{p}(t) = ie^{i\hat{H}t}[\hat{H},\hat{p}]e^{-i\hat{H}t} \tag{3.28}$$

The commutator can be evaluated without difficulties to yield

$$\begin{aligned}[\hat{H},\hat{p}] &= -\frac{m\omega^2}{2}[\hat{x}^2,\hat{p}] \\ &= -\frac{m\omega^2}{2}\{\hat{x}[\hat{x},\hat{p}] + [\hat{x},\hat{p}]\hat{x}\} \\ &= -im\omega^2\hat{x}\end{aligned} \tag{3.29}$$

so that

$$\frac{d}{dt}\hat{p}(t) = m\omega^2\hat{x}(t) \tag{3.30}$$

By a similar procedure, applied to the time evolution of the operator $\hat{x}(t)$, we get the following set of coupled first-order differential equations

$$\begin{cases} \dfrac{d}{dt}\hat{p}(t) = & m\omega^2\hat{x}(t) \\ \dfrac{d}{dt}\hat{x}(t) = & \dfrac{1}{m}\hat{p}(t) \end{cases} \tag{3.31}$$

By a simple time derivation eqs.(3.31) are decoupled

$$\frac{d^2}{dt^2}\hat{p}(t) = \omega^2\hat{p}(t) \quad , \quad \frac{d^2}{dt^2}\hat{x}(t) = \omega^2\hat{x}(t) \tag{3.32}$$

Starting from the initial conditions

$$\hat{p}(0) \equiv \hat{p} \quad , \quad \hat{x}(0) \equiv \hat{x} \tag{3.33}$$

and from the second of eqs.(3.31)

$$\hat{p}(t) = m\dot{\hat{x}}(t) \tag{3.34}$$

the natural ansatz is for solutions of the type

$$\hat{p}(t) = \hat{a}e^{\omega t} + \hat{b}e^{-\omega t} \quad , \quad \hat{x}(t) = \hat{c}e^{\omega t} + \hat{d}e^{-\omega t} \tag{3.35}$$

$\hat{a}$ and $\hat{b}$ being operator quantities to determine.
It is a simple exercise to verify that

$$\hat{p}(t) = \hat{p}\cosh(\omega t) + m\omega\hat{x}\sinh(\omega t) \tag{3.36}$$

Use of eq.(3.36) into eq.(3.14) leads seemingly to a complicate expression for the matrix element $\langle p|e^{-i\xi\hat{p}(t)}|x\rangle$, but a suitable simplification is made possible by recourse to commutator algebra. In fact

$$[\hat{x},[\hat{x},\hat{p}]] = 0 \quad , \quad [\hat{p},[\hat{x},\hat{p}]] = 0 \tag{3.37}$$

and, consequently [66]

$$e^{A\hat{x}+B\hat{p}} = e^{B\hat{p}}\, e^{A\hat{x}}\, e^{-\frac{AB}{2}[\hat{p},\hat{x}]} \tag{3.38}$$

(A, B arbitrary constants).
Eq.(3.38) translated in terms of eq.(3.14) is written

$$e^{-i\xi\hat{p}(t)} = e^{-i\xi\hat{p}\cosh\omega t}\, e^{-i\xi m\omega\hat{x}\sinh(\omega t)}\, e^{-im\omega\xi^2\sinh(\omega t)\cosh(\omega t)/2} \tag{3.39}$$

The factorization of the exponential allows a direct calculation for the matrix element:

$$< p|e^{-i\xi\hat{p}(t)}|x >= \frac{e^{-ipx}}{\sqrt{2\pi}}\, e^{-i\xi[p\cosh(\omega t)+m\omega x\sinh(\omega t)]}\, e^{-im\omega\xi^2\sinh(\omega t)\cosh(\omega t)/2} \tag{3.40}$$

This result concerning the dynamics of a parabolic barrier is exact. Its importance in the context of this thesis work can be hardly stressed. This statement will become evident going further (see, in particular, sec.3.4) when the role of eq. (3.40) as a starting point for approximations to the reactive dynamical feature in the case of general barriers will be discussed.
Two important features of eq.(3.40) should be remarked:

1. $$p_{cl}(t) = p\cosh(\omega t) + m\omega x\sinh(\omega t) \tag{3.41}$$
   is the solution for the classical moment of a particle moving under the influence of a parabolic barrier, with the initial conditions $p_{cl}(0) = p$ and $x_{cl}(0) = x$;

2. The last exponential factor in eq.(3.40) arises from the term $e^{-AB[\hat{x},\hat{p}]/2}$ and involves purely quantum effects due to the non-commutative behavior of the operators $\hat{p}$ and $\hat{x}$.

It goes without saying that the factorization between classical and quantum terms put in evidence suggests the possibility of adding quantum effects over classical dynamics simulations.

The Fourier representation of the Dirac delta allows to evaluate eq.(3.14). It is easily verified that after performing the p-integration, we get

$$\begin{aligned} k(t)Q_r = -\frac{1}{2\pi m} Re \int_{-\infty}^{+\infty} dx < x|e^{-\beta\hat{H}}|x = 0 > \times \\ \fint_{-\infty}^{+\infty} \frac{d\xi}{\xi} e^{-im\omega\xi^2\sinh(\omega t)\cosh(\omega t)/2}\, e^{-im\omega x\xi\sinh(\omega t)}\, \frac{\partial}{\partial x}\delta(x + \xi\cosh(\omega t)) \end{aligned} \tag{3.42}$$

and successively (after integration by parts)

$$\begin{aligned} k(t)Q_r = \frac{1}{2\pi m} Re \fint_{-\infty}^{+\infty} \left\{ \frac{d\xi}{\xi}\, e^{im\omega\xi^2\sinh(\omega t)\cosh(\omega t)/2} < x = -\xi\cosh(\omega t)|e^{-\beta\hat{H}}|x = 0 > \right. \\ \left. \left[\frac{\partial \ln < x|e^{-\beta\hat{H}}|x = 0 >}{\partial x} - im\omega\xi\sinh(\omega t) \right]_{x=-\xi\cosh(\omega t)} \right\} \end{aligned} \tag{3.43}$$

Using eq.(2.29) for the thermal density matrix element ($\beta\omega < \pi$)

$$\begin{aligned} k(t)Q_r &= \frac{1}{2\pi m}\left(\frac{m\omega}{2\pi\sin(\beta\omega)}\right)^{1/2} Re\left\{\fint_{-\infty}^{+\infty}\frac{d\xi}{\xi}\, e^{i\xi^2 m\omega\sinh(\omega t)\cosh(\omega t)/2}\, e^{-\frac{m\omega\xi^2}{2\tan(\beta\omega)}\cosh^2(\omega t)}\right. \\ &\qquad \left.\left[\frac{\xi m\omega\cosh(\omega t)}{\tan(\beta\omega)} - i\xi m\omega\sinh(\omega t)\right]\right\} \\ &= \frac{1}{2\pi m}\left(\frac{m\omega}{\sin(\beta\omega)}\right)^{1/2} Re\left\{\left(\frac{m\omega}{\tan(\beta\omega)} - im\omega\tanh(\omega t)\right)^{1/2}\right\} \end{aligned} \tag{3.44}$$

and finally

$$k(t)Q_r = \frac{\omega}{2\pi(\sin(\beta\omega))^{1/2}}\, Re\left[\left(\frac{1}{\tan(\beta\omega)} - i\tanh(\omega t)\right)^{1/2}\right] \tag{3.45}$$

The required real part of the complex function in eq.(3.45) can be explicited easily by noticing that

$$Re\left[(a+ib)^{1/2}\right] = \rho^{1/2}\cos(\theta/2) \qquad \rho = (a^2+b^2)^{1/2} \qquad \theta = \arctan(b/a) \tag{3.46}$$

$$\begin{aligned} \cos(\theta/2) &= \sqrt{\frac{1+\cos\theta}{2}} \\ \cos\theta &= \frac{1}{\sqrt{1+\tan^2\theta}} \end{aligned} \tag{3.47}$$

so that

$$Re\left[(a+ib)^{1/2}\right] = \left[\frac{(a^2+b^2)^{1/2}+a}{2}\right]^{1/2} \tag{3.48}$$

In the particular case of eq.(3.45), $a = 1/\tan(\beta\omega)$ and $b = -\tanh(\omega t)$.
Two immediate applications are that at ininfluent dynamics ($t = 0$) and the one in the long-time limit ($t \to \infty$), the latter giving the exact quantum rate coefficient for a parabolic barrier

$$k(0)Q_r = \frac{\omega}{2\pi}\frac{1}{(\sin(\beta\omega))^{1/2}}\, Re\left[\left(\frac{1}{\tan(\beta\omega)}\right)^{1/2}\right] = \frac{\omega}{2\pi}\frac{[\cos(\beta\omega)]^{1/2}}{\sin(\beta\omega)} \quad \text{ininfluent dynamics} \tag{3.49}$$

$$k(\infty)Q_r = \frac{\omega}{2\pi}\frac{1}{(\sin(\beta\omega))^{1/2}}\, Re\left[\left(\frac{1}{\tan(\beta\omega)} - i\right)^{1/2}\right] = \frac{\omega}{4\pi}\frac{1}{\sin(\beta\omega/2)} \qquad \text{exact result} \tag{3.50}$$

The expressions thus obtained are relative to a parabolic barrier with maximum $V_0 = 0$ at $x = 0$. For a different choice $V \neq 0$, it is straightforward to verify that the only change involves the presence of the additional factor $e^{-\beta V_0}$. It should be observed that the exact result is divergent as $\beta\omega \to 2\pi$, but the existence domain of the density matrix element is limited to $\beta\omega < \pi$.

In the previous section (sec.(3.2)) it was illustrated how our approach reduces, as it must, to a thermodynamic result in the limit $t = 0$ (eq.(3.19)). So, one can expect that applying eq.(3.19) to the case of a parabolic barrier, the same result of eq.(3.49) is regained. This is actually what happens, since from eqs.(3.19) and (2.29)

$$\begin{aligned} k(0)Q_r =& \frac{1}{2\pi m} Re \left\{ \oint_{-\infty}^{+\infty} \frac{d\xi}{\xi} \left(\frac{m\omega}{2\pi \sin(\beta\omega)} \right)^{1/2} \left[\left(-\frac{m\omega x}{\tan(\beta\omega)} \right) e^{-\frac{m\omega x^2}{2\tan(\beta\omega)}} \right]_{x=-\xi} \right\} \\ =& \frac{1}{2\pi m} \left(\frac{m\omega}{2\pi \sin(\beta\omega)} \right)^{1/2} \frac{m\omega}{\tan(\beta\omega)} \int_{-\infty}^{+\infty} d\xi \, e^{-\frac{m\omega\xi^2}{2\tan(\beta\omega)}} \\ & k(0)Q_r = \frac{\omega}{2\pi} \frac{[\cos(\beta\omega)]^{1/2}}{\sin(\beta\omega)} \end{aligned} \tag{3.51}$$

Finally, going back to the $k(\infty)$ value, it is interesting to consider the quantum correction, defined by

$$\Gamma = \frac{k(\infty)}{k^{cl}} \tag{3.52}$$

where $k^{cl} = \frac{kT}{h} e^{-\beta V_0}$ is the classical rate constant. Therefore,

$$\Gamma = \frac{u/2}{\sin(u/2)} \qquad (u = \beta\omega) \tag{3.53}$$

The result expressed by eq.(3.53) can be obtained by analitically continuing the real frequency to imaginary values in Wigner's studies about the harmonic oscillator [63]. To the same conclusion has come also Bell in his work on the tunnel effect correction for parabolic potential barriers [64].

3.3.2 The complete parabolic barrier

If one adds a term, linearly dependent on the position, to the definition of the Hamiltonian in eq.(3.27), the vertex of the parabolic barrier moves from $x^* = 0$ to the new position $x^* = v_1/(m\omega^2)$. The new Hamiltonian becomes

$$\hat{H} = \frac{\hat{p}^2}{2m} + V_0 + v_1\hat{x} - \frac{1}{2}m\omega^2\hat{x}^2 \qquad \omega \in \Re \tag{3.54}$$

In the conclusive part of sec.(3.2) it has been remarked that the exact quantum result is indipendent of the particular location of the dividing surface; so, the calculation probably will be an easier task if performed choosing $x^* = v_1/(m\omega^2)$, i.e. reducing the complete parabolic barrier to a simple one. For more complicated potentials, however, the location of the best dividing surface, presumably unknown a priori (especially for

multidimensional simulations, where entropic effects have a role in the determination of the best location for the dividing surface), so that it is fundamental to develop eq.(3.1) in the basic case $x^* = 0$.

The starting point involves a trivial reorganization of eq.(3.14)

$$\begin{aligned} k(t)Q_r = -\frac{1}{2\pi m\sqrt{2\pi}}\, Im \int_{-\infty}^{+\infty} dx < x|e^{-\beta\hat{H}}|x = 0 > \quad \times \\ \oint_{-\infty}^{+\infty} \frac{d\xi}{\xi} \int_{-\infty}^{+\infty} dp\, p < p|e^{-i\xi\hat{p}(t)}|x > \end{aligned} \tag{3.55}$$

The evolution of $\hat{p}(t)$ under the initial conditions of eq.(3.33) can be found following the scheme illustrated in sec.(3.3.1). The resulting system of coupled differential equations is

$$\begin{cases} \dfrac{d}{dt}\hat{x}(t) = \dfrac{1}{m}\hat{p}(t) \\ \dfrac{d}{dt}\hat{p}(t) = m\omega^2\hat{x}(t) - v_1 \end{cases} \tag{3.56}$$

from which, by differentiation with respect to time

$$\frac{d^2}{dt^2}\hat{x}(t) = \omega^2\hat{x}(t) - v_1/m \qquad \frac{d^2}{dt^2}\hat{p}(t) = \omega^2\hat{p}(t) \tag{3.57}$$

The solution for the momentum operator is

$$\hat{p}(t) = \hat{p}\cosh(\omega t) + m\omega\hat{x}\sinh(\omega t) - \frac{v_1}{\omega}\sinh(\omega t) \tag{3.58}$$

It is straightforward, now, to evaluate the mixed momentum-position matrix element appearing in eq.(3.55), with the result

$$< p|e^{-i\xi\hat{p}(t)}|x >= \frac{e^{-ipx}}{\sqrt{2\pi}} e^{-iA\xi} e^{-B\xi^2} \tag{3.59}$$

where

$$\begin{aligned} A &= p\cosh(\omega t) + m\omega x\sinh(\omega t) - \frac{v_1}{\omega}\sinh(\omega t) \\ B &= \frac{1}{4}m\omega\sinh(2\omega t) = \frac{m\omega}{2}\sinh(\omega t)\cosh(\omega t) \end{aligned} \tag{3.60}$$

The calculation could be continued, in analogy to sec.(3.3.1), performing the integration over p, but here a different strategy will be pursued. This procedure will be useful in the following, as we shall examine the extension to general potentials, where obtaining exact solutions for the evolution of the operatot $\hat{p}(t)$ is out of question.
The integrations involved in eq.(3.14) are carried out first with respect to ξ and then

to p and x. This alternative procedure is reliable and leads to the correct result for the simple parabolic barrier ($v_1 = 0$).

After the first integration, we are led to define the function (see Appendix A for a demonstration)

$$\begin{aligned} J(p,x) &= \frac{e^{-ipx}}{\sqrt{2\pi}} \int_{-\infty}^{+\infty} \frac{d\xi}{\xi} e^{-iA\xi} e^{-iB\xi^2} \\ &= -i\sqrt{\frac{\pi}{2}}\,\frac{A}{|A|}\; erf\left[\frac{|A|}{2\sqrt{iB}}\right] e^{-ipx} \end{aligned} \tag{3.61}$$

$J(p,x)$ reduces the principal value of the ξ-integration to an error function of complex argument, which plays a central role in the present approach. The error function, actually, contains and, consequently, "weights" the intrinsic dynamics of the problem. A correct estimation of kQ_r, forces to examine the long-time limit ($t \to \infty$) of eqs.(3.60), so that

$$\begin{aligned} A &= \frac{1}{2} e^{\omega t}\left(p + m\omega x - \frac{v_1}{\omega}\right) \quad (t \to \infty) \\ B &= \frac{m\omega}{8} e^{2\omega t} \qquad\qquad\qquad\quad (t \to \infty) \end{aligned} \tag{3.62}$$

The auxiliary function $U(x)$ follows from $J(p,x)$ according to

$$U(x) = \int_{-\infty}^{+\infty} dp\, p\, J(p,x) \tag{3.63}$$

Taking into account eqs. (3.62), after the change of variable $r = p + m\omega x - v_1/\omega$ we find

$$U(x) = -i\sqrt{\frac{\pi}{2}} \int_{-\infty}^{+\infty} dr \frac{r}{|r|} \left(r + v_1/\omega - m\omega x\right) e^{-irx} e^{-ix(v_1/\omega - m\omega x)}\, erf\left[\frac{|r|}{\sqrt{2im\omega}}\right] \tag{3.64}$$

Notice that the point $r = 0$ represents in eq.(3.64) an eliminable discontinuity, since $erf(r) \to r$ as $r \to 0$. Simple properties of the error function and the change of variable $r \to -r$ lead to

$$\begin{aligned} U(x) &= -i\sqrt{\frac{\pi}{2}}\, e^{-ix(v_1/\omega - m\omega x)} \int_{-\infty}^{+\infty} dr\, e^{-irx} \left(r + v_1/\omega - m\omega x\right) erf\left(\frac{r}{\sqrt{2im\omega}}\right) \\ &= i\sqrt{\frac{\pi}{2}}\, e^{-ix(v_1/\omega - m\omega x)} \left(v_1/\omega - m\omega x + i\frac{\partial}{\partial x}\right) \int_{-\infty}^{+\infty} dr\, e^{irx}\, erf\left(\frac{r}{\sqrt{2im\omega}}\right) \end{aligned} \tag{3.65}$$

Exploiting the following remarkable result (see Appendix B)

$$I(x) = \int_{-\infty}^{+\infty} dr\, e^{irx}\, erf\left(\frac{r}{\sqrt{2im\omega}}\right) = \begin{cases} 0 & x = 0 \\ -\dfrac{2}{ix}\, e^{-im\omega x^2/2} & x \neq 0 \end{cases} \tag{B.2}$$

$U(x)$ can be cast into the more compact form

$$U(x) = -\sqrt{\frac{\pi}{2}}\, e^{im\omega x^2/2} \frac{d}{dx}\, \left[e^{-ix(v_1/\omega - m\omega x/2)} I(x)\right] \tag{3.66}$$

Eq.(3.55) can now be properly integrated by parts to yield the rate constant,

$$k(\infty)Q_r = -\frac{1}{4\pi m}\, Im \int_{-\infty}^{+\infty} dx\, e^{-ix(v_1/\omega - m\omega x/2)}\, I(x)\, \frac{d}{dx}\, \left[e^{im\omega x^2/2} < x|e^{-\beta\hat{H}}|x = 0 >\right] \tag{3.67}$$

The Boltzmann matrix element of eq.(2.31) is conveniently written as

$$< x|e^{-\beta\hat{H}}|x' = 0 >= N\, e^{-ax^2+bx} \tag{3.68}$$

where

$$\begin{aligned} N &= \left(\frac{m\omega}{2\sin(\beta\omega)}\right)^{1/2} e^{-\beta V_0}\, e^{-\frac{\beta v_1^2}{2m\omega^2}\left(1-\frac{2\tan(\beta\omega/2)}{\beta\omega}\right)} \\ a &= \frac{m\omega}{4\tan(\beta\omega/2)}\left(1-\tan^2(\beta\omega/2)\right) = \frac{m\omega}{2\tan(\beta\omega)} \\ b &= \frac{v_1}{\omega}\tan(\beta\omega/2) \end{aligned} \tag{3.69}$$

After introducing the explicit expansion of $I(x)$, eq.(B.2), we get

$$\begin{aligned} k(\infty)Q_r &= \frac{1}{2\pi m} Im \int_{-\infty}^{+\infty} dx\, \frac{e^{-ixv_1/\omega}}{ix}\, \frac{d}{dx}\, \left[e^{im\omega x^2/2} < x|e^{-\beta\hat{H}}|x' = 0 >\right] \\ &= \frac{N}{2\pi m}\, Im \left\{ i \int_{-\infty}^{+\infty} dx\, e^{-(a-im\omega/2)x^2+(b-iv_1/\omega)x}\, [2a - im\omega - b/x] \right\} \end{aligned} \tag{3.70}$$

and finally

$$k(\infty)Q_r = \frac{N}{2\pi m}\, Im \left\{ i \int_{-\infty}^{+\infty} dx\, e^{-Ax^2+Bx}\, [2A - b/x] \right\} \tag{3.71}$$

where we have set

$$\begin{aligned} A &= a - \frac{im\omega}{2} \\ B &= b - \frac{iv_1}{\omega} \end{aligned} \tag{3.72}$$

The parameter A and B which arise from the thermal density matrix element should not be confused with those introduced in eq.(3.62), which are associated with the dynamics of the problem.

The two Gaussian integrals in eq.(3.71) can be treated separately. The former has already been encountered (see footnote (1)), while the latter

$$R(B) = \int_{-\infty}^{+\infty} \frac{dx}{x}\, e^{-Ax^2+Bx} \tag{3.73}$$

deserves greater attention. By differentiation with respect to B, we are reduced to solve the differential equation

$$\frac{\partial R}{\partial B} = \int_{-\infty}^{+\infty} dx\, e^{-Ax^2+Bx} \tag{3.74}$$

with the boundary condition $R(0) = 0$.
Simple manipulations lead to

$$R(B) = \sqrt{\frac{\pi}{A}} \int_0^B dt\, e^{t^2/4A} = -\sqrt{\frac{\pi}{A}}\, i\, \sqrt{4A} \int_0^{iB/\sqrt{4A}} dx\, e^{-x^2} = -i\pi\ erf\left(\frac{iB}{\sqrt{4A}}\right) \tag{3.75}$$

with $erf(z)$ the error function, so that

$$k(\infty)Q_r = \frac{N}{2\pi m}\, Im\left\{2Ai\sqrt{\frac{\pi}{A}}\, e^{B^2/4A} - \pi b\ erf\left(\frac{iB}{\sqrt{4A}}\right)\right\} \tag{3.76}$$

At this point, we think it interesting to verify that the procedure just developed, which differs from the one adopted in sec.(3.3.1) for the order of the integrations, leads to correct result for the simple parabolic barrier with maximum at $x^* = 0$. For this purpose, it is enough to put $v_1 = 0$. With $v_1 = 0$, from eqs.(3.69), (3.72) it follows $b = B = 0$ and therefore

$$k(\infty)Q_r = \frac{N}{2\pi m}\, Im\left[2i\sqrt{\pi A}\right] \tag{3.77}$$

At the cost of a few manipulations involving eqs. (3.62), (3.69) under the usual parabolic barrier condition $\beta\omega < \pi$, as expected, the exact result of eq.(3.50) is regained

$$k(\infty)Q_r = \frac{\omega}{4\pi}\, \frac{e^{-\beta V_0}}{\sin(\beta\omega/2)} \tag{3.78}$$

After this detailed investigation of the parabolic barrier models, the next step involves the consideration of more general forms of barrier, for which an analytically exact resolution is not possible, so that one is forced to search for approximate treatments.

3.4 Treatment of forms of barrier not analytically solvable

The basic approximation suggested in this thesis work stems from eq. (3.40), where the matrix element $< p|e^{-i\xi\hat{p}(t)}|x >$ which takes into account the role of dynamics is explicitly separated into a purely classical contribution and a quantum effect. This observation suggests a formulation which seems to be convincing and useful to the study of potential barriers of general shape.
Going back to eq.(3.40) and recalling that for the simple parabolic barrier

$$p_{cl}(t) = p\cosh(\omega t) + m\omega x \sinh(\omega t) \tag{3.79}$$

is the classical solution for the momentum, it is possible to express even the quantum factor in terms of the classical evolution of the momentum $p_{cl}(t)$, so that we can write

$$< p|e^{-i\xi\hat{p}(t)}|x >= \frac{e^{-ipx}}{\sqrt{2\pi}}\, e^{-i\xi p_{cl}(t)}\, e^{-\frac{i\xi^2}{2}\left(\frac{\partial p_{cl}(t)}{\partial p}\frac{\partial p_{cl}(t)}{\partial x}\right)} \tag{3.80}$$

x and p being respectively initial position and momentum from which the classical momentum evolves.
Eq.(3.80) is obviously a way of expressing the exact result for the case of a simple parabolic barrier and a reasonable approximation conjecture in the case of different forms of barrier. Eq.(3.80) takes one to consider classical simulations as a way for evaluating the matrix element of eq.(3.40), inclusive of quantum effects, by solving the classical dynamics problem relative to the specific potential barrier considered.
In other terms, $< p|e^{-i\xi\hat{p}(t)}|x >$ will be, from now on, calculated on the base of eq.(3.80), so that eq. (3.14) for the kinetic constant assumes the following form

$$\begin{aligned} k(t)Q_r = -\frac{1}{(2\pi)^2 m} Im \int_{-\infty}^{+\infty} dx < x|e^{-\beta\hat{H}}|x = 0 > \quad \times \\ \int_{-\infty}^{+\infty} dp\, p\, e^{-ipx} \int_{-\infty}^{+\infty} \frac{d\xi}{\xi} e^{-i\xi p_{cl}(t)}\, e^{-\frac{i\xi^2}{2}\left(\frac{\partial p_{cl}(t)}{\partial p}\frac{\partial p_{cl}(t)}{\partial x}\right)} \end{aligned} \tag{3.81}$$

As stated in sec.(3.3.2), the procedure goes on by performing first the ξ-integration, differently indeed from the simple parabolic barrier treatment, but in analogy with the complete parabolic barrier one.
At this point, there are two main ways of dealing with the principal value of the integral with respect to ξ:

1. to treat directly the integral, interpreting it in the complex domain and adopting Romberg's method for integration [67];

2. to be able to find an analytical formula which permits to avoid the integration.

Point 2 above has just been investigated in the previous section. With reference to Appendix A, we have already shown that

$$\int_{-\infty}^{+\infty} \frac{d\xi}{\xi} e^{-iA\xi}\, e^{-iB\xi^2} = -i\pi \frac{A}{|A|}\, erf\left[\frac{|A|}{2\sqrt{iB}}\right] \tag{3.82}$$

so that in conclusion the computational efforts must be addressed to the estimate of

$$kQ_r = \frac{1}{4\pi m} Re\left\{ \int_{-\infty}^{+\infty} dx < x|e^{-\beta\hat{H}}|x = 0 > \int_{-\infty}^{+\infty} dp\, p\, e^{-ipx} \frac{p_{cl}}{|p_{cl}|}\, erf\left[\frac{|p_{cl}|}{\sqrt{2i\dfrac{\partial p_{cl}}{\partial p}\dfrac{\partial p_{cl}}{\partial x}}}\right]\right\} \tag{3.83}$$

where $p_{cl}(x,p)$ is evaluated in the long time limit. Eq.(3.83) is actually valid at any time t, but the correct kinetic constant is captured only as $t \to \infty$.
The estimate according to eq.(3.83) involves some numerical problems:

1. the determination of the thermal density matrix elements. This topic will be examined carefully in the next chapter, where a Feynman path integral approach is described;

2. the partial derivatives appearing in the error function will be treated by using finite difference central formulae;

3. the error function itself will be estimated resorting to a particular algorithm, suggested by Gautschi and based on some numerical expansions [68].

4. the $p-$integrand involved in the $p-$integration is made up of an oscillatory term (e^{-ipx}) times an error function, whose value depends also on the $x-$variable. This last feature makes the auspicable application of Fast-Fourier Techniques (FFT) difficult, so that a more laborious integration procedure based on Filon's algorithm [69] has been adopted.

Chapter 4

Computational strategies

At the end of the last chapter, we have listed the problems to be tackled for successfully implementing the approach described. In this chapter, those problems are examined and suitable solutions are proposed.
In the description of the procedures we recognize the existence of two steps. The first one involves properties of the density matrix: these are initially presented, and the different behavior of diagonal and off-diagonal elements is investigated. The calculation of off-diagonal elements of the thermal density matrix (those of interest in the present approach) is performed by resorting to a formalism based on the Feynman-Kac formula, which requires the generation of Brownian random walks.
The second step is associated with the dynamics of the particle and the needed classical evolution is proved to be efficiently brought about by a velocity-Verlet integration scheme. The complex error function involved in the formalism is estimated by an algorithm suggested by Gautschi. The problem of dealing with an oscillatory integrand in the momentum space is solved by adopting the Filon's algorithm. An additional trouble connected with the double integration is that the limits are not finite: in the case of the x-integration, the matrix element fades away as x goes off from the central point $x = 0$; for the p-integration, instead, the introduction of a convergence factor becomes a necessary way out.
All these aspects play a crucial role before the present approach can be implemented; they are discussed in this chapter, while results and conclusions constitute the contents of the last one.

4.1 Step 1: the thermal density matrix

The approach described in the last chapter is characterized, among other things, by an aspect common also to the different versions of QTST treated in the introductory part of this thesis, associated with the separation between thermal and dynamical effects. While a full account of the dynamical effects is a nearly hopeless task, so that one must be satisfied with reasonably accurate estimates, for example based on the parabolic barrier approximation, thermal effects should be computed as exactly as possible, to avoid the occurrence of additional inadequacies making the analysis of the results more difficult. The fact that the thermal contribution involves an imaginary-time propagator offers the possibility of adopting appropriate Monte Carlo techniques to calculate numerically the thermal density matrix.
The thermal density matrix plays a fundamental role in the quantum mechanical description of mixed systems, since it describes how the system is populated and gives a quantitative estimate of quantum interference effects.

In the next sections of this chapter, different techniques employed for the evaluation of the thermal density matrix are described, among these the Path Integral Monte Carlo (PIMC) approach and that based on the Feynman-Kac formula. In particular, the concept of isomorphism between a quantum particle and a ring polymer of classical particles is employed, and the generation of Brownian motion is discussed. The importance of sampling multiple paths around that of minimal action (classical) will be put in evidence through the comparison between quantum and semiclassical calculations of the density matrix. A set of results will then be reported for the simple harmonic potential, the Eckart barrier and a confined system (i.e. spacially confined between infinite walls).

4.1.1 Some properties of density matrices

The formalism of density operators was introduced in 1927 by J.Von Neumann (and, independently, by L. Landau and F. Bloch) with the aim of giving a quantitative description of physical situations in which mixed states are involved; such a circumstance arises, for instance, for a quantum system in thermal equilibrium or for the entanglement of two subsystems.

A pure state is completely described by a single wavefunction $|\Psi\rangle$ (which can be expanded in terms of a complete set of eigenfunctions of a hermitian operator). The corresponding density operator is the projection operator on the pure state and is given by [70]

$$\hat{\rho} = |\Psi\rangle\langle\Psi| \tag{4.1}$$

The extension to mixed states, represented by a linear combination of pure states, is straightforward and leads to:

$$\hat{\rho} = \sum_i p_i |\Psi_i\rangle\langle\Psi_i| \tag{4.2}$$

where p_i is the weight of the i-th pure state in the mixed state.
In the case of systems kept in contact with a heat bath (i.e. at finite temperature T), p_i can be interpreted as the probability of finding the system in its i-th state at temperature T, and eq. (4.2) then defines a thermal density operator.
Choosing $\{|\Psi_i\rangle\}$ to be the eigenfunctions of the Hamiltonian operator $\hat{H}$, in the canonical ensemble $p_i \propto \exp(-\beta E_i)$, $k_B T = 1/\beta$ and the thermal density operator reads:

$$\hat{\rho} = \sum_i e^{-\beta E_i} |\Psi_i\rangle\langle\Psi_i| = e^{-\beta \hat{H}} \tag{4.3}$$

The density operator has some important features (we shall limit ourselves to consider one-dimensional systems):

- from the invariance property of the trace

$$Tr[\hat{\rho}] = \int dx \langle x|\hat{\rho}|x\rangle \tag{4.4}$$

  is a representation of the density operator in the position space; $\rho(x, x') = \langle x|\hat{\rho}|x'\rangle$ is called the density matrix. The operator defined by eq.(4.3) has an unnormalized trace, because we have chosen $p_i = e^{-\beta E_i}$ and $\sum_i p_i \neq 1$. The normalization constant $Q = \sum_i p_i = \int\, dx\, \langle x|e^{-\beta \hat{H}}|x\rangle$ is the canonical partition function of the system.

- the mean value of a generic hermitian operator $\hat{F}$, function only of the position operator $\hat{x}$, is obtained as [66]

$$\langle \hat{F} \rangle = Tr[\hat{F}\hat{\rho}] = \int dx \int dx' F(x') \rho(x', x) \delta(x' - x) \tag{4.5}$$

- the idempotency property $\hat{\rho}^2 = \hat{\rho}$ holds true only for pure states (see eq. (4.1)). For mixed states, the non validity is immediately evident, considering the case of the thermal density operator, eq. (4.3).

In general, the evaluation of the diagonal and off-diagonal elements of the (thermal) density matrix is not a trivial problem. Actually, only in a few simple cases the solution is known and can be found at the cost of less or more analytical effort.

In many situations, a practical way of proceeding has been to reduce the expression under investigation to one that contains only tractable density matrices. These, of course, include the cases of the free particle and the harmonic oscillator. Although, for simplicity, only one-dimensional systems are considered in the following, the generalization to multidimensional spaces is not difficult.

4.2 Calculation of the thermal density matrix elements

The diagonal elements of the thermal density matrix $\rho(x, x; \beta)$ represent the population of the system in the position eigenstate $|x\rangle$. By this we mean that performing N times (with N very large) the same measurement, under the same initial conditions, $N\rho(x, x; \beta)$ systems should be found in the position eigenstate $|x\rangle$.
On the other hand, the off-diagonal elements $\rho(x, x'; \beta)$, also known as coherences, represent the quantum interference between the eigenstates $|x\rangle$ and $|x'\rangle$. Coherences between two states can appear when the pure state $|\Psi_i\rangle$ is some their superposition: $\rho(x, x'; \beta)$ is nothing else than the average (over the statistical mixture) of such interferences. $\rho(x, x'; \beta) = 0$ means that the interference effects have been averaged out, while $\rho(x, x'; \beta) \neq 0$ denotes the presence of coherences.

4.2.1 Diagonal elements

The strategy of the Path Integral Monte Carlo (PIMC) techniques [71, 72, 73] is characterized by the goal of expressing the density matrix of any given systems in terms of the known result for the free particle.
The generic element of the thermal density matrix can be expressed in the basic form [66]

$$\rho(x, x'; \beta) = \int dx'' \rho(x, x''; \beta/2)\rho(x'', x'; \beta/2) \tag{4.6}$$

(see Appendix C). The decomposition in the integrand can be continued on, with the result that the searched density matrix element will be expressible in terms of a chain of integrals of density matrices involving higher and higher temperatures.

Thus, if the number of steps is P (P is called Trotter number),

$$\rho(x_0, x_P; \beta) = \int \dots \int dx_1 \dots dx_{P-1} \rho(x_0, x_1; \beta/P) \dots \rho(x_{P-1}, x_P; \beta/P) \tag{4.7}$$

The right-hand side of eq. (4.7) is referred to as a path integral representation. For P sufficiently large (usually $P \geq 10$), the role of the high temperature PT involved in the integrand is to damp the effect of the potential, so that for small intervals in the position space one can think of the potential as a smooth function of the coordinates. Indicating the free particle Hamiltonian with $\hat{H}^0$, the high-temperature density matrix

by means of the above-mentioned properties can be rewritten

$$\begin{aligned}\rho(x_n, x_{n+1}; \beta/P) &= \sum_i \Psi_i^*(x_n) e^{-\beta\left[\hat{H}^0+\hat{U}(x)\right]} \Psi_i(x_{n+1}) \\ &\approx \sum_i \Psi_i^*(x_n) e^{-\frac{\beta}{P}\hat{H}^0} \Psi_i(x_{n+1}) e^{-\frac{\beta}{2P}[U(x_n)+U(x_{n+1})]} \\ &= \rho_0(x_n, x_{n+1}; \beta/P) e^{-\frac{\beta}{2P}[U(x_n)+U(x_{n+1})]}\end{aligned} \tag{4.8}$$

The approximation in eq.(4.8) becomes exact in the limit $P \to \infty$.

For a free particle, the exact density matrix expression has been shown previously, so that for the diagonal element of the unknown density matrix one finally gets the result

$$\rho(x_0, x_0; \beta) = C^{P/2} \int \dots \int dx_1 \dots dx_{P-1}\, e^{-\beta[U_{har}+U_{ext}]} \tag{4.9}$$

with

$$C = \frac{mP}{2\pi\beta} \qquad U_{ext} = \sum_{n=0}^{P-1} U(x_n)/P \qquad U_{har} = \frac{C\pi}{\beta} \sum_{n=0}^{P-1} (x_n - x_{n+1})^2$$

Equation (4.9) is easily generalizable to the case of several degrees of freedom and, due to its form, Monte Carlo methods seem to be suitable to perform the multiple integration involved. It is also interesting to notice that it establishes an isomorphism between a single quantum particle and a polymer of P classical particles. The label *har* adopted for one of the two contributions to the potential energy is a reminder of the fact that we are actually dealing with a ring polymer ($x_P = x_0$), with the $n-$th link under the influence of an external potential $U(x_n)/P$, and two contiguous beads (n,$n+1$) coupled by a harmonic bond potential $C\pi(x_n - x_{n+1})^2/\beta$. The solution of the quantum problem relative to a particle is therefore equivalently obtained via Path Integral Monte Carlo (PIMC) method by solving that of a ring polymer of P classical particles.

From a computational point of view, it must be observed that the external potential U_{ext} is damped by larger values of P, so that larger steps are allowed to change configurations to sample the entire space. On the other hand, the oscillator strength Pm/β^2 grows up along with P; in this case smaller Monte Carlo steps are necessary. To switch from one configuration to another during the Monte Carlo simulation, the best way of proceeding is to shift first the whole polymer by a large (random) quantity and, then, to displace each individual classical particle by a small (random) amount. Once the new configuration has been determined, the variation (ΔU) in the polymer energy must be computed (i.e. being $U_{pot} = U_{har} + U_{ext}$, $\Delta U = U_{pot}^{new} - U_{pot}^{old}$) to decide, according to a Metropolis step, if the new configuration must be retained or rejected. Since the diagonal element of the density matrix in the position space,

$\rho(x, x, \beta)$, represents the probability density of finding the quantum particle at x, it can be obtained as the fraction of particles residing at x during the Monte Carlo simulation.

Figure 4.1 shows a comparison between the exact value of $\rho_{h.p.}(x, x; \beta)$ and that obtained by our PIMC code. The normalized expression for the harmonic potential density matrix is

$$\rho_{h.p.}(x, x; \beta) = \left[\frac{m\omega}{\pi} \tanh(\beta\omega/2)\right]^{1/2} \exp\left\{-m\omega x^2 \tanh(\beta\omega/2)\right\} \tag{4.10}$$

In the limit of low temperatures ($\beta \to \infty$), eq.(4.10) reduces to $(m\omega/\pi)^{1/2} \exp(-m\omega x^2)$, a fast decaying function with maximum at $x = 0$. On the other hand, in the limit $\beta \to 0$, $\rho_{h.p.}(x, x; \beta) \to 0$, leading to the expectation of plots which become wider and lower as the temperature increases. The physical explanation of this fact is that at higher temperatures it is easier to find population also in the eigenstates at some distances from the position $x = 0$, which corresponds to the minimum of the potential energy.

From a comparison of the two plots *a*) and *b*) in Fig. 4.1, the agreement between PIMC simulation and exact result can be fully appreciated; a superposition of the two plots actually would not reveal any significant discrepancies. The results *c*) and *d*) reported in Fig. 4.2 exhibit the temperature dependence in a way similar to the one of the preceding figure.

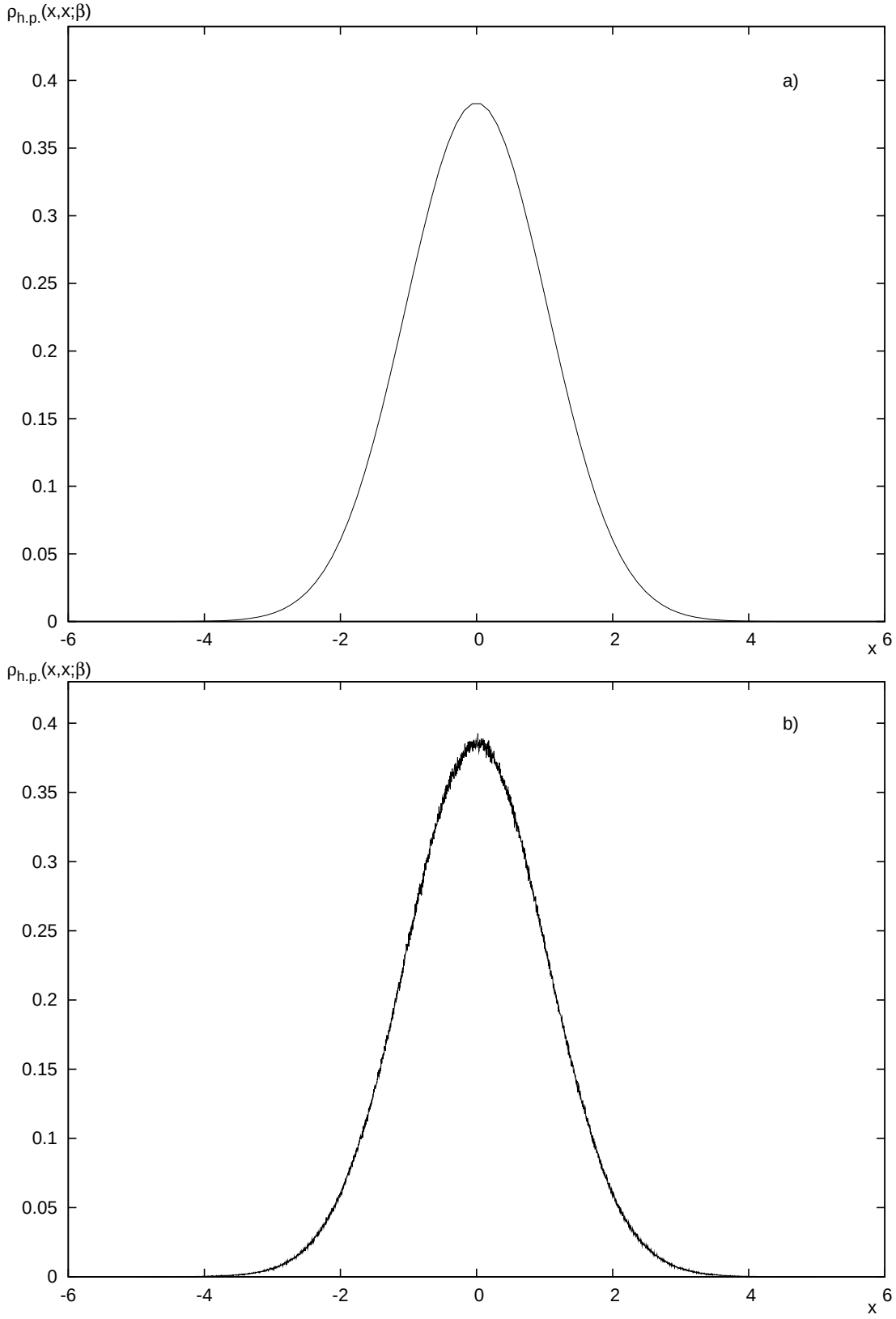

Figure 4.1: Density matrix plot for the harmonic potential ($m = 1$, $\omega = 1$). a) exact result (β=1); b) PIMC result at β=1. Distances are in a.u.

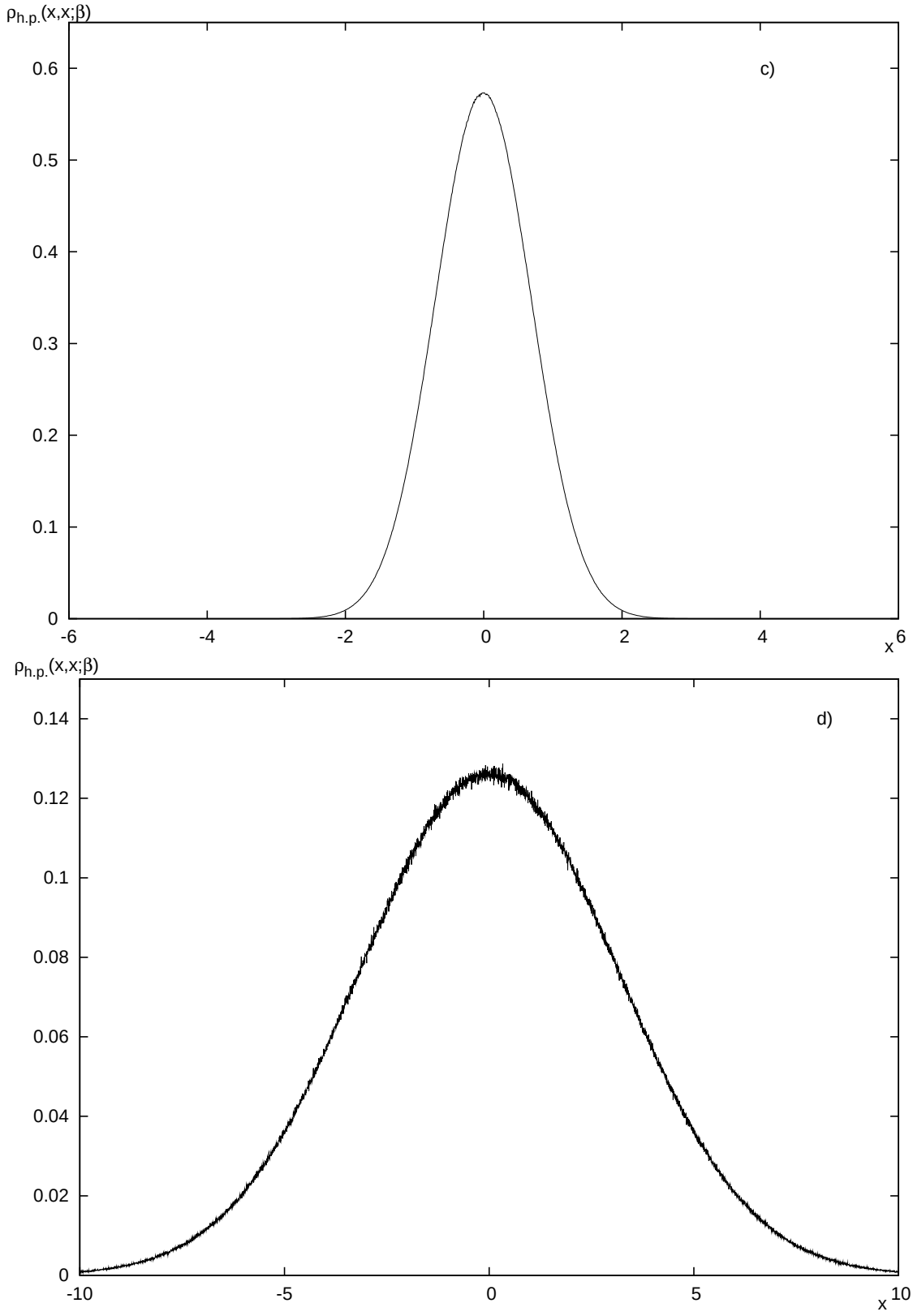

Figure 4.2: Density matrix plot for the harmonic potential ($m = 1, \omega = 1$) for different values of β. c) PIMC result (β=10); d) PIMC simulation (β=0.1). Distances are in a.u.

4.2.2 Off-diagonal elements

After the investigation of the populations, i.e. the diagonal elements of the thermal density matrix, the spotlight shifts to the calculation of the coherences, i.e. the off-diagonal elements of the matrix.
In the final formula, Eq.(3.83), of our approach, coherences should be introduced as far as possible without approximation. These matrix elements can be calculated by resorting to the Feynman-Kac relation [75, 76]

$$\rho(x, x'; \beta) = \rho_0(x, x'; \beta) \, \langle e^{-\int_0^\beta dt \, V[x(t)]} \rangle_{BRW} \tag{4.11}$$

with the free particle term (ρ_0) acting as a weight over all Brownian Random Walks (BRW), which start from x and end at x' after an imaginary time β.
Averaging over a huge number of paths is really a very time-consuming procedure. An attempt to simplify calculations leads to consider just a reduced number of the totality of the possible paths, trying to discard the minor contributions. The semiclassical approximation to the Feynman-Kac formula considers the straight path only, i.e.

$$\rho_{SC}(x, x'; \beta) = \rho_0(x, x'; \beta) \, e^{-\int_0^\beta dt V[x_{SC}(t)]} \qquad x_{SC} = \left(1 - \frac{t}{\beta}\right) x + \frac{t}{\beta} x' \tag{4.12}$$

This is surely a fast method of computing the thermal density matrix, but a careful valuation shows that such an approximation cannot be considered a reliable way of treating the problem. In fact, as shown in Fig. 4.3, the method does not work well at low temperatures, where the classical trajectory of minimum action is not the only important one, even nearby paths being influential.

Accurate off-diagonal element calculations, instead, can be obtained by means of the Feynman-Kac relation (4.11), that relies upon the idea of Brownian motion. To this aim, the concept of probability space is worth being touched upon briefly.
A probability space is defined by the triplet (Ω, B, P), where: Ω is a set whose elements ω serve as labels for the realisation of the stochastic process under investigation; **B** is the family of subsets of Ω satisfying the following conditions:

1. $\Omega \in \mathbf{B}$;

2. if $B_n \in \mathbf{B}$ (n=1,2,...) then $\bigcup_n B_n \in \mathbf{B}$;

3. if $B \in \mathbf{B}$ then $B^c \in \mathbf{B}$ ($B^c \equiv \Omega \backslash B$).

P is an additive function such that $0 \leq P(B) \leq 1 \forall B \in \mathbf{B}$, P($\Omega$)=1.
In other words, the elements $\omega \in \Omega$ are the results of the random process, $B \in \mathbf{B}$ are called events, while P(B) is the probability associated to the realisation of the event B. So, the function P is a measure of the measurable space (Ω,B) with the additional constraint that the total measure must be 1.
In the particular case of the Wiener probability space, $\Omega \equiv [0,1]$, $\mathbf{B}$ is the class of all the subsets of Ω which are Lebesgue measurable and P is the Lebesgue measure. This triplet describes the random choice of a number in the interval $[0,1]$.

Given a stochastic process $W(t,\omega)$, where $t \in T$ (T is a continuous ordered ensemble) and ω is a random variable in the probability space $(\Omega, \mathbf{W}, P)$, $W(t,\omega)$ is called a Brownian motion (or Wiener process) if [77]

$$\begin{cases} W(0,\omega) = 0 \\ W(t,\omega)(t>0) \text{ is Gaussian in } (\Omega,\mathbf{W},P) \text{ and } \forall t,h : t+h>0, \\ W(t+h,\omega) - W(t,\omega) \text{ has expectation value } 0 \text{ and variance } |h| \end{cases} \tag{4.13}$$

From these properties it follows that the Brownian motion is an additive process. According to the Feynman-Kac formula, the mean over a large number of such processes leads (after the evaluation of the imaginary-time integral) to the right estimation of the off-diagonal elements of the thermal density matrix.

There are two main routes to generate Brownian motion:

- the method due to Paley and Wiener [78], based on Fourier series expansion theory, which adopts complex functions and complex random variables;

- the second method, suggested by P. Levy [79] and based on the just mentioned additive feature of the Brownian motion, is actually the one adopted in this work. At each step, to the pre-existent $W(t,\omega)$ it is added a new term, composed of a random variable from a normal distribution of mean 0 and variance 1 ($\chi(t',\omega)$) and a factor ($\sigma(t'-t)$), which scales the variance depending on the distance between two adiacent points along the path

$$W(t',\omega) = W(t,\omega) + \sigma(t'-t)\chi(t',\omega) \tag{4.14}$$

  In this way a Brownian motion, characterized by the initial condition $W(0,\omega) = 0$, is obtained.

The Feynman-Kac relation requires that stricter conditions are met, in the sense that not only the starting point, but also the ending point of the Brownian motion is

fixed ($W(t_i,\omega) = x$, $W(t_f,\omega) = y$). A Brownian motion conditioned in a way like this is called a Brownian bridge or tied-down Brownian motion. The choice of the second construction method is explained by its direct generalization to the case of the Brownian bridge ($B(t,\omega)$)

$$B(t,\omega) = W(t,\omega) + x - \frac{t}{t_f}\{W(t_f,\omega) + x - y\} \tag{4.15}$$

$B(t,\omega)$ is a Gaussian process with mean

$$\frac{t_f - t}{t_f}x + \frac{t}{t_f}y \tag{4.16}$$

and covariance

$$\Gamma(t,s) = s\frac{t_f - t}{t_f} \quad (s < t) \tag{4.17}$$

At this point, it is interesting to study the harmonic potential density matrix obtained by the Brownian random walk technique, and to compare the results with those in fig.(4.3). Fig.(4.4) shows that the average over Brownian random walks leads to a really accurate evaluation of the off-diagonal elements $\langle x|e^{-\beta\hat{H}}|x = 0\rangle$ even in the range of low temperatures (the BRW curve is almost perfectly superimposed over the exact one). The oscillations present around the maximum could be easily averaged out by choosing a moderately higher number of paths onto which to perform the average in the Feynman-Kac formula.

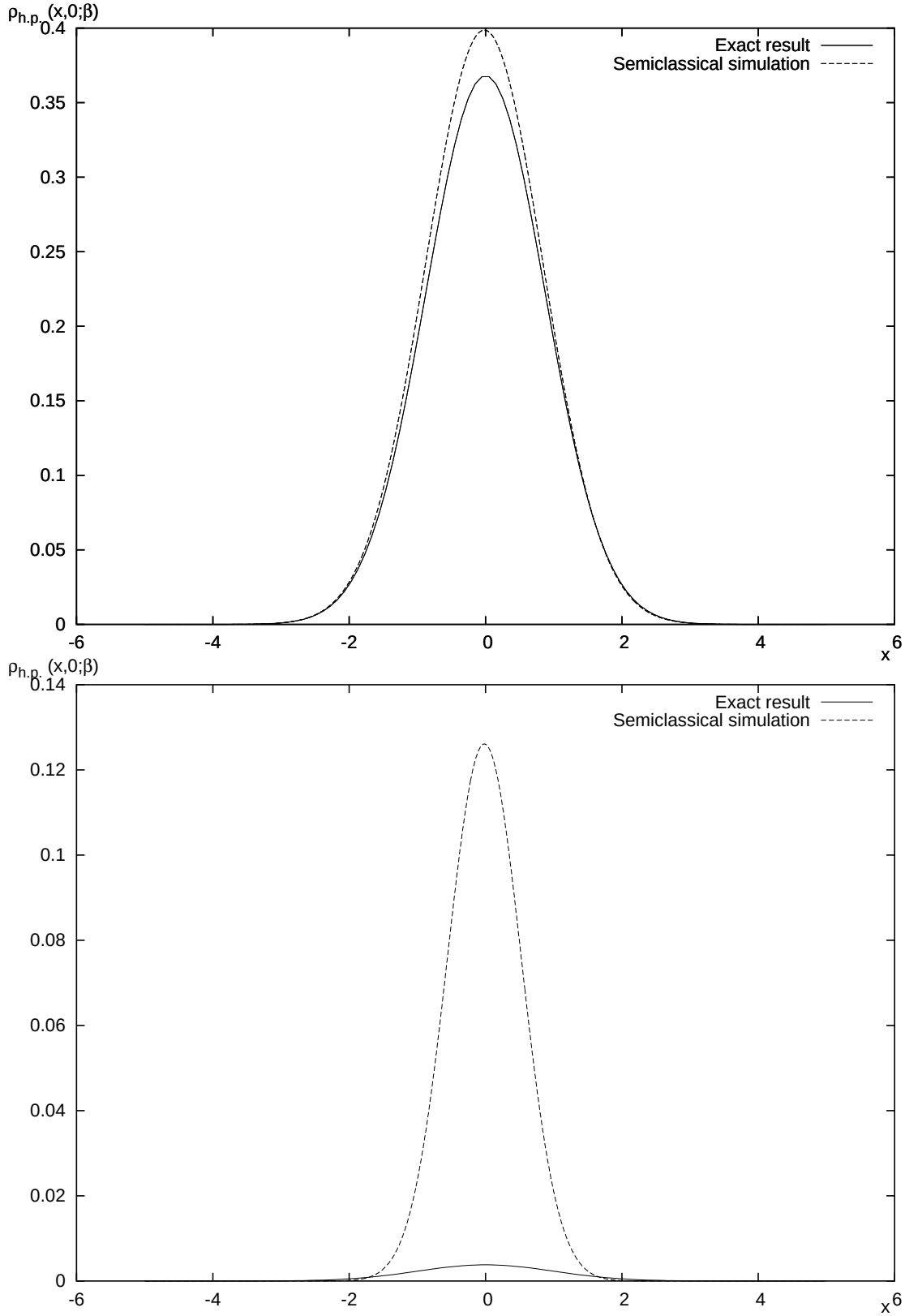

Figure 4.3: Semiclassical approximation for the harmonic potential ($m = 1$, $\omega = 1$) at different temperatures: $\beta = 1$ (upper figure) and $\beta = 10$ (lower figure)

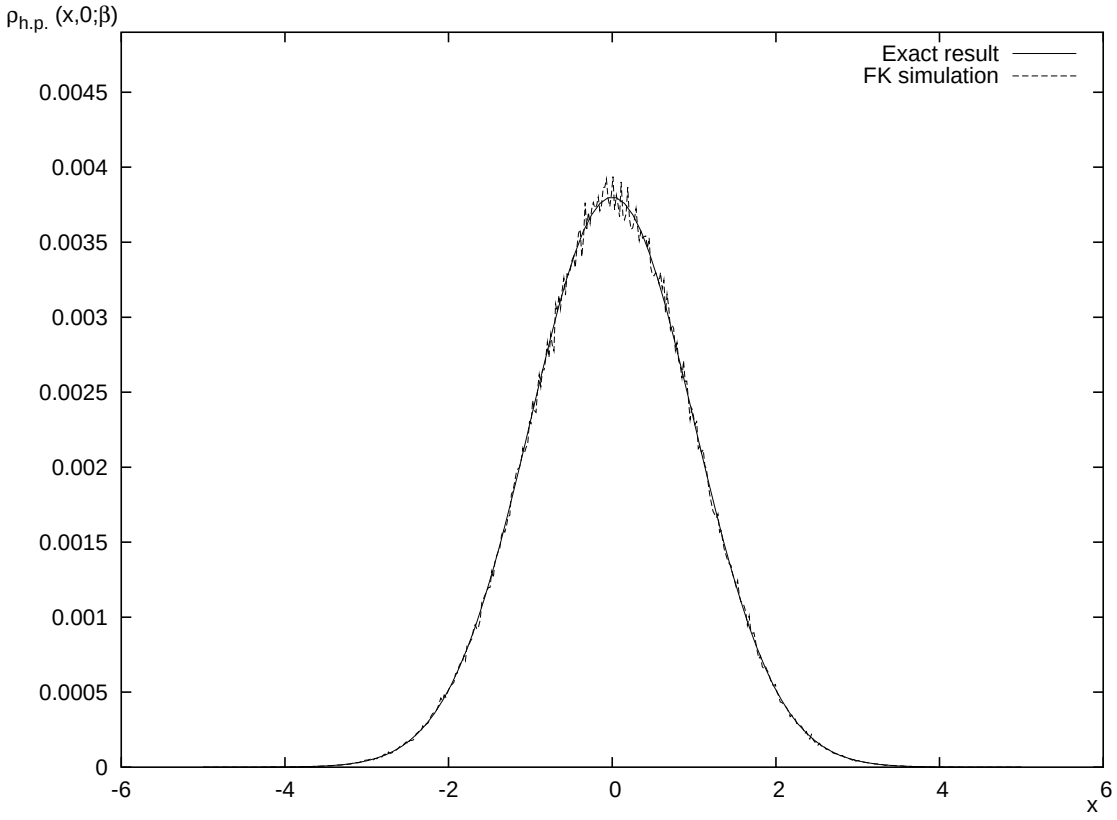

Figure 4.4: Comparison between exact result and BRW simulation based on the Feynman-Kac formula for the harmonic potential ($\beta = 10$, $m = 1$,$\omega = 1$). Distance in a.u.

4.3 The density matrix for the Eckart barrier

In view of its importance for the purposes of this thesis, we cannot get out of considering the case of the symmetrical Eckart barrier, defined by

$$V(x) = \frac{V_0}{\cosh^2(\alpha x)} \tag{4.18}$$

The shape of the barrier described by eq. (4.18), differently from the harmonic potential case, allows the particle motion to span an effetively infinite region. As a consequence, the probability of finding a particle far from the barrier is different from zero and the density matrix diagonal elements are expected to exhibit a minimum, in correspondence of the maximum of the barrier, and to be alike the free particle ones far from the barrier top. These features are, in fact, verifiable from the inspection of fig.(4.5). In the case of the Eckart barrier, it is interesting to study the results for the

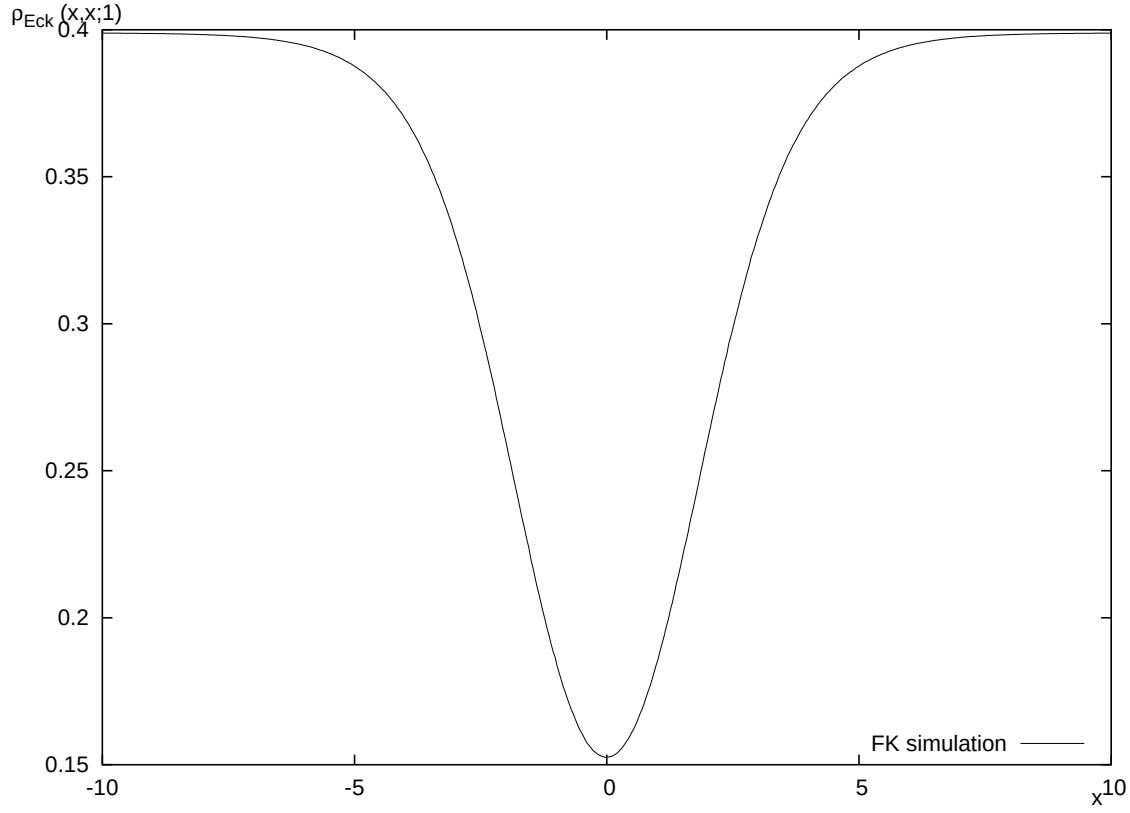

Figure 4.5: BRW simulation for the diagonal elements of the Eckart barrier ($\beta = 1,\ V_0 = 1,\ \alpha = 0.5$)

usual matrix element $\langle x|e^{-\beta \hat{H}_{E.b.}}|x = 0\rangle$ at different temperatures.

From eq. (4.3) one derives immediately the limit result

$$\lim_{\beta \to 0} \rho(x, x'; \beta) = \delta(x - x') \tag{4.19}$$

so that, in the high-temperature regime, a behavior characterized by a certain degree of localization around $x = 0$ is expected. On the other hand, in the low-temperature range, the loss of localization due to quantum effects, along with the fact that the Eckart barrier has its maximum at $x = 0$, should add up to determine a particular shape for the off-diagonal term. This is the rough explanation of the local minimum at $x = 0$ in fig.(4.6) which appears for sufficiently low temperatures

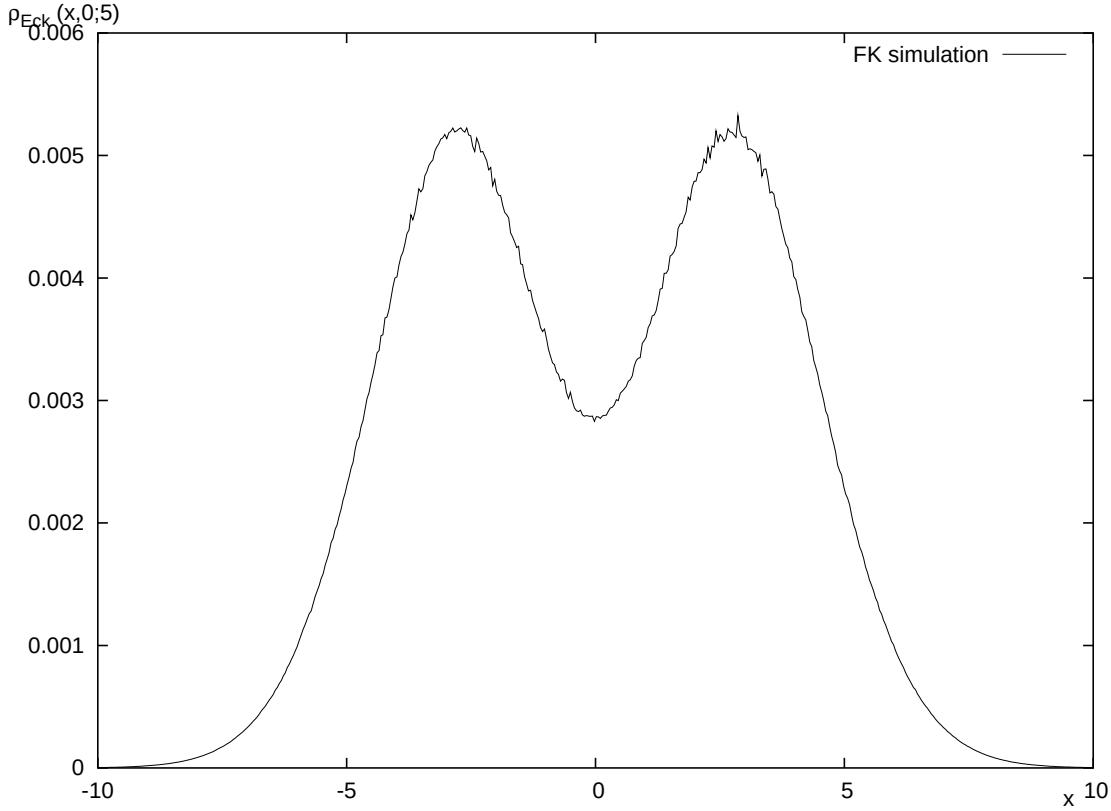

Figure 4.6: BRW simulation for off-diagonal density matrix elements of the Eckart barrier ($\beta = 5$)

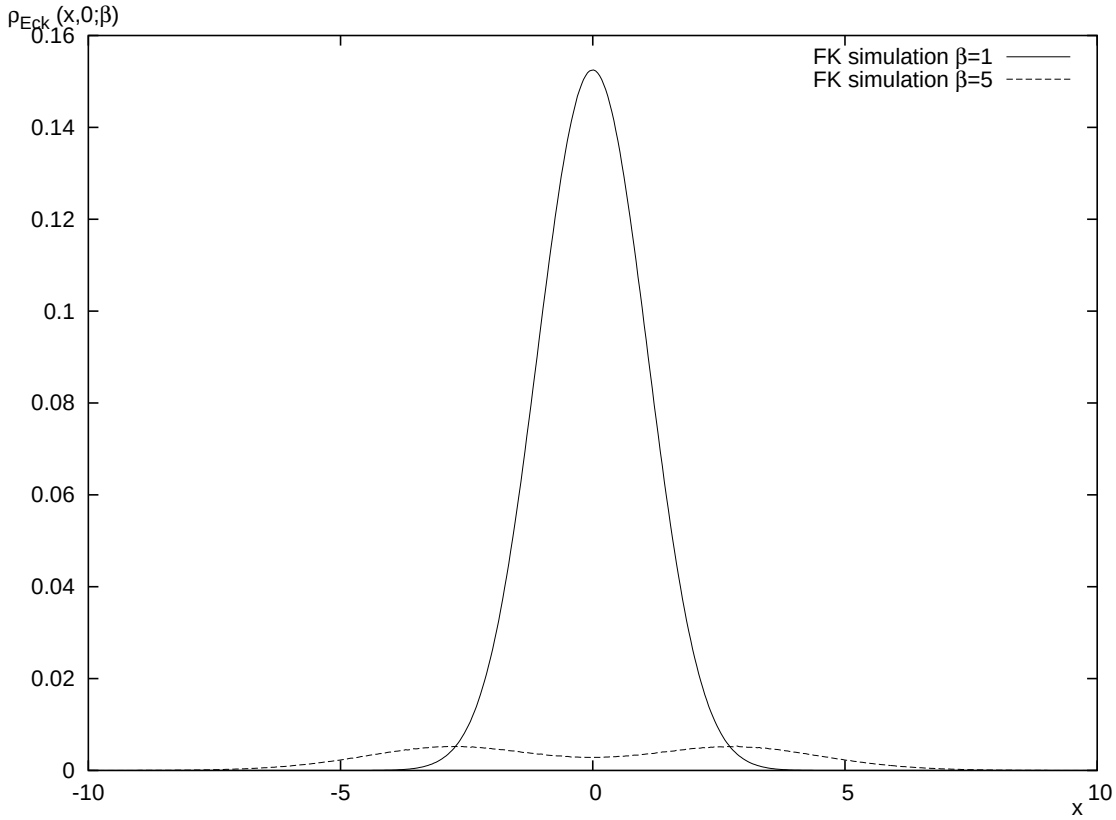

Figure 4.7: Comparison between off-diagonal density matrix elements of the Eckart barrier at different temperatures ($\beta = 1\,;\ \beta = 5$)

4.4 Confined systems

In the presence of confining infinite walls, the motion of the particle is restricted to occur within the region of finite potential; the quantum-mechanical trace of the thermal density operator, i.e. the canonical quantum partition function, is finite and the density operator is normalizable in the sense of eq.(4.4).

In the Feynman-Kac formula, the presence of confining walls is introduced by discarding the contribution of paths which go inside the walls, since that region of space is absolutely prohibited to the particle. Consequently, initial and final points must necessarily be localized within the allowed region, otherwise the matrix element equals zero.

Figure (4.8) refers to the matrix element $\langle x|e^{-\beta\hat{H}}|x = 0\rangle$ for a confined harmonic potential. As one can easily see, the position of the walls can be detected by noticing the exactly zero value of the density matrix outside their location.

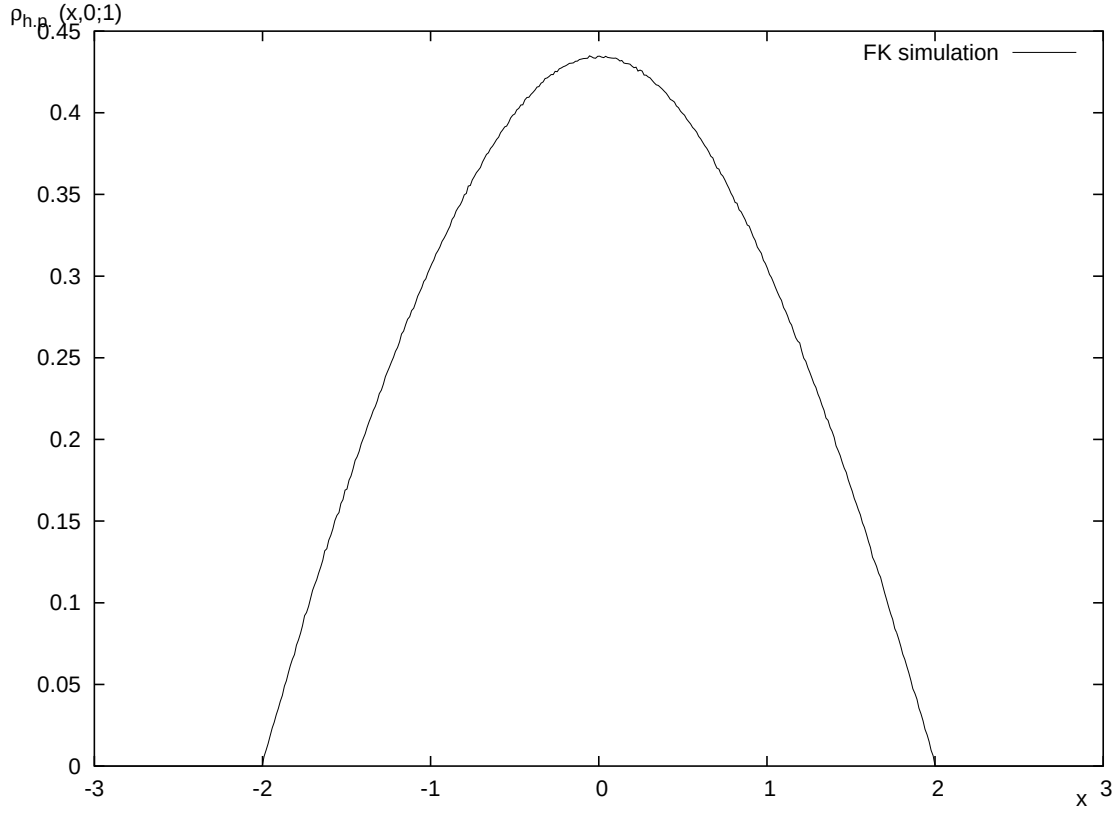

Figure 4.8: Confined harmonic potential. Walls at $x = \pm 2$. ($\beta = 1$)

The role of the temperature in both enhancing or damping the quantum effects is made explicit in fig. (4.9). The walls have been set a distance of 2 away from $x = 0$.

If $\beta \leq 1$, the off-diagonal density matrix element is still rather localized around $x = 0$, while at lower temperatures (for instance, $\beta = 5$), one notes highly non-local effects and the presence of interference phenomena.

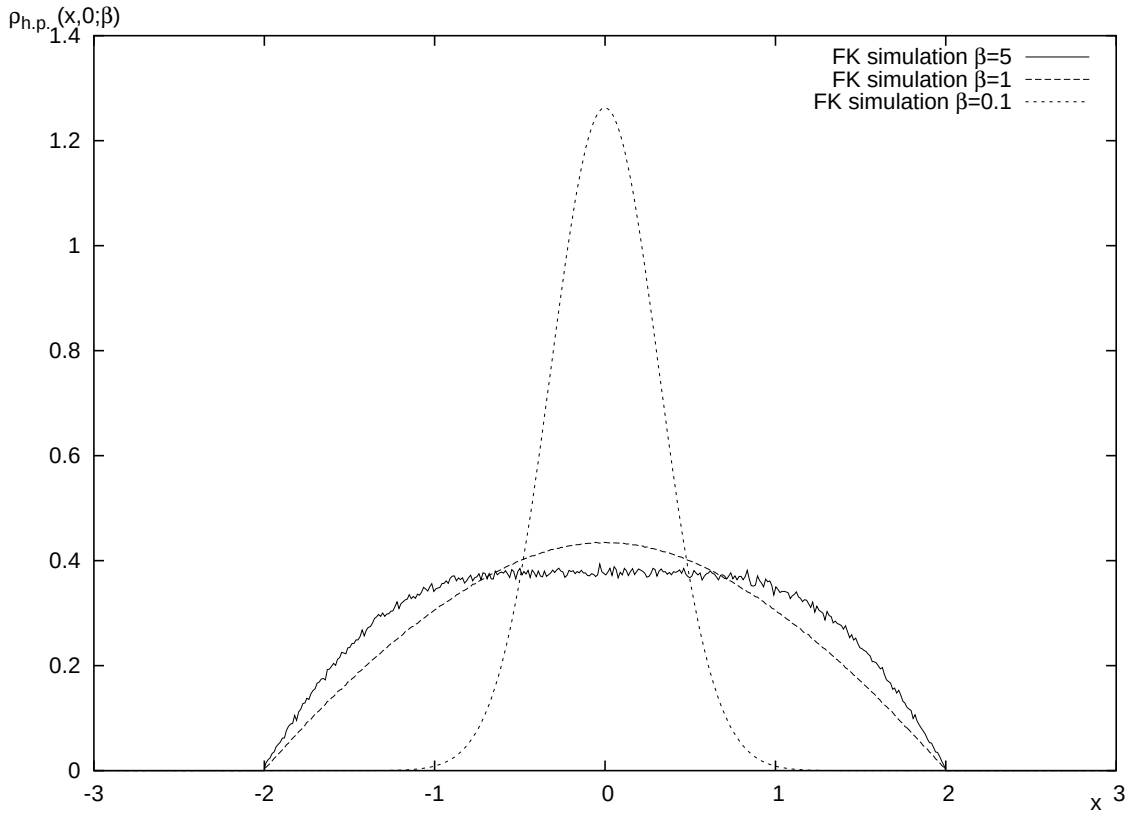

Figure 4.9: Comparison between confined harmonic potential matrix elements at different temperatures. Walls are at $x = \pm 2$.

4.5 A different algorithm for Boltzmann path integrals

Miller, Schwartz and Tromp proposed [15] a different kind of algorithm to deal with the matrix elements of the Boltzmann operator in the coordinate representation. Since the kinetic energy contribution to the exponent of the integrand (in the standard Feynman path integral expression) is quadratic, it is possible to incorporate the Gaussian factors into a proper set of integration variables and to scale all of them to have the limits $(0, 1)$. In this way, a Monte Carlo evaluation is straightforward.

The expression to evaluate is the following:

$$\langle x_N|e^{-\beta\hat{H}}|x_0\rangle = \left(\frac{m}{2\pi\beta}\right)^{1/2} \exp\left[-\frac{m}{2\beta}(x_N - x_0)^2\right] \times \tag{4.20}$$

$$\int_0^1 d\omega_1 \ldots \int_0^1 d\omega_{N-1} \exp\left[-\beta V(\omega_1, \ldots, \omega_N)\right] \tag{4.21}$$

$$\tag{4.22}$$

with

$$V(\omega_1, \ldots, \omega_N) = \frac{1}{N}\sum_{i=1}^{N} V\left(\frac{x_i + x_{i-1}}{2}\right) \tag{4.23}$$

It can be shown that the set of variables $\{x_i\}$ can be expressed in terms of the set $\{\omega_i\}$ by means of the recursion relation

$$x_i = \frac{N-i}{N-i+1}x_{i-1} + \frac{x_N}{N-i+1} + \left[\frac{2\pi\beta}{m}\frac{N-i}{N(N-i+1)}\right]^{1/2} z(\omega_i) \tag{4.24}$$

where $z(\omega)$ is the inverse of the integral function

$$w(z) = \int_{-\infty}^{z} dz' \exp(-\pi z'^2)$$

A simple rational approximation is available for $z(\omega)$ [68, 80]

$$z(\omega) = \sqrt{\frac{1}{2\pi}}\left(t - \frac{c_0 + c_1 t + c_2 t^2}{1 + d_1 t + d_2 t^2 + d_3 t^3}\right) + \varepsilon(p) \qquad 0 < p \leq 0.5 \tag{4.25}$$

where

$$\begin{aligned} p &= 1 - \omega \\ t &= \sqrt{\ln(p^{-2})} \\ |\varepsilon(p)| &< 4.5\ 10^{-4} \end{aligned}$$

and

$$\begin{array}{ll} c_0 = 2.515517 & d_1 = 1.432788 \\ c_1 = 0.802853 & d_2 = 0.189269 \\ c_2 = 0.010328 & d_3 = 0.001308 \end{array}$$

The approximation is valid for $0.5 \geq \omega < 1$. In the case $0 < \omega \leq 1$ the relation $Z(\omega) = -Z(1-\omega)$ stands.
The multiple integral over the variables $\{\omega_i\}$ is conveniently carried out by Monte Carlo techniques. So, the algorithm in question looks like the one described before, since the desired matrix element is given by a first factor which is the free particle matrix element and a second factor which is the average of the exponential over the random path generated by means of the recursion relation (4.24) and the rational approximation (4.25). Obviously, the correct result would require to average over an infinite number of simulations, but it is a fact that different applications need different accuracy.
The procedure of changing the integration variables so as to incorporate part of the integrand is an example of importance sampling. Since the harmonic potential gives rise to a contribution which is quadratic in the integration variables $\{x_i\}$, it can be factorized out, leading to

$$\langle x_N | e^{-\beta \hat{H}} | x_0 \rangle = \langle x_N | e^{-\beta \hat{H}_0} | x_0 \rangle \langle e^{-\beta V} \rangle \tag{4.26}$$

where $\hat{H}_0$ is the harmonic potential Hamiltonian, for which the analytic expression of the matrix element has been found previously. This procedure, of course, results to be very useful in the case of additional degrees of freedom, many of which are oscillators: the harmonic part of the potential can be incorporated explicitly, resulting in a huge simplification of the calculations and a drastic reduction of computational time.

4.6 Step 2: dynamics and integration

From eq.(3.83) one sees explicitly that its implementation involves the knowledge of $p_{cl}(p,q)$ along with that of its partial derivatives with respect to the initial conditions. Two different problems arise due to this quest: first of all, the dynamics of the particle must be evolved for a sufficiently long time from given initial conditions (p,q) and, secondly, an appropriate computational procedure must be employed to get the partial derivatives. The latter task is easily accomplished by means of central finite difference formulae: the finite difference, in fact, is the discrete analogue of the derivative. Realizing the former demand, instead, requires to set up an integration scheme. One of the most common integration procedures in molecular dynamics (actually the one adopted in this work) is the velocity-Verlet algorithm [81].
The velocity-Verlet algorithm, an evolution of the previous Verlet algorithm [82, 83], is a scheme based on two (one forward and one backward in time) third-order Taylor expansions for the trajectory $\mathbf{r}(t)$. The great advantage of this algorithm is that positions, velocities and accelerations at time $t+\Delta t$ are obtained from the same quantities at time t, according to the following scheme:

$$\begin{aligned}
\mathbf{r}(t+\Delta t) &= \mathbf{r}(t) + \mathbf{v}(t)\Delta t + \frac{1}{2}\mathbf{a}(t)\Delta t^2 \\
\mathbf{v}(t+\Delta t/2) &= \mathbf{v}(t) + \frac{1}{2}\mathbf{a}(t)\Delta t \\
\mathbf{v}(t+\Delta t) &= \mathbf{v}(t+\Delta t/2) + \frac{1}{2}\mathbf{a}(t+\Delta t)\Delta t
\end{aligned}$$

$\mathbf{a}(t+\Delta t)$ can be calculated from $\mathbf{r}(t+\Delta t)$, through the motion equation $\mathbf{a}(t+\Delta t) = -\frac{1}{m}\nabla V(\mathbf{r}(t+\Delta t))$. The step involving $\mathbf{v}(t+\Delta t/2)$ is necessary, so positions, velocities and accelerations are stored simultaneously at the same time, but never at two different times.

Once the dynamics has been evolved, the problem of the evaluation of the complex error function present in eq.(3.83) arises. To come through this issue, an algorithm suggested by W.Gautschi [84, 85] is adopted. This is based on the computation of the complex function

$$w(z) = e^{-z^2}\left[1 + \frac{2i}{\sqrt{\pi}}\int_0^z e^{t^2}\,dt\right], \tag{4.27}$$

which is easily expressed in terms of the searched complex error function

$$w(z) = e^{-z^2}\left[1 - erf(-iz)\right] \tag{4.28}$$

Gautschi's algorithm is characterized by an extremely high degree of precision (it is exact to the tenth decimal digit), but it was written for the first quadrant only.

The extension to the other quadrants, however, is readily obtained. In fact, in the notation of ref. [68],

$$w(-z) = 2\,e^{-z^2} - w(z) \qquad w(z^*) = [w(-z)]^* \tag{4.29}$$

The complex integral function

$$F(z) = e^{-z^2} \int_0^z e^{t^2}\, dt, \tag{4.30}$$

known as Dawson's integral, can be calculated by means of the approximation

$$F(z) = \lim_{h\to 0} \frac{1}{\sqrt{\pi}} \sum_{n\ odd} \frac{e^{-(z-nh)^2}}{n} \tag{4.31}$$

which is characterized by an increasing accuracy with decreasing h.

Coming back to discuss eq.(3.83), there is an additional point, a not negligible one, connected with the range of integration, which is not limited, along with the fact that $\lim_{z\to\infty} erf(z) = 1$: thus, the p-integration involved can be argued to lead to possible problems. To "cure" this trouble, an appropriate smoothing factor has been introduced, transforming the p-integral as follows:

$$\lim_{\varepsilon\to 0} \int_{-\infty}^{+\infty} dp\, p\, e^{-ipx}\, e^{-\varepsilon|p|} \frac{p_{cl}}{|p_{cl}|}\, erf\left[\frac{|p_{cl}|}{\sqrt{2i\dfrac{\partial p_{cl}}{\partial p}\dfrac{\partial p_{cl}}{\partial x}}}\right] \tag{4.32}$$

so that the integration must be performed under the limit $\varepsilon \to 0$. The convergence factor $e^{-\varepsilon|p|}$ acts as a sort of adiabatic switching (a technique adopted to describe interactions in many fields, such as solid state physics or quantum electrodynamics), in which the role of the dynamics (i.e. the importance of the interactions) is switched on slowly between $p \to -\infty$ and $p = 0$ and switched off slowly between $p = 0$ and $p \to \infty$. In other words, momenta which are too large are not influenced in a significant way by the potential and cancel out mutually with those opposite in sign. The Taylor expansion of the term $e^{-\varepsilon|p|}$ keeps only the linear term for ε sufficiently small, so that the search for the requested limit is conjectured to be feasible by linear extrapolation for suitable ε. The actual magnitude of ε needed was found to depend on the type of potential under examination.

Anyway, from a computational point of view, an accurate evaluation of integrals often means to face some problems. Three of the most common troubles are related to the following occurrences:

1. the integrand is discontinuous in the integration range;

2. the integrand has some singularities;

3. the range of integration is infinite.

In most cases, these problems cannot be dealt with directly by numerical techniques and, consequently, some preparatory manipulation of the integrand is required. In the first case, which, anyway, is not of interest in our case, the position of the discontinuities must be found and the integral split into a sum of two or more integrals, the ranges of which avoid the discontinuities.
The second point (i.e. the presence of singularities) is most frequently tackled by resorting to changes of variable, integration by parts or splitting of the integral. Actually, in our case this problem is intrinsically avoided since the possible presence of caustic points is embedded in the error function, which is well-behaved.
Finally, the problem of the infinite range of integration can be treated by means of particular methods (for instance use of Gauss-Laguerre and Gauss-Hermite formulae) or, sometimes, by means of a preliminar treatment fit to reduce the range of integration within finite limits.

There are many quadrature techniques able to provide accurate estimations also to difficult integration problems. However, as a general rule, it is known that even the best quadrature methods meet with difficulties as the functions involved vary very rapidly due to small changes in the independent variable, i.e. in the case of highly oscillatory integrands.
To deal with the oscillatory integrand which characterizes the p-integration in formula (3.83), we have resorted to the Filon's method [69]. To reduce the overall number of calculations required, there exist some adaptive methods (like Patterson's technique), able to thicken the intervals only in those regions where the function is changing very rapidly.

Filon's technique can successfully be applied to integrals of the form $\int_a^b f(x)\cos kxdx$ and $\int_a^b \sin kxdx$. For instance, considering the first of the two integrals above, by the method of undetermined coefficients an approximation can be obtained. Let

$$\int_0^{2\pi} f(x)\cos xdx = A_1 f(0) + A_2 f(\pi) + A_3 f(2\pi) \tag{4.33}$$

Requiring that this should be exact for $f(x) = 1, x, x^2$

$$\int_0^{2\pi} f(x)\cos xdx = [2f(0) - 4f(\pi) + 2f(2\pi)]/\pi \tag{4.34}$$

More general results can be developed as follows:

$$\int_a^b f(x)\cos kx dx = h\left[A\{f(x_n)\sin kx_n - f(x_0)\sin kx_0\} + BC_e + DC_0\right] \tag{4.35}$$

$$\int_a^b f(x)\sin kx dx = h\left[A\{f(x_0)\cos kx_0 - f(x_n)\cos kx_n\} + BS_e + DS_0\right] \tag{4.36}$$

where $h = (b-a)/n$, $q = kh$ and

$$\begin{aligned}
A =& \left[q^2 + q\sin 2q/2 - \sin^2 q\right]/q^3 \\
B =& 2\left[q(1+\cos^2 q) - \sin 2q\right]/q^3 \\
D =& 4\left[\sin q - q\cos q\right]/q^3 \\
C_0 =& \sum_{i=1,3,5}^{n-1} f(x_i)\cos kx_i \\
C_e =& \left[f(x_0)\cos kx_0 + f(x_n)\cos kx_n\right]/2 + \sum_{i=2,4,6}^{n-2} f(x_i)\cos kx_i
\end{aligned}$$

It can be seen that C_0 and C_e involve odd and even sums of cosine terms. S_0 and S_e are similarly defined with respect to sine terms.
It is important to note that Filon's method, when applied to functions of the form given above, usually gives better results than Simpson's method, the number of intervals being equal.
It is sometimes useful (even though not adopted in this work) to use approximations to the expressions for A, B, C, and D given above, by expanding them in a series of ascending powers of q. This leads to the following results:

$$\begin{aligned}
A =& 2q^2\left(q/45 - q^3/315 + q^5/4725 + \ldots\right) \\
B =& 2\left(1/3 + q^2/15 + 2q^4/105 + q^6/567 + \ldots\right) \\
D =& 4/3 - 2q^2/15 + q^4/210 - q^6/11340 + \ldots
\end{aligned}$$

When the number of intervals becomes very large, h and q become small. As q tends to zero, A tends to zero, B tends to 2/3 and D tends to 4/3. Substituting these values into the formula for Filon's method, it can be shown that it becomes equivalent to the Simpson's rule.

Chapter 5

Reaction rates and conclusions

The utilization of all the techniques analysed in the previous chapter allows in principle the complete and final application of the approach advocated in this thesis. After having presented some results relative to the thermal density matrix and the few cases where an analytical solution for the real-time propagator is possible, we get ready to move onto models where the kinetics is associated with simple one-dimensional barriers, in particular truncated parabola and Eckart barrier (symmetrical and asymmetrical).

The main difficulties met with the simulations lie in the choice of an adequate discretization of the phase space, (in turn related to the accuracy of the integration algorithm) and the determination of the integration ranges.
The integration bounds are essentially controlled by the density matrix element and the convergence factor $e^{-\varepsilon|p|}$, for the x- and p-integration respectively. As a matter of fact, the matrix element $\langle x|e^{-\beta\hat{H}}|x=0\rangle$ drops to zero for x sufficiently far from $x=0$, while $pe^{-\varepsilon|p|}$ becomes negligible for sufficiently large values of p (depending on the value of ε), so that the individuation of suitable bounds for the integrations is not so difficult.
Calculations are necessarily performed for different values of ε and the final result follows by extrapolation. The smaller ε, the larger the integration range in the p-variable. Considering that the Filon's algorithm is the truly time-consuming step in the procedure, this aspect represents the real bottleneck to overcome: in particular, we have found that the need of small ε values is more marked for highly asymmetrical barriers.

5.1 The truncated parabolic barrier

The first kind of one-dimensional barrier investigated in this thesis is the truncated parabolic barrier, i.e. a barrier having parabolic shape in the positive region of the potential, which becomes abruptly zero out of that region. Explicitly,

$$V(x) = \frac{E^*}{a^2}(x^2 - a^2)\Theta(a - |x|) \tag{5.1}$$

where E^* is the height of the barrier and $2a$ its width. Fig. (5.1) is a plot of the potential corresponding to $E^* = 4$, $a = 2$ (in arbitrary units).

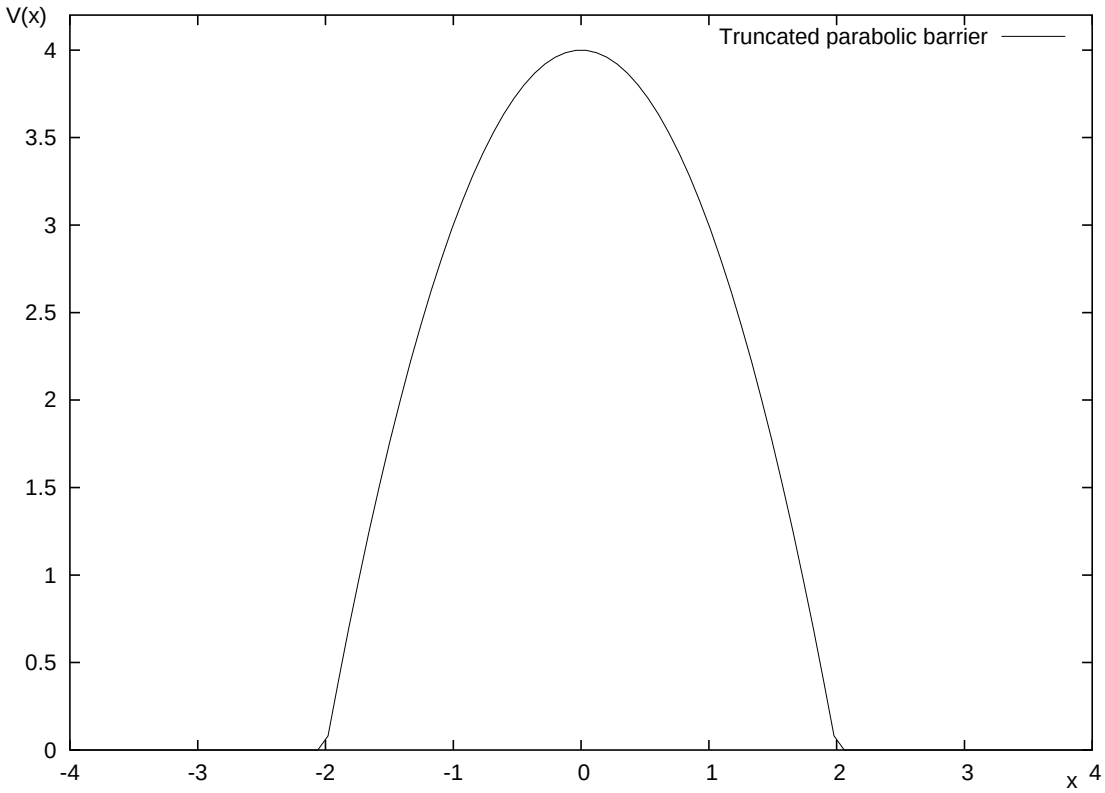

Figure 5.1: Truncated parabolic potential $V(x) = (4 - x^2)\Theta(2 - |x|)$.

Expressions for the tunnel-effect correction in the case of a truncated parabola of given curvature ω_B have been proposed by Bell [64, 86, 87]. These are in accordance with previous results by Bigeleisen [88] (their validity, actually, extends to a broader range).
The approach consists in choosing a permeability function $G(E)$ for the barrier, satisfying some conditions that hold true for an exact solution:

- to reduce to the WKB approximation at low energies ($E \ll E^*$);

- to approach the value $G(E^*) = 1/2$.

A simple function with these characteristics, able to give good results also for energies next to the barrier top E^*, is

$$G(E) = [1 + \exp(\beta' y)]^{-1} \qquad y = 1 - E/E^* \tag{5.2}$$

In eq.(5.2) β' is a parameter that depends on the energy E, the mass of the particle and the width of the barrier:

$$\beta' = \pi a (2mE)^{1/2} \tag{5.3}$$

In the cases of chemical interest (i.e. when the ratio between the energy E and thermal energy β^{-1} is less than β'), the quantum correction found by Bell is

$$\Gamma = \frac{1}{2} u / \sin\left(\frac{1}{2}u\right) \qquad (u = \beta\omega_B) \tag{5.4}$$

which can be expanded as

$$\Gamma = 1 + \frac{u^2}{24} + \frac{7u^4}{5760} + \ldots \qquad (u < 2\pi) \tag{5.5}$$

a result equivalent, in the low-order terms, to that obtained by Wigner through a general treatment for the passage of a particle over a multidimensional energy surface.

Simulations relative to the truncated-parabola potential were performed by the present approach for different temperatures, assuming the parabola parameters (in a.u.) $2a = 4$, $\omega_B = 0.95493$ and the maximum of the potential $E^* = 1.82378$, i.e. the values employed by Bell. The values reported in Table (5.5) have been obtained by the basic result $k(T)Q = \Gamma e^{-\beta E^*}/2\pi\beta$ (see sec. 3.3.1). The validity of eq.(5.4), in the range of energies considered, shows that, for truncated-parabola barriers which are wide compared to their height, the quantum correction reduces to that of the simple parabolic barrier.

u	Γ_{Bell}	Γ_{calc}
0.1	1.0041	1.00184
0.5	1.01049	1.01355
1.0	1.04288	1.04818

Table 5.1: Results for the truncated-parabola potential. Bell's results are based on eq.(5.5)

5.2 The Eckart barrier

A role similar to that of the truncated parabolic barrier is played by the Eckart barrier, a potential which changes smoothly and continuously, proposed by C. Eckart in 1930 [89]. Eckart evaluated the probability, $\kappa(E)$, of crossing the barrier for a particle of energy E, while Johnston [90] introduced statistical effects performing numerical integration of the transmission probability $\kappa(E)$ over a Boltzmann distribution of incident particles (see below).

The potential relative to the Eckart barrier can be written as

$$V = \frac{Ay}{1-y} - \frac{By}{(1-y)^2} \tag{5.6}$$

with

$$y = -\exp(2\pi x/L) \tag{5.7}$$

A, B and L (a characteristic length) are adjustable parameters.

By denoting with V_1 the separation between the maximum value and $\lim_{x\to-\infty} V(x)$, V_2 the analogous separation between the maximum and the $V(x)$ value as $x \to +\infty$ and F^* the second derivative of the function at its maximum, the following relations are easily derived:

$$V_1 = (A+B)^2/4B \tag{5.8}$$

$$V_2 = (A-B)^2/4B \tag{5.9}$$

$$F^* = -\frac{\pi^2(A^2-B^2)^2}{2L^2B^3} \tag{5.10}$$

$$\tag{5.11}$$

Obviously, the case of the symmetrical barrier corresponds to $A = 0$.
A particle of mass m and energy E which approaches the barrier is characterized by

$$\nu^* = \frac{1}{2\pi}(-\frac{F^*}{m})^{1/2}, \qquad u^* = h\nu^*/kT \tag{5.12}$$

$$\alpha_1 = 2\pi V_1/h\nu^* \tag{5.13}$$

$$\alpha_2 = 2\pi V_2/h\nu^* \tag{5.14}$$

$$\xi = E/V_1 \tag{5.15}$$

$$\tag{5.16}$$

The transmission probability through the barrier is found by solving the Schrödinger's equation, with the following result

$$\kappa(E) = 1 - \frac{\cosh 2\pi(a-b) + \cosh 2\pi d}{\cosh 2\pi(a+b) + \cosh 2\pi d} \tag{5.17}$$

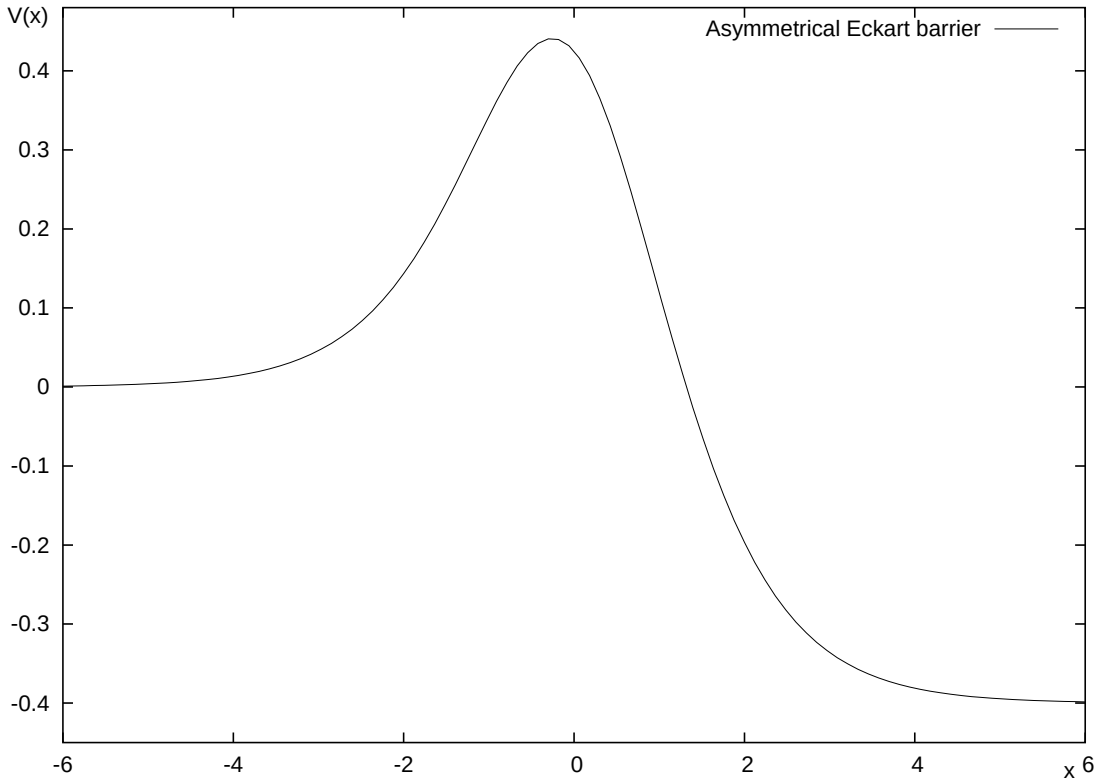

Figure 5.2: A typical shape of asymmetrical Eckart barrier ($A = 0.4$, $B = 2.5$, $L = 5$, arbitrary units).

where

$$2\pi a = 2(\alpha_1 \xi)^{1/2} \left(\frac{1}{\alpha_1^{1/2}} + \frac{1}{\alpha_2^{1/2}} \right)^{-1} \tag{5.18}$$

$$2\pi b = 2[(1+\xi)\alpha_1 - \alpha_2]^{1/2} \left(\frac{1}{\alpha_1^{1/2}} + \frac{1}{\alpha_2^{1/2}} \right)^{-1} \tag{5.19}$$

$$2\pi d = 2[\alpha_1 \alpha_2 - (2\pi)^2/16]^{1/2} \tag{5.20}$$

Whenever d is imaginary, the term $\cosh 2\pi d$ in eq. (5.18) transforms into $\cos 2\pi|d|$. The kinetic constant is directly related to $\kappa(E)$; in particular, the ratio between the quantum mechanical barrier crossing rate and the classical mechanical prediction is

$$\Gamma^* = \frac{R_{qu}}{R_{cl}} = \frac{\exp(V_1/kT)}{kT} \int_0^\infty \kappa(E) \exp(-E/kT) dE \tag{5.21}$$

5.2.1 Symmetrical Eckart barrier

It is easily verified that the symmetrical Eckart barrier can also be expressed in an alternative form. Starting from eq. (5.6) with $A = 0$ (symmetrical barrier) it follows that

$$V = \frac{Be^{\alpha}}{(1+\alpha)^2}, \qquad \alpha = \frac{2\pi x}{L} \tag{5.22}$$

After rearrangement, this expression yields

$$V = \frac{B}{(e^{\alpha/2} + e^{-\alpha/2})^2} = \frac{B}{4[\cosh(\alpha/2)]^2} = \frac{B}{4}[sech(\alpha/2)]^2 \tag{5.23}$$

and, finally,

$$V(x) = V_0 \, \mathrm{sech}^2(x/L) \tag{5.24}$$

where L is a new length parameter. The next comments are facilitated by the introduction of the following two dimensionless parameters:

$$\alpha = 2\pi V_0/\omega_B \tag{5.25}$$

$$u = \beta\omega_B \tag{5.26}$$

where $\omega_b^2 = 2V_0/(mL^2)$, m being the mass of the crossing particle.

Fig.(5.3) summarizes effectively many points discussed in the previous chapters. The full line (label c) corresponds to the exact solution as calculated by Johnston [90], while the classical transition state theory result is that represented by the straight line d. The increasing deviation of the classical prediction from the exact solution as the temperature decreases (i.e. when quantum effects become more and more important) should be noticed. The three dotted and/or dashed lines labeled e, b, f correspond to estimates obtained by means of different approximations for the dynamical z factor introduced by Voth, Chandler and Miller [17]. They refer specifically to free particle (e), parabolic barrier (b) and semiclassical (f) estimates of the z factor. Finally, the results plotted by adopting a parabolic-barrier approximation for both thermal and dynamical factors (line a), put in clear evidence the inadequacy of a model entirely based on the standard parabolic-barrier behavior.

The approach elaborated in this thesis has been tested by performing calculations on the symmetrical Eckart barrier with values for the parameters corresponding to the maximum of the potential and the correspondent curvature equal to those (V_0, ω_B) adopted for the truncated parabolic barrier previously analysed (see Fig.(5.4)). The results have been obtained for values of the parameters α and u, $\alpha = 12$ and $u \in [2, 6]$, identical to those of Fig. (5.3).

The application of the approach leads to results in good agreement with both Bell (truncated parabolic barrier) and Johnston (exact quantum mechanical solution).

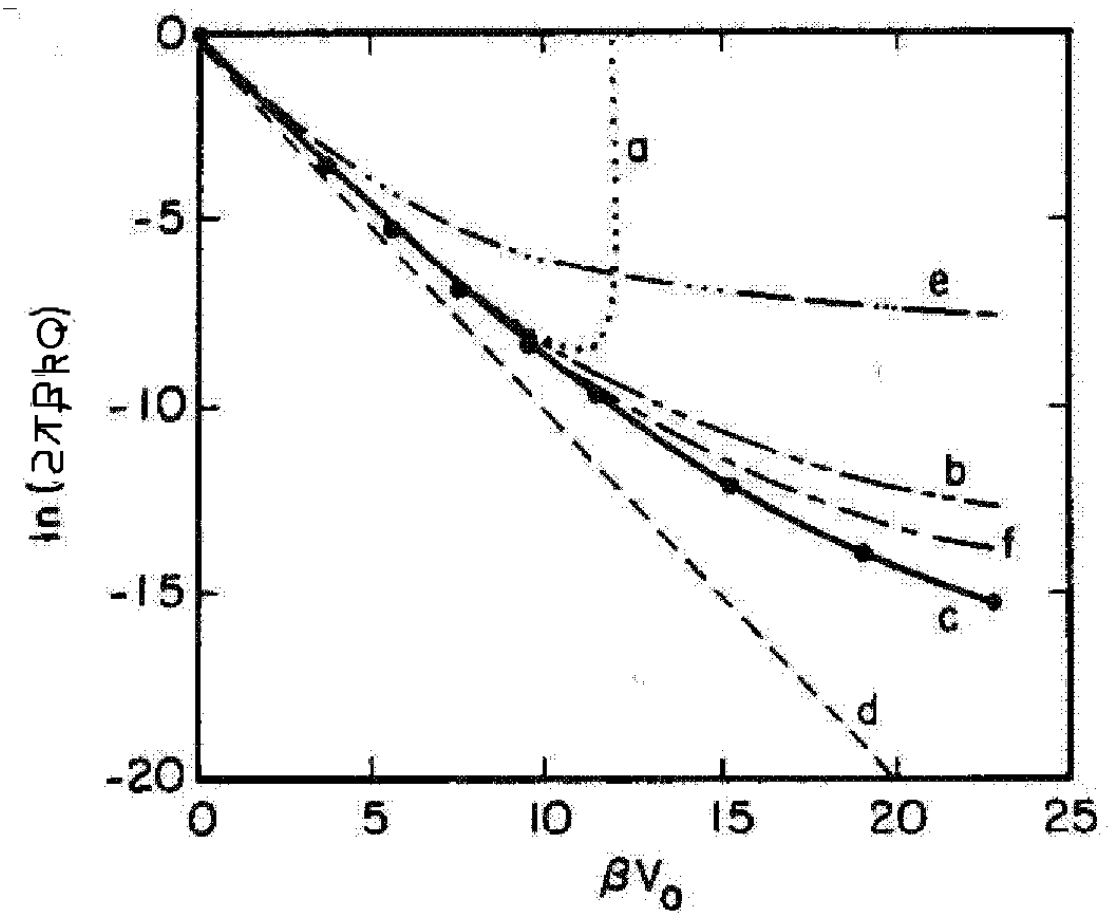

Figure 5.3: Comparison between kinetic constant results obtained by different approaches for a symmetrical Eckart barrier. The plots refer to $\alpha = 12$ and $u \in [2, 12]$ (see text).

The philosophy at the basis of the long-standing ideas pioneered by W. H. Miller, P. Pechukas et al., in particular the separation between thermal and dynamical effects, suggests itself as a satisfying alternative to the ineluctability of full quantum scattering calculations.
The fact that the approach works well in the cases tested induces to believe that it can be extended to different and even more realistic potentials, such as, for instance, the asymmetrical Eckart barrier, which is the topic briefly touched in the next subsection.

5.2.2 Asymmetrical Eckart barrier

Our study concerning an asymmetrical Eckart barrier has been simulated for values of the involved parameters (see eq. (5.12)) $\alpha_1 = 4$ and $\alpha_2 = 8$, with the cur-

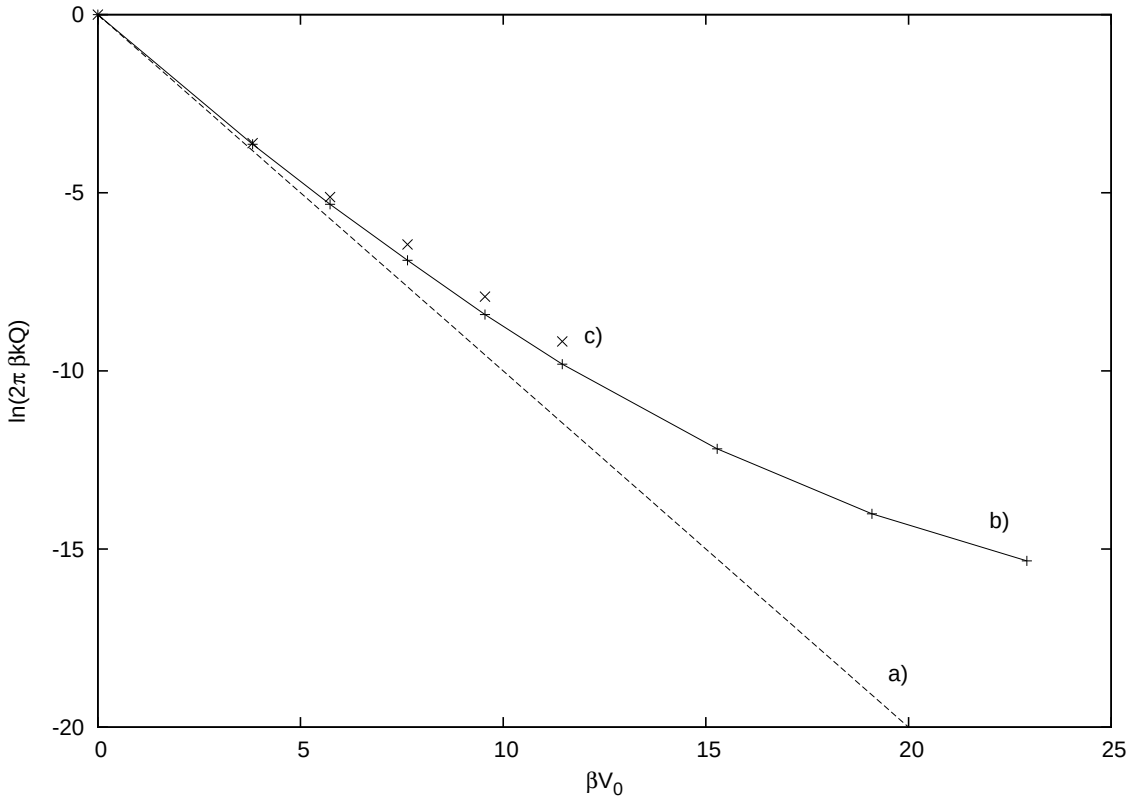

Figure 5.4: Test for a symmetrical Eckart barrier: a) Classical result; b) Exact quantum mechanical result derived by Johnston [90]; c) our approach.

vature at the maximum kept identical to that assumed in the study of both truncated parabola and symmetrical Eckart barrier ($\omega_B = 0.954929 a.u.$). Explicitly, $V_1 = 0.608\, a.u.$ and $V_2 = 1.216\, a.u.$
The simulations, performed in the temperature range $u \in [2, 8]$, lead to the results collected in Table (5.2.2).

u	$ln(2\pi\beta kQ)_{q.m.}$	$ln(2\pi\beta kQ)_{calc.}$
2	-1.050	-1.064
4	-1.889	-1.884
6	-2.550	-2.207
8	-3.069	-2.687

Table 5.2: Kinetic constant results for the asymmetrical Eckart barrier ($\alpha_1 = 4$, $\alpha_2 = 8$). Second column: exact quantum mechanical findings by Johnston [90]. Last column: estimates according to the approach discussed in this thesis.

Specifically, our results have been extrapolated from simulations which required ε values so small as $\varepsilon = 0.005$ and $|p_{max}| = 3000$ as cutoff for the momenta involved. Again, the parabolic barrier approximation overestimates the correct rate, with better behavior at higher temperatures.

5.3 Conclusions and perspectives

A first point on which to dwell is the role played by statistical and dynamical effects in the estimation of rate constants. The thermal density matrix, being calculated essentially without approximations, cannot be responsible for the discrepancies observed between the results obtained by our approach and the reference ones. Thus it is evident that blame for the overestimation cannot but lay in the insufficient appreciation of dynamics.
The expectation that dominant features of quantum dynamics involved in barrier crossing can be grasped looking at the exactly soluble case of the parabolic barrier has largely bonafide motivation. Actually what we see is that the specificity of a given barrier becomes less influential only at sufficiently high temperature, an indication that there are more specific quantum effects left out from our analysis. These few considerations suggest also that deficiencies caused by the introduction in the treatment of poor or insufficient dynamical approximations could probably be compensated by use of modified parabolic potentials involving temperature-dependent parameters. To this regard, it is worth of mention that effective potentials of this type have been employed in various physical contexts.
The truncated parabolic barrier, along with the symmetrical Eckart barrier, constitute two good tests for judging the reliability of our approach. Our results are quantitatively acceptable (even though some different techniques and methods can lead to better accuracy), a good reason for extending the test to the more demanding problem involving an asymmetrical Eckart potential. The importance of such extension lies in the fact that some realistic reactions, for instance the well-studied reactive process $H + H_2$ [91], can be properly modeled in terms of such potential. Even in this case the few simulations performed appear to confirm the preceeding judgement. The application of the approach to multidimensional systems, to depict reactions involving many degrees of freedom, appears, intuitively, a natural extension. To this regard, we think that the SC-IVR (SemiClassical Initial Value Representation) strategy, advocated particularly by W. H. Miller is, nowadays, the best way to take on complex reactions, since all the degrees of freedom are treated equivalently and the old limitation dating back to Wigner, i.e. of a reaction taking place on a single potential energy surface (adiabatic reaction), can be surpassed so as to make possible the study of photoelectronic reactions.

The possible development of our approach in this direction appears, at this moment, only a stimulating challenge for the future. A few comments on this point, however, are in order. The extension of the calculation of the thermal density matrix to several dimensions does not seem to grow any particular problems. The strategy

described in the fourth chapter is easily generalizable to the multidimensional case: from a computational point of view, many independent one-dimensional paths (actually one for each degree of freedom) would be generated.
On the other hand, the same cannot be said about the dynamical part, for which a more careful treatment is required. The extension of the quantum mechanical treatment described in chapter three to a multidimensional space is not impossible, but the basic parabolic barrier approximation exploited in the one-dimensional case should be replaced, if possible, by a working multidimensional analogue.
Alternatively, a sort of mixed quantum/classical approach could be preferred, with one degree of freedom (i.e. the reaction coordinate) treated according to the quantum approach adopted in the one-dimensional case, and all the remaining degrees of freedom described by classical dynamics.
Additional difficulties to reckon with would originate from the multiple integration involved. Probably, the Filon's algorithm would no longer be competitive and other procedures, such as Monte Carlo methods for oscillatory integrands or FFT techniques, should be devised.

As a final conclusion, we want to spend a few words about the approach. As pointed out above, its implementation should be further elaborated to permit the study of complex reactions, which involve multidimensional potential energy surfaces. To this regard it is right to say that strategies like the Semiclassical Initial Value Representation, which has been widely developed and applied to a variety of different reactions, or the recent approach suggested by Craig and Manolopoulos, that is more direct and straightforward to apply, are probably preferable in facing really complicated kinetic problems.

All the same, some merits should be recognized to our efforts, in particular the fact that some important points have been put in evidence: first of all, quantum scattering calculations have been avoided, in harmony with modern formulations of theoretical chemical kinetics implemented after the pioneer suggestions by W. H. Miller, P. Pechukas et al.; secondly, the general lines of the approach, developed quantum mechanically on rigorous grounds, lead to a clear separation between thermal and dynamical effects (associated with imaginary and real time dynamics, respectively), with the standard parabolic barrier approximation to the real time dynamics introduced only as a final step. The approximation, presented in an original and appealing way, involves the appearance in the formalism of an error function. In this manner, the problem of caustic points is avoided, while the presence of a suitable convergence factor acts as a cutoff limiting the integrations to a finite range.

Altogether, then, the study of the approach, even though anything but exhaustive, has come to a positive point, with acceptable results for the cases we minded to face.

Appendix A

A remarkable relation between a principal value integral and a complex error function

The main goal of this appendix is to show the validity of the relation

$$I = \fint_{-\infty}^{+\infty} \frac{d\xi}{\xi} e^{-iA\xi}\, e^{-iB\xi^2} = -i\pi \frac{A}{|A|}\, erf\left[\frac{|A|}{2\sqrt{iB}}\right] \tag{A.1}$$

The principal value integral can be evaluated as the limit of the sum of two integrals

$$\begin{aligned} I &= \lim_{\varepsilon\to 0} \int_{-\infty}^{-\varepsilon} \frac{d\xi}{\xi}\, e^{-iA\xi}\, e^{-iB\xi^2} + \int_{\varepsilon}^{+\infty} \frac{d\xi}{\xi}\, e^{-iA\xi}\, e^{-iB\xi^2} \\ &= \lim_{\varepsilon\to 0} \int_{+\infty}^{\varepsilon} \frac{d\xi}{\xi}\, e^{iA\xi}\, e^{-iB\xi^2} + \int_{\varepsilon}^{+\infty} \frac{d\xi}{\xi}\, e^{-iA\xi}\, e^{-iB\xi^2} \\ &= \lim_{\varepsilon\to 0} \int_{\varepsilon}^{+\infty} \frac{d\xi}{\xi} e^{-iB\xi^2} \left(e^{-iA\xi} - e^{iA\xi}\right) \\ &= -2i \int_0^{+\infty} d\xi\, e^{-iB\xi^2}\, \frac{\sin(A\xi)}{\xi} \end{aligned} \tag{A.2}$$

It is possible to generalize this result for any argument of the sine function, finding the equivalent formula

$$I = -2i \frac{A}{|A|} \int_0^{+\infty} d\xi\, e^{-iB\xi^2}\, \frac{\sin\left(|A|\xi\right)}{\xi} \tag{A.3}$$

In this way, indipendently of the effective value of A, the substitution $\eta = |A|\xi$ preserves the integration limits, leading to

$$I = -2i \frac{A}{|A|} \int_0^{+\infty} d\eta\, e^{-iB\eta^2/|A|^2}\, \frac{\sin\eta}{\eta} \tag{A.4}$$

To proceed it is convenient to introduce the auxiliary function

$$K(\alpha) = \int_0^{+\infty} d\eta \, e^{-i\alpha\eta^2} \, \frac{\sin\eta}{\eta} \tag{A.5}$$

where $\alpha = B/|A|^2$. The calculation of $K(\alpha)$ follows a quite standard procedure. First, a derivation with respect to α gives

$$\begin{aligned} \frac{dK(\alpha)}{d\alpha} &= -i \int_0^{+\infty} d\eta \, \eta \sin\eta \, e^{-i\alpha\eta^2} \\ &= -\frac{e^{i/4\alpha}}{2} \int_0^{+\infty} d\eta \, \eta \left[e^{-i\alpha(\eta-1/2\alpha)^2} - e^{-i\alpha(\eta+1/2\alpha)^2} \right] \end{aligned} \tag{A.6}$$

Simple manipulations lead to the result

$$\begin{aligned} \frac{dK(\alpha)}{d\alpha} &= -\frac{e^{i/4\alpha}}{2} \left[\int_{-1/2\alpha}^{+\infty} d\eta' \left(\eta' + \frac{1}{2\alpha} \right) e^{-i\alpha\eta'^2} - \int_{1/2\alpha}^{+\infty} d\eta' \left(\eta' - \frac{1}{2\alpha} \right) e^{-i\alpha\eta'^2} \right] \\ &= -\frac{e^{i/4\alpha}}{2} \left[\int_{1/2\alpha}^{-\infty} d\eta' \left(\eta' - \frac{1}{2\alpha} \right) e^{-i\alpha\eta'^2} - \int_{1/2\alpha}^{+\infty} d\eta' \left(\eta' - \frac{1}{2\alpha} \right) e^{-i\alpha\eta'^2} \right] \end{aligned} \tag{A.7}$$

and successively to

$$\begin{aligned} \frac{dK(\alpha)}{d\alpha} &= \frac{e^{i/4\alpha}}{2} \left[\int_{-\infty}^{+\infty} d\eta' \left(\eta' - \frac{1}{2\alpha} \right) e^{-i\alpha\eta'^2} \right] \\ &= -\frac{e^{i/4\alpha}}{4\alpha} \int_{-\infty}^{+\infty} d\eta' \, e^{-i\alpha\eta'^2} \\ &= -\frac{e^{i/4\alpha}}{4\alpha} \sqrt{\frac{\pi}{i\alpha}} \end{aligned} \tag{A.8}$$

The solution of eq.(A.5) is obtained by integration of eq.(A.8)

$$K(\alpha) = K(0) + \int_0^{\alpha} d\alpha' \, \frac{dK}{d\alpha'} \tag{A.9}$$

where

$$K(0) = \int_0^{+\infty} d\eta \, \frac{\sin\eta}{\eta} = \frac{\pi}{2} \tag{A.10}$$

Thus

$$K(\alpha) = \frac{\pi}{2} - \frac{1}{4} \int_0^{\alpha} d\alpha' e^{i/4\alpha'} \sqrt{\frac{\pi}{i\alpha'^3}} \tag{A.11}$$

The integral in eq.(A.11) is evaluated by means of suitable variable changes. If $\beta = \frac{1}{4\alpha'}$, eq.(A.11) becomes

$$\begin{aligned} K(\alpha) &= \frac{\pi}{2} + \frac{1}{2}\sqrt{\frac{\pi}{i}} \int_{\infty}^{1/4\alpha} d\beta \frac{e^{i\beta}}{\sqrt{\beta}} \\ &= \frac{\pi}{2} - \sqrt{\frac{\pi}{i}} \int_{1/2\sqrt{\alpha}}^{\infty} du\, e^{iu^2} \end{aligned} \tag{A.12}$$

At this point it is a trivial task to express the above result in terms of the error function. If we put $s = u/\sqrt{i}$, it follows

$$K(\alpha) = \frac{\pi}{2} - \sqrt{\pi} \int_{1/2\sqrt{i\alpha}}^{\infty} ds\, e^{-s^2} \tag{A.13}$$

From the definition of the error function $erf(z)$

$$\begin{aligned} erf(z) &= \frac{2}{\sqrt{\pi}} \int_0^z ds\, e^{-s^2} \\ &= \frac{2}{\sqrt{\pi}} \left[\frac{\sqrt{\pi}}{2} - \int_z^{\infty} ds\, e^{-s^2} \right] \\ &= 1 - \frac{2}{\sqrt{\pi}} \int_z^{\infty} ds\, e^{-s^2} \end{aligned} \tag{A.14}$$

the following result for $K(\alpha)$ is found

$$K(\alpha) = \frac{\pi}{2}\, erf\left(\frac{1}{2\sqrt{i\alpha}}\right) \tag{A.15}$$

Finally, the starting I integral can be written

$$I = -i\pi \frac{A}{|A|}\, erf\left(\frac{|A|}{2\sqrt{iB}}\right) \tag{A.16}$$

Appendix B

Calculation of an integral of the error function

We find it interesting to show in detail the technique employed to evaluate the integral

$$I(x) = \int_{-\infty}^{+\infty} dr\, e^{irx}\, erf\left(\frac{r}{\sqrt{2im\omega}}\right) \tag{B.1}$$

which is involved in the resolution of the problem of the complete parabolic barrier (sec.(3.3.2)).
First of all, we observe that for $x = 0$ the integrand is odd, so that

$$I(0) = \int_{-\infty}^{+\infty} dr\, erf\left(\frac{r}{\sqrt{2im\omega}}\right) = 0 \tag{B.2}$$

On the basis of simple parity reasons, in eq. (B.1) $I(x)$ is expected to be purely imaginary. Assuming for the error function its integral representation, we are led to

$$I(x) = \frac{2}{\sqrt{\pi}} \int_{-\infty}^{+\infty} dr\, e^{irx} \int_0^{r/\sqrt{2im\omega}} dt\, e^{-t^2} \tag{B.3}$$

and successively, by the variable change $T = t\sqrt{2im\omega}/r$,

$$\begin{aligned} I(x) &= \frac{2}{\sqrt{\pi}} \int_{-\infty}^{+\infty} dr\, e^{irx} \int_0^1 dT \frac{r}{\sqrt{2im\omega}}\, e^{-r^2T^2/2im\omega} \\ &= \frac{2}{\sqrt{2\pi im\omega}} \int_0^1 dT \int_{-\infty}^{+\infty} dr\, r\, e^{-r^2T^2/2im\omega}\, e^{irx} \end{aligned} \tag{B.4}$$

The integral

$$\int_{-\infty}^{+\infty} dr\, r\, e^{-r^2T^2/2im\omega}\, e^{irx} \tag{B.5}$$

can be evaluated making use of known results for Gaussian-like integrals, arriving at

$$\int_{-\infty}^{+\infty} dr\, r\, e^{-r^2T^2/2im\omega}\, e^{irx} \;=\; -m\omega x\sqrt{2\pi im\omega}\;\frac{e^{-im\omega x^2/2T^2}}{T^3} \tag{B.6}$$

The change of variable $\beta = x/T$ provides

$$\begin{aligned} I(x) &= \frac{2m\omega}{x}\int_{\infty}^{x} d\beta\,\beta\, e^{-im\omega\beta^2/2} \\ &= -\frac{2}{ix}\, e^{-im\omega x^2/2} \end{aligned} \tag{B.7}$$

Hence, the final result is

$$I(x) = \int_{-\infty}^{+\infty} dr\, e^{irx}\, erf\left(\frac{r}{\sqrt{2im\omega}}\right) = \begin{cases} 0 & x = 0 \\ -\dfrac{2}{ix}\, e^{-im\omega x^2/2} & x \neq 0 \end{cases} \tag{B.8}$$

Appendix C

Basic path integral method for the calculation of thermal density matrix elements

In this appendix, we wish to provide the basic formulation of the path integral method which leads to the relations adopted in sec.(4.2). For evaluating the matrix element of interest

$$K(x,y;\beta) =< x|e^{-\beta(\hat{T}+\hat{V})}|y >, \tag{C.1}$$

the starting point is the operatorial equality

$$e^{\hat{A}} = (e^{\hat{A}/N})^N \tag{C.2}$$

so that

$$K(x,y;\beta) =< x| \left[e^{-\beta\left(\hat{T}+\hat{V}\right)/N}\right]^N |y > \tag{C.3}$$

By resorting to the Trotter product formula

$$e^{-\lambda(\hat{T}+\hat{V})} = \lim_{N\to\infty}\left[e^{-\lambda\hat{T}/N}e^{-\lambda\hat{V}/N}\right]^N \tag{C.4}$$

eq.(C.3) transforms into

$$K(x,y;\beta) = \lim_{N\to\infty} < x|(e^{-\beta T/N}e^{-\beta V/N})^N|y > \tag{C.5}$$

At this point, it is convenient to introduce $N-1$ complete sets of eigenstates of the position operator $\int dx_j|x_j >< x_j|$, labelled by the indexes $j = 1,\ldots,N-1$, so that

$$K(x,y;\beta) = \lim_{N\to\infty}\int dx_1\ldots dx_{N-1}\prod_{j=0}^{N-1} < x_{j+1}|e^{-\beta T/N}e^{-\beta V/N}|x_j >, \quad y = x_0\,,\, x = x_N \tag{C.6}$$

The operator $V(\hat{x})$ is multiplicative in the position representation

$$e^{-\beta\hat{V}/N}|x_j>=|x_j>\ e^{-\beta V(x_j)/N} \tag{C.7}$$

Consequently, $K(x,y;\beta)$ (eq.(C.6)) becomes

$$K(x,y;\beta)=\lim_{N\to\infty}\int dx_1\dots dx_{N-1}\prod_{j=0}^{N-1}e^{-\beta V(x_j)/N}<x_{j+1}|e^{-\beta\hat{T}/N}|x_j> \tag{C.8}$$

The matrix elements $<x_{j+1}|e^{-\beta\hat{T}/N}|x_j>$ are readily evaluated by introducing a complete set of eigenstates of the momentum operator,

$$\begin{aligned}<x_{j+1}|e^{-\beta\hat{T}/N}|x_j>&=\int_{-\infty}^{+\infty}dp<x_{j+1}|p><p|e^{-\beta\hat{T}/N}|x_j>\\&=\frac{1}{2\pi}\int_{-\infty}^{+\infty}dp\,e^{-\frac{\beta p^2}{2mN}}\,e^{ip(x_{j+1}-x_j)}\\&=\sqrt{\frac{mN}{2\pi\beta}}\,e^{-mN(x_{j+1}-x_j)^2/2\beta}\end{aligned} \tag{C.9}$$

The final result for the matrix element of eq. (C.1) is

$$K(x,y;\beta)=\lim_{N\to\infty}\int dx_1\dots dx_{N-1}\sqrt{\frac{mN}{2\pi\beta}}\prod_{j=0}^{N-1}\exp\left\{-\frac{mN(x_{j+1}-x_j)^2}{2\beta}+\frac{\beta V(x_j)}{N}\right\} \tag{C.10}$$

Bibliography

[1] *Trans. Faraday Soc.* **34** (1938).

[2] W.H.Miller, *Faraday Discuss.* **110**, 1 (1998).

[3] D.G. Truhlar, B.C. Garrett and S.J. Klippenstein, *J.Phys.Chem.* **100**, 12771 (1996).

[4] M.J.Gillan, *J.Phys.C* **20**, 3621 (1987).

[5] G.A.Voth, *J.Phys.Chem.* **97**, 8365 (1993).

[6] N.F.Hansen and J.C.Andersen, *J.Chem.Phys.* **101**, 6032 (1994).

[7] N.F.Hansen and J.C.Andersen, *J.Phys.Chem.* **100**, 1137 (1996).

[8] T.Yamamoto, *J. Chem. Phys.* **33**, 281 (1960).

[9] W.H.Miller, *J.Chem.Phys.* **61**, 1823 (1974).

[10] F.J.McLafferty and P.Pechukas, *Chem.Phys.Lett.* **27**, 511 (1974).

[11] T.F.George and W.H.Miller, *J.Chem.Phys.* **57**, 2458 (1972).

[12] W.H.Miller, *Acc. Chem. Res.* **9**, 306 (1976).

[13] S.Chapman, B.C.Garrett and W.H.Miller, *J.Chem.Phys.* **63**, 2710 (1975).

[14] W.H.Miller, *J.Chem.Phys.* **62**, 1899 (1975).

[15] W.H.Miller, S.D.Schwartz and J.W.Tromp, *J.Chem.Phys.* **79**, 4889 (1983).

[16] J.Ankerhold, F.Grossmann and D.J.Tannor, *Phys.Chem.Chem.Phys.* **1**, 1333 (1999).

[17] G.A.Voth, D.Chandler and W.H.Miller, *J.Phys.Chem.* **93**, 7009 (1989).

[18] R.Zwanzig, *Annu.Rev.Phys.Chem* **16**, 67 (1965).

[19] E.Pollak and J. Liao, *J.Chem.Phys.* **108**, 2733 (1998).

[20] J.W.Tromp. *Chemical reaction rates via the flux correlation funcion*, Ph.D. thesis, University of California, Berkeley (1988).

[21] J.W.Tromp and W.H.Miller, *J.Phys.Chem.* **90**, 1986 (3482).

[22] I.R.Craig and D.E.Manolopoulos, *J.Chem.Phys.* **121**, 3368 (2004).

[23] I.R.Craig and D.E.Manolopoulos, *J.Chem.Phys.* **122**, 084106 (2005).

[24] I.R.Craig and D.E.Manolopoulos, *J.Chem.Phys.* **123**, 034102 (2005).

[25] J.H.Van Vleck, *Proc. Natl. Acad. Sci.* **14**, 178 (1928).

[26] W.H.Miller, *J.Phys.Chem.A* **105**, 2942 (2001).

[27] W.H.Miller, *J.Chem.Phys.* **53**, 3578 (1970).

[28] G.A.Voth, D.Chandler and W.H.Miller, *J.Chem.Phys.* **91**, 7749 (1989).

[29] W.H.Miller, *J.Chem.Phys.* **95**, 9428 (1991).

[30] P.Pechukas, in *Dynamics of Molecular Collisions*, Part B, W.H.Miller(Ed.), Modern Theoretical Chemistry, Vol.2, Plenum, New York (1976), Chapter 6.

[31] D.P.Landau and K.Binder, *A guide to Monte Carlo Simulations in Statistical Physics*, Cambridge University Press, Cambridge (2000).

[32] J.M.Hammersley and D.C.Handscomb, *Monte Carlo Methods*, John Wiley & Sons, New York (1964).

[33] S.C.Tucker, in *New Trends in Kramers' Reaction Rate Theory*, P. Talkner and P.Hänggi (Eds.), Kluwer Academic Publishers, The Netherlands (1995), Chapter 2.

[34] D.G.Truhlar and B.C.Garrett, *Accts. Chem. Res.* **13**, 440 (1980).

[35] D.G.Truhlar and B.C.Garrett, *Ann. Rev. Phys. Chem.* **35**, 159 (1984).

[36] F.J.McLafferty and P.Pechukas, *J. Chem. Phys.* **58**, 1622 (1973).

[37] S.Chapman, S.M.Hornstein and W.H.Miller, *J.Am.Chem.Soc.* **97**, 892 (1975).

[38] W.H.Miller, in *New Trends in Kramers' Reaction Rate Theory*, P. Talkner and P.Hänggi (Eds.), Kluwer Academic Publishers, The Netherlands (1995), Chapter 11.

[39] H.S.Johnston and D.Rapp, *J.Amer.Chem.Soc.* **83**, 1 (1961).

[40] R.A.Marcus and M.E.Coltrin, *J.Chem.Phys.* **67**, 2609 (1977).

[41] N.Makri and W.H.Miller, *J.Chem.Phys.* **91**, 4026 (1989).

[42] S.Caratzoulas and P.Pechukas, *J.Chem.Phys.* **104**, 6265 (1996).

[43] D.Thirumalai and B.J.Berne, *J.Chem.Phys.* **79**, 5029 (1983).

[44] D.Thirumalai, E.J.Bruskin and B.J.Berne, *J.Chem.Phys.* **79**, 5063 (1983).

[45] D.Chandler and P.G.Wolynes, *J.Chem.Phys.* **74**, 4078 (1981).

[46] K.S.Schweizer, R.M.Stratt, D.Chandler and G.P.Wolynes, *J.Chem.Phys.* **75**, 1347 (1981).

[47] D.Chandler, *J.Phys.Chem.* **88**, 3400 (1984).

[48] N.Makri and W.H.Miller, *Chem.Phys.Lett.* **139**, 10 (1987).

[49] N.Makri, *Chem.Phys.Lett.* **159**, 489 (1989).

[50] J.D.Doll, R.D.Coalson and D.L.Freeman, *J.Chem.Phys.* **87**, 1641 (1987).

[51] J.D.Doll, D.L.Freeman and M.J.Gillian, *Chem.Phys.Lett.* **143**, 277 (1988).

[52] E.Wigner, *Phys.Rev.* **40**, 749 (1932).

[53] N. Makri and K. Thompson, *Chem.Phys.Lett.***291**, 101 (1998).

[54] N.Makri and K.Thompson, *J.Chem.Phys.* **110**, 1343 (1999).

[55] G.Wahnström and H. Metiu, *J.Phys.Chem.* **92**, 3240 (1988).

[56] K.G.Kay, *Annu.Rev.Phys.Chem.* **56**, 255 (2005).

[57] J.D.Doll, *J.Chem.Phys.* **81**, 3536 (1984).

[58] N.Makri, *Comp.Phys.Comm.* **63**, 389 (1991).

[59] L.A.Beauregard, *Am.J.Phys.* **33**, 1084 (1965).

[60] B.Felsager, *Geometry, Particles and Fields*, Odense University Press (1981).

[61] L.S.Schulman, *Techniques and Applications of Path Integration*, John Wiley & Sons (1981).

[62] I.Fujiwara, *Progr. Theoret. Phys. (Kyoto)* **21**, 902 (1959).

[63] E.P.Wigner, *Z. Physik Chem. B* **19**, 203 (1932).

[64] R.P.Bell, *Trans. Faraday Soc.* **55**, 1 (1959).

[65] G.Barton, *Ann. Phys.* **166**, 322 (1986).

[66] L.D.Landau and E.M.Lifsits, *Kvantovaja mechanika*, Mir Editions (1947).

[67] W.H. Press, S.A. Teulosky, W.T. Vetterling and B.P. Flannery, *Numerical Recipes in fortran 77 - The Art of Scientific Computing*, Cambridge University Press, 2nd ed, (1992).

[68] M. Abramowitz and I.A. Stegun,*Handbook of mathematical functions*, Dover Publications, INC., New York (1970).

[69] G.R.Lindfield and J.E.T. Penny, *Microcomputers in numerical analysis*, Ellis Horwood Limited, Chichester (1989).

[70] J.J.Sakurai, *Modern Quantum Mechanics. Revised Edition*, Addison-Wesley Publishing Company, Inc. (1985).

[71] B.Militzer, *Path Integral Monte Carlo Simulations of Hot Dense Hydrogen*, Ph.D. thesis, University of Illinois, Urbana-Champaign (2000).

[72] D.M.Ceperley, *Rev. Mod. Phys.* **67**, 280 (1995).

[73] B. Bernu and D.M. Ceperley, in *Quantum Simulations of Complex Many-Body Systems: From Theory to Algorithms*, Lecture Notes, J. Grotendorst, D.Marx, A.Muramatsu (Eds), John Von Neumann Institute for Computing, Jülich, vol **10**, pp. 51-61 (2002).

[74] H.F.Trotter, *Proc. Am. Math. Soc.* **10**, 545 (1959).

[75] M.Kac, *Trans. Amer. Math. Soc.* **65**, 1 (1949).

[76] M.Kac, *Trans. Amer. Math. Soc.* **59**, 401 (1946).

[77] T.Hida, *Brownian Motion*, Springer-Verlag, New York (1980).

[78] R.E.A.C. Paley and N. Wiener, *Fourier Transforms in the Complex Domain*, Amer. Math. Soc. Colloq. Pub. XIX (1934).

[79] P.Lévy, *Processus stochastiques et mouvement brownien*, Gauthier-Villars, Paris (1948).

[80] C.Hastings, Jr., *Approximations for digital computers*, Princeton Univ. Press, Princeton, N.J. (1955).

[81] W.C.Swope, H.C.Andersen, P.H.Berens, and K.R.Wilson, *J. Chem. Phys.* **76**, 637 (1982).

[82] L.Verlet, *Phys. Rev.* **159**, 98 (1967).

[83] L.Verlet, *Phys. Rev.* **165**, 201 (1968).

[84] W.Gautschi, Algorithm 363, Complex Error Function, *Collected Algorithms from CACM* (1969).

[85] W.Gautschi, *SIAM J. Numer. Anal.* **7**, 187 (1970).

[86] R.P.Bell, *Proc. Roy. Soc. A* **148**, 241 (1935).

[87] R.P.Bell, *Proc. Roy. Soc. A* **158**, 128 (1937).

[88] J.Bigeleisen, *J. Chem. Phys.* **17**, 675 (1949).

[89] C.Eckart, *Phys. Rev.* **35**, 1303 (1930).

[90] H.S.Johnston, *Gas Phase Reaction Rate Theory*, Ronald Press, New York (1966).

[91] U.Manthe, *J. Chem. Phys.* **102**, 9205 (1995).